unesp

PROGRAMA DE PÓS-GRADUAÇÃO EM GEOCIÊNCIAS E MEIO AMBIENTE

CONTRIBUIÇÃO DE PROCESSOS ENDÓGENOS E EXÓGENOS PARA A DENUDAÇÃO CENOZOICA E A EVOLUÇÃO DO RELEVO NA PORÇÃO OESTE DO DOMO DE ANGOLA: APLICAÇÃO DA TERMOCRONOLOGIA MULTIMÉTODO

Bruno Venancio da Silva

Instituto de Geociências e Ciências Exatas
Campus de Rio Claro

Rio Claro/SP - 2022

UNIVERSIDADE ESTADUAL PAULISTA
“Júlio de Mesquita Filho”
Instituto de Geociências e Ciências Exatas
Câmpus de Rio Claro

Bruno Venancio da Silva

Contribuição de processos endógenos e exógenos para a denudação cenozoica e a evolução do relevo na porção oeste do Domo de Angola: aplicação da termocronologia multimétodo

Tese de Doutorado apresentada ao Instituto de Geociências e Ciências Exatas do Câmpus de Rio Claro, da Universidade Estadual Paulista “Júlio de Mesquita Filho”, como parte dos requisitos para obtenção do título de Doutor em Geociências e Meio Ambiente.

Orientador: George Luiz Luvizotto

Rio Claro - SP

2022

S586c

Silva, Bruno Venancio da

Contribuição de processos endógenos e exógenos para a denudação cenozoica e a evolução do relevo na porção oeste do Domo de Angola: aplicação da termocronologia multimétodo / Bruno Venancio da Silva. -- Rio Claro, 2022

124 f. : il., tabs., fotos, mapas, 8 v.

Tese (doutorado) - Universidade Estadual Paulista (Unesp), Instituto de Geociências e Ciências Exatas, Rio Claro

Orientador: George Luiz Luvizotto

1. Geociências. 2. Geotectônica. 3. Geomorfologia. 4. Termocronologia. I. Título.

Bruno Venancio da Silva

Contribuição de processos endógenos e exógenos para a denudação cenozoica e a evolução do relevo na porção oeste do Domo de Angola: aplicação da termocronologia multimétodo

Tese de Doutorado apresentada ao Instituto de Geociências e Ciências Exatas do Câmpus de Rio Claro, da Universidade Estadual Paulista "Júlio de Mesquita Filho", como parte dos requisitos para obtenção do título de Doutor em Geociências e Meio Ambiente.

Comissão Examinadora

Prof. Dr. GEORGE LUIZ LUVIZOTTO
IGCE / UNESP/Rio Claro (SP)

Dr. DANIEL FRANÇOSO DE GODOY
IGCE / UNESP/Rio Claro (SP)

Dr. SILVIO TAKASHI HIRUMA
Instituto de Pesquisas Ambientais / SIMA/São Paulo (SP)

Dr. JOSÉ PAULO DONATTI FILHO
Pesquisador Colaborador / UNICAMP/Campinas (SP)

Dr. JOÃO MARINHO DE MORAIS NETO
E&P / Petrobras/Rio de Janeiro (RJ)

Conceito: Aprovado.

Rio Claro/SP, 07 de fevereiro de 2022.

Dedico esta Tese aos meus pais Paulo e Rosangela, à minha noiva Jéssica, à minha filha Manuela e à memória de Peter Christian Hackspacher

AGRADECIMENTOS

À minha família, que sempre esteve presente e me apoiou durante o desenvolvimento do trabalho.

Ao professor e amigo Peter Christian Hackspacher, que me orientou durante a maior parte do trabalho e me ensinou a sempre buscar pela ciência de qualidade.

Ao amigo Daniel Françoso de Godoy, que rotinizou o método por traços de fissão em zircão por microssonda eletrônica no Departamento de Geologia da UNESP, possibilitando a realização de uma parte importante da pesquisa.

Aos colegas Daniel Henrique de Souza, Alessandra Petruz, Marli Carina Siqueira Ribeiro, Regiane Fumes, Marly Aparecida e Cibele Montibeller pelo auxilio e supervisão durante as atividades de laboratório ou de tratamento dos dados.

Aos parceiros em Angola, professor Antônio Olimpio Gonçalves, Tinta Manuel Vunda e João Gaspar Correia, por todo o suporte durante a etapa de campo.

Ao professor e colega George Luiz Luvizotto, que possibilitou o desenvolvimento da pesquisa junto ao laboratório de microssonda eletrônica do Departamento de Geologia e aceitou me orientar na reta final do trabalho.

Aos professores e colegas Guillermo Navarro, Antenor Zanardo e Vania Rosolen, pelas discussões construtivas que me auxiliaram na caracterização e interpretação das amostras de rocha.

Ao professor Didier Gastmans, que enquanto presidente do conselho do programa de pós-graduação em Geociências e Meio Ambiente, esteve sempre aberto ao diálogo após o meu religamento no programa.

À Sociedade Mineira de Catoca LDA pela disponibilização de alojamento, transporte e materiais durante a etapa de campo da pesquisa.

O presente trabalho foi realizado com apoio da Coordenação de Aperfeiçoamento de Pessoal de Nível Superior - Brasil (CAPES) - Código de Financiamento 001. Também foi realizado com apoio do Conselho Nacional de Desenvolvimento Científico e Tecnológico – CNPq, processo 140361/2019-7.

A theory is nothing but the generalization of particular facts; and, in a theory of the earth, those facts must be taken from the observations of natural history. (HUTTON, 1795, p. 297)

Resumo

Para entender a origem de parte do relevo relacionado ao Domo de Angola, África, as histórias de denudação de *long-term* da Escarpa de Chela (porção sudoeste do Domo) e do Planalto Antigo (porção noroeste do Domo) foram obtidas através dos métodos por traços de fissão e (U-Th-Sm)/He em apatita. Uma possível contribuição do manto terrestre para a evolução de *long-term* da paisagem foi testada a partir da datação de kimberlitos, localizados na região da cabeceira do rio Longa (porção noroeste do Domo), utilizando-se o método por traços de fissão em zircão via microssonda eletrônica. Os resultados sugerem que a maior parte do relevo de ambas as regiões tem se desenvolvido durante a segunda metade do Cenozoico, assim como processos no manto profundo parecem ter impulsionado os eventos de soerguimento e denudação continentais associados à formação da Zona Costeira, do *Great Escarpment* e do Planalto Antigo em Angola, feições estas também típicas da paisagem da África meridional.

Palavras-chave: Topografia da África. Soerguimento dinâmico. Relevo de Angola. Termocronologia. Kimberlito cenozoico. Escudo Angolano. Região do Longa.

Abstract

To understand the origin of part of the relief related to the Angola Dome, Africa, the *long-term* denudation history of the Chela Escarpment (southwestern portion of the Dome) and the Ancient plateau (northwestern portion of the Dome), were accessed by means of apatite fission-track and (U-Th-Sm)/He methods. A possible contribution of the Earth's mantle to the long-term evolution of the landscape, was tested from the dating of kimberlites localized in the region of the Longa river headwater (northwestern portion of the Dome), by using the electron microprobe zircon fission- track method. The results suggest that most of the relief of both regions has developed since Late Cenozoic times, as well as deep mantle processes appear to account for the uplift and denudation events associated to the formation of the Coastal Zone, the Great Escarpment, and the Ancient Plateau in Angola, features that are also typical of the southern African landscape.

Keywords: Africa topography. Dynamic uplift. Relief of Angola. Thermochronology. Cenozoic kimberlite. Angolan Shield. Longa region.

SUMÁRIO

CAPÍTULO 1 - INTRODUÇÃO

1.1 A topografia da África meridional

A África meridional apresenta uma das paisagens mais enigmáticas do mundo, caracterizada principalmente por um planalto interior elevado (acima de 1000 m) e de relevo predominantemente baixo, limitado por um escarpamento íngreme em quase todo o seu perímetro (*Great Escarpment*), o qual o separa da região costeira circundante (FLOWERS; SCHOENE, 2010; KING, 1956; MOORE; BLENKINSOP; COTTERILL, 2009; STANLEY; FLOWERS; BELL, 2015) (Fig. 1a). O interior deste planalto é dominado por uma extensa *etchplain,* conhecida como a superfície de aplainamento africana (BURKE; GUNNELL, 2008; KING, 1976; PARTRIDGE; MAUD, 1987), a qual se caracteriza por apresentar deflexões de escala continental (acima de 1000 km de diâmetro), configurando extensos domos e bacias (AL-HAJRI; WHITE; FISHWICK, 2009; HOLMES, 1944).

Apesar de mais de 100 anos de pesquisa, existe pouco consenso entre os pesquisadores a respeito dos mecanismos formadores e da idade desta topografia. De um ponto de vista geotectônico, três grandes “motores”, capazes de explicar amplas deflexões na superfície terrestre, têm sido requeridos:

- Fluxo vertical e viscoso do manto devido à incidência de plumas mantélicas e/ou a convexões profundas;
- Processos no manto litosférico, subjacentes ao continente;
- Esforços tectônicos de longa distância, relacionados a fluxos laterais do manto e a movimentações laterais das placas tectônicas.

A ideia de que processos mantélicos, subjacentes ao continente, tem sido os motores para a topografia (BUNGE; GLASMACHER, 2018) surge a partir de características geomorfológicas, tais como a existência de amplos domos na superfície, de contornos quase circulares e que apresentam sistema de drenagem radial (HOLMES, 1944).

A influência do manto é reforçada a partir da caracterização da *Superswell* africana, que consiste em uma região de topografia e batimetria anômalas que se estende desde o planalto do leste africano até a porção sudeste do oceano Atlântico Sul (NYBLADE; ROBINSON, 1994), aliada à existência de uma ampla zona de baixa-velocidade sísmica na transição entre o núcleo e o manto terrestre (*large low* *shear velocity province* - LLSVP) (GURNIS et al., 2000; LITHGOW-BERTELLONI; SILVER, 1998; RITSEMA; VAN HEIJST; WOODHOUSE, 1999). Neste mesmo contexto, diversos trabalhos têm levantado evidências geoquímicas e geofísicas de que a região foi afetada pela incidência de plumas mantélicas (EBINGER; SLEEP, 1998; GIULIANI et al., 2017). Entretanto, em várias partes da África meridional, não existem evidências suficientes suportando uma possível conexão entre a LLSVP e a superfície terrestre, de forma que a sua influência direta na topografia ainda é especulativa. Neste sentido, alguns trabalhos têm combinado evidências geoquímicas e geofísicas para propor processos ocorridos no manto raso (não ligados à incidência de plumas), como pequenas variações nas temperaturas da astenosfera associadas ao afinamento/erosão da litosfera (KLÖCKING et al., 2020).

Em contrapartida, dados estruturais e geomorfológicos ao longo da margem e do interior da África meridional indicam a formação de arqueamentos crustais causados por esforços compressivos laterais. A formação destas estruturas tem sido atribuída a eventos tectônicos globais, tais como mudanças nas velocidades e nos polo de rotação de placas litosféricas (COLLI et al., 2014; GUIRAUD; BOSWORTH, 1997; MOORE; BLENKINSOP; COTTERILL, 2009). Alguns autores propõem que margens continentais elevadas, ou seja, aquelas caracterizadas pela ocorrência de um escarpamento costeiro (GREEN et al., 2018; JAPSEN et al., 2012), são formadas a partir destes arqueamentos crustais (JAPSEN et al., 2012; MOORE; BLENKINSOP; COTTERILL, 2009). Deste modo, existem evidências suportando cada um dos três grandes mecanismos mencionados acima, de forma que a topografia da África meridional parece ser o resultado da combinação de cada um deles.

Com relação à idade da topografia, duas correntes de pensamento principais advogam a seguinte cronologia:

- Idade Mesozoica, desenvolvida entre ~ 150 e 80 Ma;
- Idade Cenozoica, formada a partir de ~ 40 ou 30 Ma.

Dados regionais de termocronologia indicam que os maiores pulsos de denudação/erosão continental ocorreram no Mesozoico, nos intervalos entre ~ 150 e 120 Ma e entre ~ 90 e 70 Ma (BICCA et al., 2019; BROWN et al., 2014, 1990; BROWN; SUMMERFIELD; GLEADOW, 2002; COCKBURN et al., 2000; FLOWERS; SCHOENE, 2010; GALLAGHER; BROWN, 1999; GREEN; MACHADO, 2015; KOUNOV et al., 2009; RAAB et al., 2002a; SILVA et al., 2019; STANLEY;

FLOWERS; BELL, 2015; TINKER; DE WIT; BROWN, 2008; WILDMAN et al., 2015, 2016). Estes pulsos de denudação coincidem com períodos de altas taxas de sedimentação siliciclástica *offshore*, associadas à formação de grandes depocentros ao longo das bacias marginais (BRAUN et al., 2014; DE VERA; GRANADO; MCCLAY, 2010; GUILLOCHEAU et al., 2012; MACGREGOR, 2013; MAYSTRENKO et al., 2013; MCMILLAN, 2003; PATON et al., 2007; ROUBY et al., 2009; SAID et al., 2015; SÉRANNE; ANKA, 2005). Estes períodos de denudação continental juntos coincidem com a incidência de plumas mantélicas, relacionadas à tectônica rifte de abertura do Atlântico Sul e à erupção da *Large Igneous Province* (LIP) Paraná – Etendeka (BRAUN et al., 2014; KROB et al., 2020; O'CONNOR et al., 2018; RENNE et al., 1996), assim como parecem coincidir com eventos tectônicos associados à propagação de esforços compressivos de longa distância (MOORE; BLENKINSOP; COTTERILL, 2009) e à magmatismo kimberlítico intra-placa (JELSMA et al., 2009, 2004; STANLEY; FLOWERS, 2016).

A corrente de pensamento mesozoica se baseia no princípio de que o ganho substancial de elevação e de formação do relevo é contemporâneo às principais fases de magmatismo, soerguimento e de denudação/erosão continentais (FLOWERS; SCHOENE, 2010). A maior parte dos estudos termocronológicos desenvolvidos na África meridional (Fig. 1a) estima taxas de denudação/erosão relativamente baixas para o Cenozoico (BICCA et al., 2019; BROWN et al., 1990; BROWN; SUMMERFIELD; GLEADOW, 2002; FLOWERS; SCHOENE, 2010; KOUNOV et al., 2009; RAAB et al., 2002b; TINKER; DE WIT; BROWN, 2008; WILDMAN et al., 2015, 2016), da mesma forma que estudos baseados em isótopos cosmogênicos, concentrados principalmente na Namíbia, também indicam taxas de erosão recentes relativamente baixas (BIERMAN; CAFFEE, 2001; COCKBURN et al., 2000; VAN DER WATEREN, 2001). Estes aspectos, portanto, têm sido interpretados como um indício da longevidade do relevo nestas regiões.

Por outro lado, trabalhos de termocronologia nas margens continentais de Angola (GREEN; MACHADO, 2015; JACKSON; HUDEC; HEGARTY, 2005; SILVA et al., 2019), da Namíbia (MARGIRIER et al., 2019) e da África do Sul (GREEN et al., 2016), além dos eventos do Cretáceo, interpretam eventos de denudação/erosão pronunciados no Cenozoico. A maior parte destes eventos coincide com as deformações de longa amplitude na superfície africana a partir de ~ 40 - 30 Ma, associadas à formação, por exemplo, dos Domos do Oeste Africano e de Angola

(GUILLOCHEAU et al., 2018). Coincidem também com deformações de estratos marinhos *onshore* e com a formação de discordâncias erosivas, dentre as quais está a do limite Eoceno – Oligoceno reconhecida ao longo da margem africana (ANKA et al., 2009; BURKE, 1996; BURKE; GUNNELL, 2008; LAVIER; STECKLER; BRIGAUD, 2001; PARTRIDGE; MAUD, 1987). Em Angola, por exemplo, sedimentos maastrichtianos (Cretacéo Superior) recobrem uma discordância que se encontra inclinada para *offshore* (GREEN; MACHADO, 2015; MARSH; SWART, 2016) e esta é truncada em direção ao continente por outra discordância mais jovem, de idade cenozoica (FEIO, 1964). Estes processos iniciados a partir de ~ 40 – 30 Ma também coincidem com a formação da corrente circumpolar antartica associada a transição de um clima global quente para um clima predominantemente frio, o que pode explicar o aumento da erosão continental no período, que culmina no aumento da sedimentação siliciclástica *offshore* em bacias como as de Angola, do Baixo Congo (LAVIER; STECKLER; BRIGAUD, 2001; SÉRANNE; ANKA, 2005) e de Moçambique (SAID et al., 2015). Em resumo, a corrente de pensamento cenozoica se baseia basicamente em correlações entre superfícies de aplainamento e discordâncias erosivas regionais, onde se estabelece idades para estas superfícies (e discordâncias) por meio de suas relações de truncamento e de sobreposição com rochas, sedimentos e mantos de intemperismo de idades preestabelecidas (GUILLOCHEAU et al., 2018). Também se baseia em estudos termocronológicos que utilizam estas informações estratigráficas e de superfícies de aplainamento para a construção de histórias térmicas (GREEN; MACHADO, 2015; SILVA et al., 2019).

As observações anteriormente apresentadas mostram que os eventos de soerguimento e denudação tanto do Cretáceo quanto do Cenozoico parecem ter sido importantes para a formação da topografia e do relevo da África meridional; no entanto, é importante ressaltar que as duas correntes de pensamento apresentam limitações, principalmente devido à carência de dados quantitativos, ou à limitações das técnicas empregadas na quantificação dos processos geológicos e geomorfológicos envolvidos. Isótopos cosmogênicos são capazes de estimar taxas de erosão relativamente muito recentes, enquanto a termocronologia por traços de fissão em apatita é menos sensível a processos erosivos de baixa magnitude (da ordem de ~ 1 - 2 km). Muitos pesquisadores questionam a extensão espacial e longevidade da superfície de aplainamento africana, principalmente devido à carência de datações radiométricas, exceto em algumas regiões do planalto meridional africano (DE PUTTER; RUFFET, 2020).

1.2 O Domo de Angola

Angola, localizada na margem sudoeste da África meridional (Fig. 1a, b), consiste em um laboratório natural para o entendimento dos processos que regem a evolução do relevo daquela região. Sua topografia revela a existência do Domo de Angola, com um diâmetro de aproximadamente 1000 km e cujo flanco oeste é voltado para o oceano (Fig. 1b). O início do soerguimento deste Domo é estimado do Oligoceno, mas o maior pulso de soerguimento é atribuído ao Neogeno (GUILLOCHEAU et al., 2018; ROBERTS; WHITE, 2010; WALKER et al., 2016). Estas estimativas se baseiam principalmente em modelos de inversão de perfis longitudinais de rios, os quais assumem valores para variáveis difíceis de serem mensuradas (ROBERTS; WHITE, 2010); portanto, tais modelos possuem um elevado grau de incerteza de forma que a idade desta estrutura ainda é incerta. Desse modo, apesar de dados termocronológicos suportarem denudação cenozoica pronunciada ao longo da margem angolana (GREEN; MACHADO, 2015; JACKSON; HUDEC; HEGARTY, 2005; SILVA et al., 2019), a falta de dados na região do escarpamento e do planalto interior não permite assegurar se o relevo regional tem sido formado no Cenozoico, ou se a denudação cenozoica somente tem realçado um relevo pretérito.

Em relação aos mecanismos de formação da topografia, também há controvérsias. Dados geofísicos indicam que o manto sotoposto ao Domo é caracterizado por anomalias gravimétricas *free-air* positivas e anomalias sísmicas de baixa-velocidade, ambas compatíveis com soerguimento dinâmico (AL-HAJRI; WHITE; FISHWICK, 2009; KLÖCKING et al., 2020). O fato é que estes dados geofísicos mostram a situação atual, de forma que ainda não se sabe quando estes processos mantélicos se iniciaram. Outra característica importante do Domo de Angola é a ocorrência de kimberlitos e carbonatitos distribuídos ao longo de notáveis alinhamentos estruturais (Fig. 1c). O maior deles, o alinhamento de Lucapa, atravessa o território angolano na direção NE-SW e hospeda as maiores províncias diamantíferas do país (JELSMA et al., 2004; MCCOURT et al., 2013; USTINOV et al., 2018) (Fig. 1c). Kimberlitos são formados em profundidade no manto e além de sua importância econômica, constituem registros da astenosfera e da litosfera da época das erupções (STANLEY; FLOWERS; BELL, 2015, 2013). Apesar de ser peça-chave no entendimento de como processos mantélicos interferem na superfície terrestre (STANLEY; FLOWERS; BELL, 2015, 2013), a maior parte das intrusões conhecidas não possui idade estabelecida. Na região kimberlítica próxima a cabeceira rio Longa (Fig. 1c), algumas intrusões kimberliticas estão em estreita associação com sedimentos paleogenos da Formação “Grès Polymorphes” e são truncados por uma superfície de aplainamento regional denominada “Upper surface 2” (GUILLOCHEAU et al., 2015). Deste modo, estabelecer a idade destes kimberlitos pode fornecer informações valiosas a respeito dos mecanismos que regem a topografia.

1.3 Problema, Hipóteses e Objetivos

Esta Tese se concentra na seguinte questão: Qual é a idade e quais são os principais mecanismos que atuaram na formação do Domo de Angola e de seu relevo associado? A partir da literatura preexistente, duas hipóteses são formuladas:

- A denudação cenozoica tem contribuído substancialmente para a formação do relevo;
- O manto subjacente ao Domo de Angola tem sido um dos principais motores para a topografia.

Para se testar a primeira hipótese, pretende-se estabelecer os principais eventos de denudação continental nas porções sudoeste (área 1) e noroeste (área 2) do Domo de Angola (Fig. 1b). Para se testar a segunda hipótese, pretende-se estabelecer as possíveis idades de três intrusões kimberlíticas localizadas na região do rio Longa (área 3), porção noroeste do Domo de Angola (Fig. 1c). Desta forma, o objetivo principal é estabelecer a correlação temporal entre os eventos de denudação continental e o episódio (ou episódios) de vulcanismo kimberlítico.

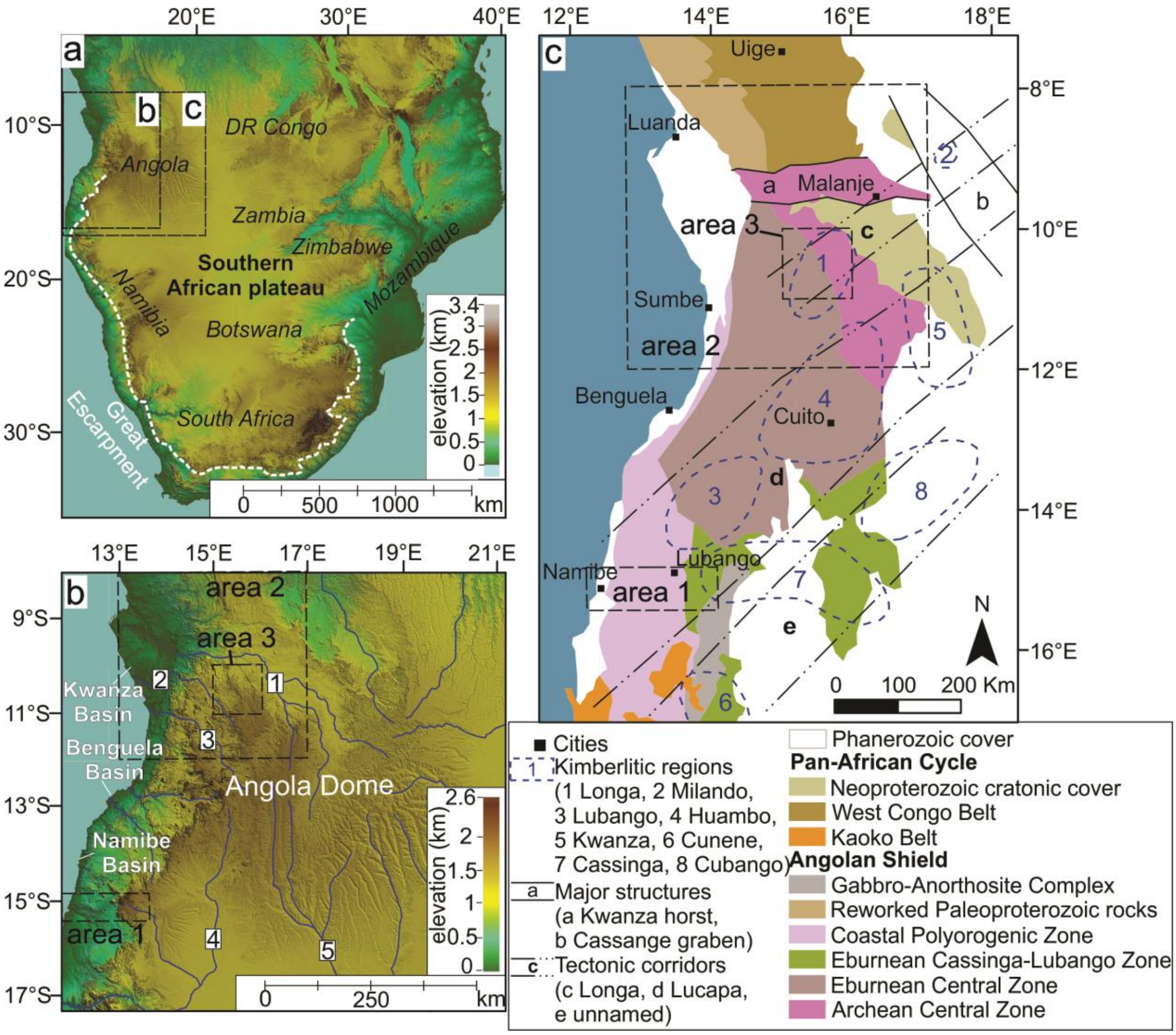

Fig. 1 a) Mapa de elevação do planalto meridional africano mostrando o escarpamento, a zona costeira e a localização das figuras b e c. b) Mapa de elevação mostrando o Domo de Angola associado a um padrão de drenagem radial (rios: 1 Kwanza; 2 Longa; 3 Cuvo; 4 Cunene; 5 Cubango) e a localização aproximada das bacias angolanas costeiras e das áreas de estudo. c) Mapa geotectônico simplificado da porção leste do Escudo Angolano, mostrando as unidades tectônicas principais, estruturas do embasamento e as áreas de estudo (modificado de (HEILBRON et al., 2008; USTINOV et al., 2018)

Detalhadamente, os objetivos específicos são:

- Acessar o padrão de denudação continental utilizando-se (U-Th-Sm)/He em apatita (AHe) e traços de fissão em apatita (AFT);
- Entender a dinâmica de evolução da paisagem utilizando-se índices morfométricos da rede de drenagem;
- Estimar possíveis temperaturas de formação e profundidades de erosão das intrusões kimberlíticas, através da caracterização petrográfica e mineralógica (difratometria de raios-X) de amostras de rocha coletadas em afloramentos;

- Estabelecer as possíveis idades das intrusões kimberlíticas utilizando-se traços de fissão em zircão por microssonda eletrônica (EP-FT).

1.4 Estrutura da Tese

Esta Tese é apresentada em mais quatro capítulos, sendo que os **Capítulos 2, 3 e 4** estão organizados na forma de artigos científicos individuais e o **Capítulo 5** apresenta uma síntese das discussões e das principais contribuições da Tese.

O **Capítulo 2** (submetido para o *International Journal of Earth Sciences*) apresenta novos dados de AHe da região da Escarpa de Chela (Fig 1b, área 1), os quais são combinados a dados prévios de AFT da mesma região para a construção de histórias térmicas pelo método inverso. Em complemento, índices morfométricos são extraídos da rede de drenagem regional e são analisados por meio de mapas e de perfis longitudinais de rios. Os dados suportam a ocorrência de denudação cenozoica diferencial entre a base e o topo da escarpa, possibilitando a proposta de um modelo genético para a Escarpa de Chela.

O **Capítulo 3** apresenta novos dados de AHe da porção noroeste do Escudo Angolano, porção noroeste do Domo de Angola (Fig. 1b, c, área 2), os quais são utilizados para a construção de histórias térmicas pelo método inverso. As novas histórias térmicas indicam eventos de denudação continental no Carbonífero – Permiano e no Cretáceo Superior, sendo o Cenozoico caracterizado por uma denudação relativamente mais limitada. Estas informações combinadas a dados de AFT e lito-estratigráficos da margem continental (Bacia do Kwanza, Fig. 1b), sugerem que o relevo regional tem se desenvolvido predominantemente no Cenozoico.

O **Capítulo 4** apresenta a caracterização petrográfica e idades EP-FT obtidas a partir de amostras de três kimberlitos (Tchiandongo, QTB-20 e K-3), localizados na região do rio Longa (Fig. 1c, área 3). Os novos dados indicam possíveis temperaturas de formação das amostras analisadas, assim como sugerem eventos de reativação térmica do Escudo Angolano no Neoproterozoico e no Paleogeno.

Referências

AL-HAJRI, Y.; WHITE, N.; FISHWICK, S. Scales of transient convective support beneath Africa. **Geology**, v. 37, n. 10, p. 883–886, 2009.

ANKA, Z. et al. The long-term evolution of the Congo deep-sea fan: A basin-wide view of the interaction between a giant submarine fan and a mature passive margin (ZaiAngo project). **Tectonophysics**, v. 470, n. 1–2, p. 42–56, 2009.

BICCA, M. M. et al. Mesozoic-Cenozoic landscape evolution of NW Mozambique recorded by apatite thermochronology. **Journal of Geodynamics**, v. 125, n. January 2018, p. 48–65, 2019.

BIERMAN, P. R.; CAFFEE, M. Slow rates of rock surface erosion and sediment production across the Namib Desert and escarpment, Southern Africa. **American Journal of Science**, v. 301, n. 4–5, p. 326–358, 2001.

BRAUN, J. et al. Rapid erosion of the Southern African Plateau as it climbs over a mantle superswell. **Journal of Geophysical Research: Solid Earth**, v. 119, p. 6093–6112, 2014.

BROWN, R. et al. Intracontinental deformation in southern Africa during the Late Cretaceous. **Journal of African Earth Sciences**, v. 100, p. 20–41, 2014.

BROWN, R. W. et al. An Early Cretaceous phase of accelarated erosion on the South-Western margin of Africa: Evidence from apatite fission track analysis and the offshore sedimentary record. **Nucl. Tracks Radiat. Meas.**, v. 17, n. 3, p. 339–350, 1990.

BROWN, R. W.; SUMMERFIELD, M. A.; GLEADOW, A. J. W. Denudational history along a transect across the Drakensberg Escarpment of southern Africa derived from apatite fission track thermochronology. **Journal of Geophysical Research**, v. 107, n. B12, p. 2350, 2002.

BUNGE, H.; GLASMACHER, U. A. Models and observations of vertical motion (MoveOn) associated with rifting to passive margins : Preface. **Gondwana Research**, v. 53, p. 1–8, 2018.

BURKE, K. The African plate. **South African Journal of Geology**, v. 99, n. 4, p. 341–409, 1996.

BURKE, K.; GUNNELL, Y. **The african erosion surface: A Continental-Scale Synthesis of Geomorphology, Tectonics, and Environmental Change over the Past 180 Million Years**. Memoir 201 ed. Boulder, Colorado: Geological Society of America, 2008.

COCKBURN, H. A. P. et al. Quantifying passive margin denudation and landscape development using a combined fission-track thermochronology and cosmogenic isotope analysis approach. **Earth and Planetary Science Letters**, v. 179, n. 3–4, p. 429–435, 2000.

COLLI, L. et al. Rapid South Atlantic spreading changes and coeval vertical motion in surrounding continents: Evidence for temporal changes of pressure-driven upper mantle flow. **Tectonics**, v. 33, n. 7, p. 1304–1321, 2014.

DE PUTTER, T.; RUFFET, G. Supergene manganese ore records 75 Myr-long Campanian to Pleistocene geodynamic evolution and weathering history of the

Central African Great Lakes Region – Tectonics drives, climate assists. **Gondwana Research**, v. 83, p. 96–117, 2020.

DE VERA, J.; GRANADO, P.; MCCLAY, K. Structural evolution of the Orange Basin gravity-driven system, offshore Namibia. **Marine and Petroleum Geology**, v. 27, n. 1, p. 223–237, 2010.

EBINGER, C. J.; SLEEP, N. Cenozoic magmatism throughout east Africa resulting from impact of a single plume. **Nature**, v. 395, n. October, p. 788–791, 1998.

FEIO, M. A evolução da escadaria de aplanações do sudoeste de Angola. **Garcia da Orla (Lisboa)**, v. 12, n. 2, p. 323–354, 1964.

FLOWERS, R. M.; SCHOENE, B. (U-Th)/He thermochronometry constraints on unroofing of the eastern Kaapvaal craton and significance for uplift of the southern African plateau. **Geology**, v. 38, n. 9, p. 827–830, 2010.

GALLAGHER, K.; BROWN, R. Denudation and uplift at passive margins: the record on the Atlantic Margin of southern Africa. **Philosophical Transactions of the Royal Society A: Mathematical, Physical and Engineering Sciences**, v. 357, n. 1753, p. 835–859, 1999.

GIULIANI, A. et al. Southwestern Africa on the burner: Pleistocene carbonatite volcanism linked to deep mantle upwelling in Angola. **Geology**, v. 45, n. 11, p. 971–974, 2017.

GREEN, P. F. et al. Post-breakup burial and exhumation of the southern margin of Africa. **Basin Research**, v. 29, n. 1, p. 1–32, 2016.

GREEN, P. F. et al. Post-breakup burial and exhumation of passive continental margins : Seven propositions to inform geodynamic models. **Gondwana Research**, v. 53, p. 58–81, 2018.

GREEN, P. F.; MACHADO, V. Pre-rift and synrift exhumation, post-rift subsidence and exhumation of the onshore Namibe Margin of Angola revealed from apatite fission track analysis. **Geological Society, London, Special Publications**, v. 438, p. 99–118, 2015.

GUILLOCHEAU, F. et al. Quantification and causes of the terrigeneous sediment budget at the scale of a continental margin: A new method applied to the Namibia-South Africa margin. **Basin Research**, v. 24, n. 1, p. 3–30, 2012.

GUILLOCHEAU, F. et al. Cenozoic Landscape Evolution in and Around the Congo Basin: Constraints from Sediments and Planation Surfaces. In: DE WIT, M. J.; GUILLOCHEAU, F.; DE WIT, M. C. J. (Eds.). . **Geology and Resource Potential of the Congo Basin**. Berlin-Heidelberg: Springer, 2015. p. 1–417.

GUILLOCHEAU, F. et al. Planation surfaces as a record of mantle dynamics: The case example of Africa. **Gondwana Research**, v. 53, p. 82–98, 2018.

GUIRAUD, R.; BOSWORTH, W. Senonian basin inversion and rejuvenation of rifting in Africa and Arabia: synthesis and implications to plate-scale tectonics. **Tectonophysics**, v. 282, n. 1–4, p. 39–82, 1997.

GURNIS, M. et al. Constraining mantle density structure using geological evidence of surface uplift rates: The case of the African Superplume. **Geochemistry, Geophysics, Geosystems**, v. 1, n. 7, 2000.

HEILBRON, M. et al. Correlation of Neoproterozoic terrane between te Ribeira Belt, SE Brazil and its African countepart: comparative tectonic evolution and open questions. **Geological Society, London, Special Publications**, v. 294, n. 1, p. 2011–237, 2008.

HOLMES, A. **Principles of Physical Geology**. Edinburgh: Thomas Nelson and Sons Limited, 1944.

JACKSON, M. P. A.; HUDEC, M. R.; HEGARTY, K. A. The great West African Tertiary coastal uplift: Fact or fiction? A perspective from the Angolan divergent margin. **Tectonics**, v. 24, n. 6, p. 1–23, 2005.

JAPSEN, P. et al. Elevated, passive continental margins: Not rift shoulders, but expressions of episodic, post-rift burial and exhumation. **Global and Planetary Change**, v. 90–91, p. 73–86, 2012.

JELSMA, H. et al. Tectonic setting of kimberlites. **LITHOS**, v. 112, p. 155–165, 2009.

JELSMA, H. A. et al. Preferential distribution along transcontinental corridors of kimberlites and related rocks of Southern Africa. **South African Journal of Geology**, v. 107, n. (1-2), p. 301–324, 2004.

KING, L. C. A Geomorphological comparison between eastern Brazil and Africa (Central and Southern). **Quarterly Journal of the Geological Society of London**, v. 112, n. 1–4, p. 445–474, 1956.

KING, L. C. Planation remnants upon high lands. **Zeitschrift für Geomorphologie**, v. 20, p. 133–148, 1976.

KLÖCKING, M. et al. A tale of two domes: Neogene to recent volcanism and dynamic uplift of northeast Brazil and southwest Africa. **Earth and Planetary Science Letters**, v. 547, p. 116464, 2020.

KOUNOV, A. et al. Denudation along the Atlantic passive margin: new insights from apatite fission-track analysis on the western coast of South Africa. **Geological Society, London, Special Publications**, v. 324, n. September, p. 287–306, 2009.

KROB, F. C. et al. Application of stratigraphic frameworks and thermochronological data on the Mesozoic SW Gondwana intraplate environment to retrieve the Paraná-Etendeka plume movement. **Gondwana Research**, v. 84, p. 81–110, 2020.

LAVIER, L. L.; STECKLER, M. S.; BRIGAUD, F. Climatic and tectonic control on the Cenozoic evolution of the West African margin. **Marine Geology**, v. 178, n. 1–4, p. 63–80, 2001.

LITHGOW-BERTELLONI, C.; SILVER, P. Dynamic topography, plate driving forces and the African superswell. **Nature**, v. 395, n. September, p. 345–348, 1998.

MACGREGOR, D. S. Late Cretaceous – Cenozoic sediment and turbidite reservoir supply to South Atlantic margins. **Geological Society, London, Special Publications**, v. 369, p. 109–128, 2013.

MARGIRIER, A. et al. Climate control on Early Cenozoic denudation of the Namibian margin as deduced from new thermochronological constraints. **Earth and Planetary Science Letters**, v. 527, 2019.

MARSH, J. S.; SWART, R. The Bero Volcanic Complex: Extension of the Paraná-Etendeka Igneous Province into SW Angola. **Journal of Volcanology and Geothermal Research**, 2016.

MAYSTRENKO, Y. P. et al. Structural features of the Southwest African continental margin according to results of lithosphere-scale 3D gravity and thermal modelling. **Tectonophysics**, v. 604, p. 104–121, 2013.

MCCOURT, S. et al. New U-Pb SHRIMP ages from the Lubango region, SW Angola: insights into the Palaeoproterozoic evolution of the Angolan Shield, southern Congo Craton, Africa. **Journal of the Geological Society**, v. 170, n. 2, p. 353–363, 2013.

MCMILLAN, I. K. Foraminiferally defined biostratigraphic episodes and sedimentation pattern of the Cretaceous drift succession (Early Barremian to Late Maastrichtian) in seven basins on the South African and southern Namibian continental margin. **South African Journal of Science**, v. 99, n. 11–12, p. 537–576, 2003.

MOORE, A.; BLENKINSOP, T.; COTTERILL, F. Southern African topography and erosion history: Plumes or plate tectonics? **Terra Nova**, v. 21, n. 4, p. 310–315, 2009.

NYBLADE, A. A.; ROBINSON, S. W. The African Superswell. **Geophysical Research Letters**, v. 21, n. 9, p. 765–768, 1994.

O'CONNOR, J. et al. Hotspot tracks in the South Atlantic located above bands of fast flowing asthenosphere driven by waning pulsations from the African LLSVP. **Gondwana Research**, v. 53, p. 197–208, 2018.

PARTRIDGE, T. C.; MAUD, R. R. Geomorphic evolution of southern Africa since the Mesozoic. **South African Journal of Geology**, v. 90, n. 2, p. 179–208, 1987.

PATON, D. A. et al. Insights into the Petroleum System Evolution of the southern Orange Basin, South Africa. **South African Journal of Geology**, v. 110, n. 2–3, p. 261–274, 2007.

RAAB, M. J. et al. Late Cretaceous reactivation of major crustal shear zones in northern Namibia: Constraints from apatite fission track analysis. **Tectonophysics**, v. 349, n. 1–4, p. 75–92, 2002a.

RAAB, M. J. et al. Late Cretaceous reactivation of major crustal shear zones in northern Namibia: Constraints from apatite fission track analysis. **Tectonophysics**, v. 349, n. 1–4, p. 75–92, 2002b.

RENNE, P. R. et al. Age of Etendeka flood volcanism and associated intrusions in southwestern Africa. **Geology**, v. 24, n. 7, p. 659–662, 1996.

RITSEMA, J.; VAN HEIJST, H. J.; WOODHOUSE, J. H. Complex shear velocity structure imaged beneath {A}frica and {I}celand. **Science**, v. 286, n. 5446, p. 1925–1928, 1999.

ROBERTS, G. G.; WHITE, N. Estimating uplift rate histories from river profiles using African examples. **Journal of Geophysical Research: Solid Earth**, v. 115, n. 2, p. 1–24, 2010.

ROUBY, D. et al. Sediment supply to the Orange sedimentary system over the last 150 My: An evaluation from sedimentation/denudation balance. **Marine and Petroleum Geology**, v. 26, n. 6, p. 782–794, 2009.

SAID, A. et al. Cretaceous-Cenozoic sedimentary budgets of the Southern Mozambique Basin: Implications for uplift history of the South African Plateau. **Journal of African Earth Sciences**, v. 109, p. 1–10, 2015.

SÉRANNE, M.; ANKA, Z. South Atlantic continental margins of Africa: A comparison of the tectonic vs climate interplay on the evolution of equatorial west Africa and SW Africa margins. **Journal of African Earth Sciences**, v. 43, n. 1–3, p. 283–300, 2005.

SILVA, B. V. et al. Evolution of the Southwestern Angolan Margin: episodic burial and exhumation is more realistic than long-term denudation. **International Journal of Earth Sciences**, v. 108, n. 1, p. 89–113, 2019.

STANLEY, J. R.; FLOWERS, R. M. Dating kimberlite emplacement with zircon and perovskite (U-Th)/He geochronology. **Geochemistry Geophysics Geosystems**, v. 17, p. 4517–4533, 2016.

STANLEY, J. R.; FLOWERS, R. M.; BELL, D. B. Erosion patterns and mantle sources of topographic change across the southern African Plateau derived from the shallow and deep records of kimberlites. **Geochemistry, Geophysics, Geosystems**, v. 16, p. 1–22, 2015.

STANLEY, J. R.; FLOWERS, R. M.; BELL, D. R. Kimberlite (U-Th)/He dating links surface erosion with lithospheric heating, thinning, and metasomatism in the southern African Plateau. **Geology**, v. 41, n. 12, p. 1243–1246, 2013.

TINKER, J.; DE WIT, M.; BROWN, R. Mesozoic exhumation of the southern Cape, South Africa, quantified using apatite fission track thermochronology. **Tectonophysics**, v. 455, n. 1–4, p. 77–93, 2008.

USTINOV, V. N. et al. Kimberlites distribution in Angola and prospective areas for new discoveries. **Mineralogy and Petrology**, v. 112, p. 383–396, 2018.

VAN DER WATEREN, F. Late Neogene passive margin denudation historyâ□”cosmogenic isotope measurements from the central Namib desert. **Global and Planetary Change**, v. 30, p. 271–307, 2001.

WALKER, R. T. et al. Rapid mantle-driven uplift along the Angolan margin in the late Quaternary. **Nature Geoscience**, v. 9, n. 12, p. 909–914, 14 dez. 2016.

WILDMAN, M. et al. Post break-up tectonic inversion across the southwestern cape of South Africa: New insights from apatite and zircon fission track thermochronometry. **Tectonophysics**, v. 654, p. 30–55, 2015.

WILDMAN, M. et al. The chronology and tectonic style of landscape evolution along the elevated Atlantic continental margin of South Africa resolved by joint apatite fission track and (U-Th-Sm)/He thermochronology. **Tectonics**, v. 35, n. 3, p. 511–545, 2016.

CAPÍTULO 2 - THE CHELA ESCARPMENT AS THE RESULT OF THE DISSECTION AT THE ANGOLA DOME FLANK, SOUTHWESTERN MARGIN OF AFRICA: INSIGHTS FROM THERMOCHRONOLOGY AND DRAINAGE NETWORK MORPHOMETRY

1 INTRODUCTION

Southern Africa presents one of the most enigmatic landscapes in the world, characterized by a high, low-relief inland plateau (above ~ 1000 m) that is separated from the low-lying coastal region by a prominent escarpment (the Great Escarpment) encircling almost all the plateau perimeter (LITHGOW-BERTELLONI; SILVER, 1998; MOORE; BLENKINSOP; COTTERILL, 2009; NYBLADE; SLEEP, 2003; VAN DER BEEK et al., 2002) (Fig. 1a). The plateau interior is also dominated by a conspicuous basin and swell topography, characterized by the occurrence of long wavelength domes (up to over 1000 km) standing out above the average altitude of the plateau (AL-HAJRI; WHITE; FISHWICK, 2009; GUILLOCHEAU et al., 2018; HOLMES, 1944). Despite more than 100 years of research, there is little consensus among researchers about the age and mechanisms controlling the Southern Africa topography and relief (BABY et al., 2020; BURKE; GUNNELL, 2008; COCKBURN et al., 2000; FLOWERS; SCHOENE, 2010; GILCHRIST; KOOI; BEAUMONT, 1994; GREEN et al., 2016; GREEN; MACHADO, 2015; GUILLOCHEAU et al., 2018; LITHGOW-BERTELLONI; SILVER, 1998; PARTRIDGE; MAUD, 1987; PICART et al., 2020; STANLEY; FLOWERS; BELL, 2015; VAN DER BEEK et al., 2002; WILDMAN et al., 2016).

Regional thermochronology data acquired mainly around the southern African margin, support that the larger pulses of continental denudation took place at ~ 160 – 120 Ma and at ~ 90 – 70 Ma (BICCA et al., 2019; BROWN et al., 2014, 1990; BROWN, 2002; COCKBURN et al., 2000; FLOWERS; SCHOENE, 2010; GALLAGHER; BROWN, 1999; GREEN et al., 2016; GREEN; MACHADO, 2015; JACKSON; HUDEC; HEGARTY, 2005; KOUNOV et al., 2009; KROB et al., 2020a; MARGIRIER et al., 2019; RAAB et al., 2002; SILVA et al., 2019; STANLEY, 2015; TINKER; DE WIT; BROWN, 2008; WILDMAN et al., 2015, 2016). These denudation events overlap in time with the South Atlantic rifting (BUMBY; GUIRAUD, 2005), the emplacement of the Paraná-Etendeka Large Igneous Province (LIP) (MARZOLI et al., 1999; RENNE et al., 1996), episodes of intra-plate kimberlite volcanism (JELSMA et al., 2004), and major continental uplifts attributed to lithospheric updoming, tilting, and faulting (BRAUN et al., 2014; KROB et al., 2020b; SALOMON; PASSCHIER; KOEHN, 2017). Following the rationale that the main phases of elevation gain and relief formation are contemporaneous with the main phases of tectonism, magmatism, uplift, and continental denudation, some researchers argue that in many parts of the Southern Africa, the relief and topography were mostly developed during Mesozoic times, despite these works do not preclude the possibility for a minor contribution occurring in the Cenozoic (COCKBURN et al., 2000; DE WIT, 1999; FLOWERS; SCHOENE, 2010). On the other hand, some thermochronological studies in addition to the Mesozoic denudation events, also interpret substantial continental denudation arising in the Cenozoic (GREEN et al., 2016; GREEN; MACHADO, 2015; JACKSON; HUDEC; HEGARTY, 2005; MARGIRIER et al., 2019; SILVA et al., 2019), and most of these proposed episodes coevally overlap with the onset of continental uplifts at ~ 40 – 20 Ma, which have been often interpreted as the result of compressional tectonics induced by far-field stresses (COLLI et al., 2014; GUIRAUD; BUTA-NETO; QUESNE, 2010; JAPSEN et al., 2012), or underlying mantle upwelling and/or convection acting beneath the African plate (AL-HAJRI; WHITE; FISHWICK, 2009; BURKE, 1996; BURKE; GUNNELL, 2008; CELLI et al., 2020; FISHWICK; BASTOW, 2011; GUILLOCHEAU et al., 2018; KLÖCKING et al., 2020; LITHGOW-BERTELLONI; SILVER, 1998; MVONDO; DAUTEUIL; GUILLOCHEAU, 2011; WALKER et al., 2016). Additionally, some researchers argue that the southern African plateau is dominated by an extensive erosion surface (etchplain) known as the African surface (BURKE; GUNNELL, 2008; KING, 1976; PARTRIDGE; MAUD, 1987). Recently, (GUILLOCHEAU et al., 2018) interpret that this surface is deformed following the basin and swell topography, and they propose that such deformations and hence the central Africa topography (the authors include the northern portion of the southern African plateau in this central area) have been developed essentially since ~ 40 – 20 Ma. In this context, but particularly focusing the discussion regarding the first-order relief of southern Africa (i.e., the configuration coastal region, Great Escarpment, and inland plateau), (BURKE; GUNNELL, 2008) claim that the Great Escarpment has been developed by backward erosion affecting the flanks of major domes uplifted since ~ 30 Ma.

The southwestern margin of Angola consists in a natural laboratory for the understanding of how large-scale deep Earth (e.g. mantle upwelling, tectonics) and climate-driven (e.g. denudation) processes interact to create the regional topography and relief. This margin segment lies at the southwestern half of a very long-wavelength (~1000 km diameter) swell refered as “Bié” (AL-HAJRI; WHITE; FISHWICK, 2009; FISHWICK; BASTOW, 2011) or “Angola” Dome (CELLI et al., 2020) (Fig. 1 a,b), and this margin segment contains the Chela Escarpment, one of the most steep stretches of the African Great Escarpment (showing up to ~ 1500 m of relief from base to summit) that separates the inland plateau from the coastal region (Fig 2a). Pioneering work based on correlations between planation surfaces and sedimentary strata onshore, suggest that the region below the present-day Chela Escarpment undergone a denudation phase in the Miocene (FEIO, 1964). In agreement, (GREEN; MACHADO, 2015) combine stratigraphic information onshore with estimates of rock paleotemperatures derived from apatite fission-track (AFT) data, and interpret that the Chela Escarpment has been shaped by a denudation pulse since ~ 45 Ma.

In this work we provide new thermochronological and river morphometric data, which strengthen the hyphotesis of the previous work that the Chela Escarpment is a Late Cenozoic landform. First, we performed new inverse thermal history modelling by combining new apatite (U-Th-Sm)/He (AHe) data with published AFT data, in order to refine the long-term denudation pattern across the escarp. Second, we performed morphometric analysis to access how rivers have responded to the balance between uplift and erosion, an approach that has been used to interpret the tendency of the landscape evolution (KIRBY; WHIPPLE, 2012; WILLETT et al., 2014). Therefore, we used the integrated data to ultimately access the interplay between denudation processes and the tectonic/mantle forcing in shaping the landscape of the southwestern Angolan margin.

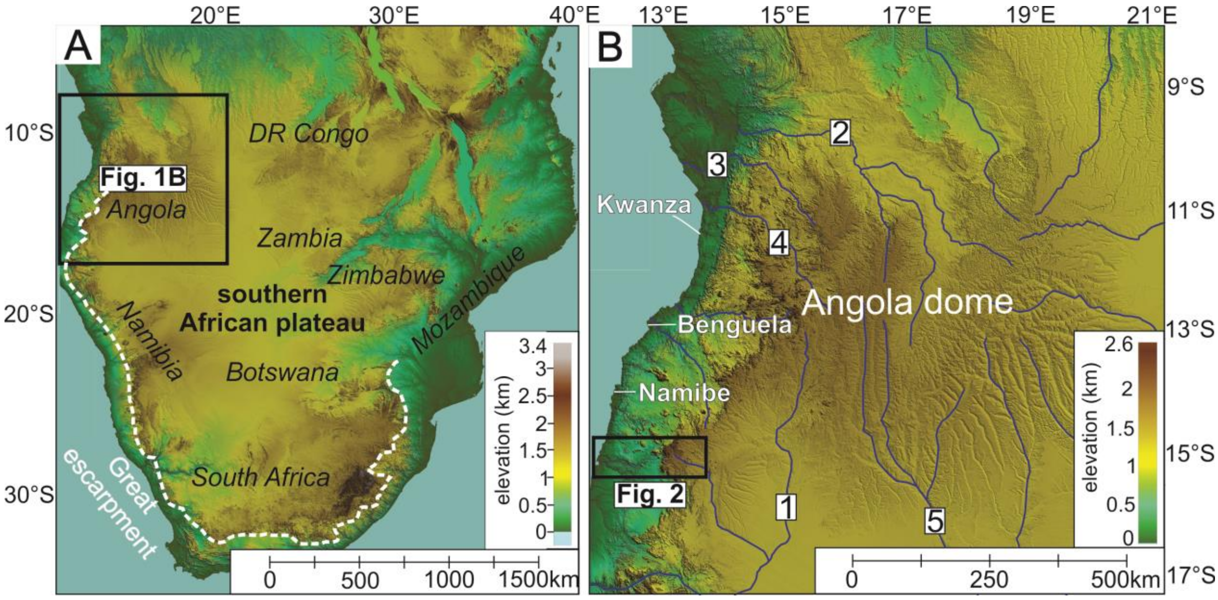

Fig. 1 Elevation maps showing the regional geomorphic context: A) The southern African plateau showing the Great Escarpment and the location of the Angola Dome; B) Detail of the Angola Dome showing important Angolan rivers (1 - Cunene, 2 - Kwanza, 3 - Longa, 4 - Cuvo, 5 - Cubango), the marginal basins, and the location of the study area represented by the Fig. 2 rectangle

2 GEOLOGIC AND GEOMORPHIC SETTING

The Angola Dome consists in a macro-geomorphic landform with a roughly circular shape, radial drainage pattern (ROBERTS; WHITE, 2010) (Fig. 1b), positive free-air gravity anomalies coupled with low shear-wave velocity anomalies underneath (AL-HAJRI; WHITE; FISHWICK, 2009), stratigraphic evidence of Cenozoic uplift (KLÖCKING et al., 2020), and also marks an upward deformation of the African surface (GUILLOCHEAU et al., 2018). The rivers that drain the Angola Dome have tipically upward convex longitudinal profiles, defined by knickpoints that mostly do not coincide with changes on lithology, probably reflecting recent uplift and a transient landscape (GUIRAUD; BUTA-NETO; QUESNE, 2010; LETURMY; LUCAZEAU; BRIGAUD, 2003; ROBERTS; WHITE, 2010). These aspects together indicate that the Angola Dome has been formed, at least in part, by dynamic uplift, although its associated mechanisms within the underlying mantle remains controversial (GIULIANI et al., 2017; KLÖCKING et al., 2020).

The southwestern Angolan margin, at the latitude of the Chela Escarpment, encompasses four coast-parallel geomorphic domains (DINIZ, 1973) (Fig. 2a), also showing distinct geological features (Fig. 2b). Far west, the low relief Coastal Zone forms a 10-150 km wide strip with elevations of up 200 m, characterized by broad and narrow river valleys, cliffs up 100 m, and marine terraces (BEERNAERT, 1997; DINIZ, 1973; FEIO, 1964; HUNTLEY, 2019). The Coastal Zone is most underlain by sedimentary rocks of the Namibe Basin that also unconformably overlain Archean to Paleoproterozoic gneisses and granites of the Angolan Shield (Congo Craton) (DE WAELE; JOHNSON; PISAREVSKY, 2008). Remnants of the Early Cretaceous Bero volcanics (correlative to Etendeka) outcrop at the eastern edge of the Basin (Fig. 2b) and overlain an erosion surface that truncates both the Jurassic-Cretaceous pre-rift rocks and the Precambrian basement rocks (GINDRE-CHANU et al., 2016; MARSH; SWART, 2016). These volcanic rocks are locally carved by valleys infilled with Albian conglomerates, and are also covered by a transgressional marine sequence including Aptian evaporites (MARSH; SWART, 2016), which display diagenetic features consistent with its burial (by up to 2 km) and later exhumation to the surface (GINDRE-CHANU et al., 2015).

Another notable feature is a Late Cretaceous erosion surface cutting across the Bero volcanics and the Precambrian basement rocks, and overlain by marine Maastrichtian and younger (Cenozoic) sedimentary cover (FEIO, 1964; GREEN; MACHADO, 2015; MARSH; SWART, 2016) (Fig. 2c). Thus, at least a post-Maastrichtian exhumation event is required to expose these marine rocks at the surface, which agree with the occurrence of Cretaceous to Pleistocene sedimentary strata elevated up to hundreds of meters above the present-day sea level, providing evidence for the Cenozoic uplift of the margin (GIRESSE; HOANG; KOUYOUMONTZAKIS, 1984; GUIRAUD; BUTA-NETO; QUESNE, 2010). Those geological aspects provide evidence that the southwestern Angolan margin has evolved from burial and exhumation events, which may have affected the basement further inland as suggested, for example, by the projection of the Maastrichtian surface and the overlying strata to the inland (FEIO, 1964) (Fig. 2c), as well as by AFT and AHe thermal histories (GREEN; MACHADO, 2015; SILVA et al., 2019).

To the east of the Coastal Zone, the Escarpment Zone is characterized by low relief plateaus reaching mean elevations between 400 and 600 m (HUNTLEY, 2019). This zone encompasses a 100 km wide pediment defined as the “Serra-Abaixo” erosion surface (correlative to the Post-African surface of (KING, 1962) that truncates the Maastrichtian one to the west, indicating that the former is younger in age (FEIO, 1964) (Fig. 2c).

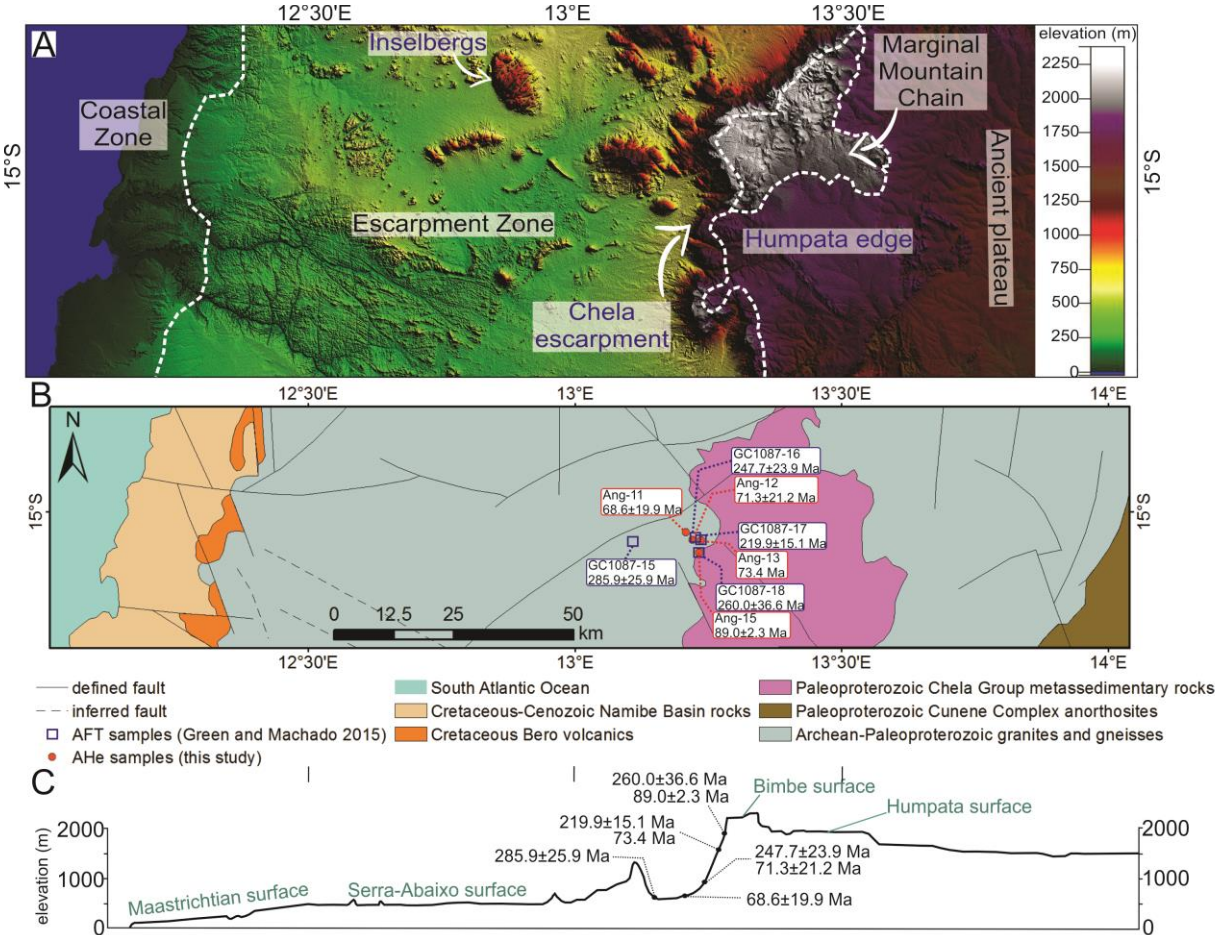

Fig. 2 a) Elevation map from the Chela Escarpment region showing the geomorphological domains based on (HUNTLEY, 2019). b) Simplified regional geological map showing the main units and faults based on (ARAÚJO; GUIMARÃES, 1992), and samples utilised in this study. c) W-E topographic profile at 15 °S showing the erosion surfaces according to (FEIO, 1964). The analised samples are also projected over this profile

At the eastern boundary of this Zone, the Chela Escarpment reaches about 1800 m of elevation and forms a conspicuous feature where recent erosion and rockfalls can be observed (LOPES et al., 2016). Whereas the small plateaus are underlying by Archean and Paleoproterozoic gneisses and granites, the Chela Escarpment is supported at its top by 600 m of Palaeoproterozoic quartzites from the volcano-sedimentary Chela Group (PEREIRA et al., 2011) (Fig. 2a,b), suggesting that litology may have played a role on the relief development.

To the east, the Escarpment Zone transitions to the Marginal Mountain Chain Zone comprising a rugged-relief highland domain that reaches over 2,300 m at its western edge (BEERNAERT, 1997; HUNTLEY, 2019; MARQUES, 1977). Finally, this mountainous domain gives way eastwards and southwards to the low-relief Ancient Plateau that in the study area is named Humpata Plateau (LOPES et al., 2016) (Fig.

2a). The Humpata Plateau is mostly sustained by Chela Group rocks (FEIO, 1964; LOPES et al., 2016) and is characterized by two steps of flat surfaces: the Bimbe surface (with mean elevations of 2300 m) and the Humpata surface (that reaches elevations of 2000 m) (FEIO, 1964) (Fig. 2c). The Humpata surface is correlative with the African surface (BURKE; GUNNELL, 2008; GUILLOCHEAU et al., 2018; KING, 1962), which was subjected to deep lateritic weathering that implies periods of relatively humid climate and low denudation during the Palaeocene and Eocene times (DE PUTTER; RUFFET, 2020; MACGREGOR, 2013). The preservation of these lateritic profiles, as well as remnants of Cenozoic sedimentary cover of the Kalahari Group along the Cunene river catchment (HOUBEN et al., 2020) (Fig. 1b) indicate that low Cenozoic denudation has prevailed at least in parts of the inland plateau.

3 SAMPLING AND METHODS

3.1 Apatite (U-Th-Sm)/He Analysis

Four basement samples, collected in outcrops from base to top of the Chela Escarpment, were analysed for AHe (Fig. 2c). Samples consist of Eburnean granites and Chela Group quartzites ranging between 777 m and 1,682 m of elevation, collected close to samples previoulsly analysed for AFT (GREEN; MACHADO, 2015). The goal was to perform inverse thermal modelling combining the new AHe data with available AFT data in order to identify possible contrasting denudation patterns across the escarp.

In total, fifteen idiomorphic apatite grains were analysed for AHe. The grains were obtained by rock crushing, sieving, panning, magnetic separation, and heavy liquid separation, and then the idiomorphic ones, without visible fractures or inclusions, were separated under a binocular glass for AHe analysis. The selected grains were measured in length and width under a stereomicroscope (Zeiss Discovery V8) coupled with the AxioVision software. Afterthat, the apatite crystals were placed into platinum tubes that were introduced in a noble gas spectrometer (Helix SFT) for ^{4}He extraction. First, the platinum tubes were heated by a laser beam (Fusions 960, Photon Machines) that fully extracted the ^{4}He gas of the crystals. The gas was then purified under a high vacuum pressure (~10^{-9} mbar) by using getters and a cryogenics system. The purified gas was ionized into the spectrometer by a Nier-type ion source and the ^{4}He concentrations were determined by using a Faraday cup.

Apatite grains were then fully dissolved over a hot plate (~110°C) in a spiked solution containing certified amounts of ^{235}U, ^{230}Th, and ^{149}Sm. The solution was introduced into an Inductively Coupled Plasma Mass Spectrometer (ICP-MS, Element 2) for U, Th, and Sm determinations. Single-grain AHe ages were determined following the equation of (MEESTERS; DUNAI, 2005). Further details of the analytical procedure are described by (SIQUEIRA-RIBEIRO et al., 2019). All the steps were carried out at the Noble Gas laboratory of the Department of Geology, São Paulo State University (Unesp), Rio Claro, Brazil.

3.2 Inverse Thermal History Modelling

The thermal history of the Chela Escarpment region was determined by time-temperature simulations (t-T paths) generated by the QTQt software (GALLAGHER, 2012) that makes use of the Bayesian Trans-dimensional Markov Chain Monte Carlo (MCMC) algorithm (GALLAGHER et al., 2009). The inversion approach was used, in which a suite of thermal simulations generated by QTQt tries to reproduce individually and simultaneously the single-grain AHe data (age, eU, grain morphology and size) and the AFT data (age, track length, kinetic parameter) for each sample. The AFT data utilized here are published in (GREEN; MACHADO, 2015) (samples GC1087-15, -16, -17, and -18). The reproducibility of track length distributions (TLD) and mean track length (MTL) are found in the Fig. 3. The integrated modelling combining AFT and AHe data usually improves the robustness of the thermal histories models in comparison to such ones derived from a single thermochronometer data (STOCKLI, 2005). The multi-kinetic annealing model of (KETCHAM et al., 2007) for the AFT data and the radiation damage model of (GAUTHERON et al., 2009) for the AHe data were used. The t-T paths were interpreted in terms of their weighted mean within 95% confidence limit intervals (GALLAGHER, 2012).

The t-T initial constraint applied to all models was 70 ± 70°C at 300 ± 20 Ma to account for the presence of the basement rocks at an upper crustal level during the onset of the Karoo Supergroup deposition (Fig. 3). This is supported by paleogeography reconstructions showing that the entire region underwent glacial erosion in the Carboniferous-Permian (ISBELL et al., 2012) that shaped an erosion surface currently preserved in parts of the Ancient Plateau (DE WIT, 2007; GUILLOCHEAU et al., 2018). In addition, fluvio-glacial rocks of the Dwyka Formation (Karoo Sequence) are exposed by the Cunene river further southeast of the study area (HIPONDOKA, 2005), and Karoo-correlated rocks rest over a basement unconformity in the onshore Namibe Basin to the west (GINDRE-CHANU et al., 2015, 2016). Another imposed constraint was a current surface temperature of 20° ± 5°C for the basement.

3.3 Morphometric Analysis of River Profiles

River profile analysis has been extensively used for extracting valuable information regarding tectonic, mantle, and climate driven forcing of the landscape (ROBERTS; WHITE, 2010) as the topography of a river profile results from the interplay between uplift (associated to rock uplift and/or base-level fall) and fluvial incision (WHIPPLE; TUCKER, 1999). Such processes led to variations in the river gradient (slope) that are positively correlated with variations in incision rate into river channel (CASTILLO; MUÑOZ-SALINAS; FERRARI, 2014); however, other parameters related to drainage area (used as a proxy for discharge) also influence the competence of a river in eroding its substratum besides its topographic gradient (MUDD et al., 2018). Therefore, gradients along a river channel in equilibrium commonly show a negative relationship with upstream drainage area (SHALER, 1899), which is decribed by a stream power law equation (FLINT, 1974):

$$S = K_s A^{-\theta}$$

where S is the channel local slope, A is the upstream drainage area, K_s is the channel steepness index, and Ɵ is the concavity index that reflects the rate at which a channel slope decreases as drainage area increases downstream (KIRBY; WHIPPLE, 2012; MUDD et al., 2018). Whereas Ɵ is an intrinsic metric of the river, K_s is sensitive to variations on lithology, rock uplift and erosion rates, as demonstrated by a growing set of research (WOBUS et al., 2006), and in such wise, it is a common routine normalise K_s (K_{sn}) through a fixed concavity index ($Ɵ_{ref}$) to allow comparisons of K_{sn} values among rivers and basins of different sizes and shapes (KIRBY; WHIPPLE, 2012; MILLER et al., 2013; WOBUS et al., 2006).

K_{sn} values are acquired by the continuous measurements of S and A along the stream length. S data may be directly extracted from Digital Elevation Models (DEMs), however, DEMs may contain inconvenient noise and imprecisions, propagating error in S and hence in K_{sn} values (PERRON; ROYDEN, 2013; WOBUS et al., 2006). Instead, in the integral or Chi (χ) analysis, the horizontal coordinate of the river long profile (x) is converted in the χ variable through an integration from the base level (x_b) towards upstream, which is made via modifications of the stream-power equation (PERRON; ROYDEN, 2013). The χ parameter shows a linear relationship with elevation (z) at the x position according to the following equation,

$$z(x) = z(x_b) + (\frac{U}{K{A_0}^m})^{\frac{1}{n}}\chi$$

rewrite as,

$$\chi = \int_{x_b}^{x} (\frac{A_0}{A(x)})^{\theta} dx$$

Where K is the erodibility coefficient, A_0 is a reference drainage area (commonly A_0 = 1), U is the rock uplift rate, and m and n are erosional constants where ϴ = m/n. Therefore, steady state river profiles appear as straight lines in χ - z plots or χ plots (PERRON; ROYDEN, 2013), provided that all the analised rivers share the same base level and a proper ϴ value is used. A best-fit ϴ may be obtained through testing which ϴ value best linearizes the river profiles in the χ plots (MUDD et al., 2018; PERRON; ROYDEN, 2013; WANG et al., 2017). K_{sn} metrics correspond to the slope of the χ – z regression line (for A_0 = 1), thus, changes in slope along the profile in the χ plot indicate variations in K_{sn} values.

K_{sn} and χ maps of drainage networks have been also utilised to access the tendency of the landscape evolution (BEESON; MCCOY; KEEN-ZEBERT, 2017; DE SOUZA et al., 2019; STRUTH et al., 2017). Particularly, as K_{sn} usually correlates positively with independent estimates of incision/erosion rates at the catchment scale (KIRBY; WHIPPLE, 2012), K_{sn} maps are usefull in proving a planform view of the variations in the fluvial incision rates, whereas χ maps might indicate the stationary (steady state) or mobile nature of drainage divides (WILLETT et al., 2014). (WILLETT et al., 2014) propose that between basins sharing relatively homogeneous uplift rates, bedrock erodibility, and climate, constrasting cross-divide χ values suggest erosional disequilibrium, and hence the divide tends to migrate towards the side characterized by higher χ values. However, under conditions of spatially variable uplift rate and bedrock erodibility, χ maps may not accuratelly indicate the current migration direction of drainage divides, or these maps may be usefull in indicating at least a long-term, future trend of divide mobility (FORTE; WHIPPLE, 2018; WHIPPLE et al., 2017). A good strategy for interpretation of the landscape dynamics is to combine distinct metrics and testing them at regions where independent estimates of erosion rates are also available.

Here, morphometric parameters were obtained from a 30 m fine resolution DEM (NASADEM, available in the NASA EarthData Search at https://search.earthdata.nasa.gov/search?q=nasadem) and calculated by the Topographic Analysis Kit (TAK) (FORTE; WHIPPLE, 2019) within TopoToolbox 2 (SCHWANGHART; SCHERLER, 2014). For determination of the best-fit Θ_{ref}, we first used the mnoptim tool that utilises Bayesian optimization to find a minimum (i.e., an optimal Θ_{ref} value) of an objective function whose Θ is the variable. The flatness of the function around the minimum defined a range of suitable Θ_{ref} values between ~ 0.15 and 0.5, thus, χ values were determined based on a Θ_{ref} of 0.5, taking into consideration that it was previously utilised for the region based on Monte Carlo simulations (ROBERTS; WHITE, 2010). Afterthat, K_{sn} values were calculated by derivatives from the χ – z correlations (FORTE; WHIPPLE, 2019). The morphometric data is presented as longitudinal river profiles and χ plots, and K_{sn} and χ maps.

4 RESULTS AND DISCUSSION

4.1 Assessment of the Apatite (U-Th-Sm)/He Ages

Sample Ang-12 yielded single-grain AHe ages from 98.3 ± 3.2 to 40.6 ± 1.6 Ma that show moderate intra-sample dispersion (29.6 %) (Tab. 1). This sample also does not show a clear relationship between ages and eU concentrations (6.8 to 30.3 ppm) or with R_s values, i.e., the contribution of radiation damage or grain size for the scatter in ages is not evident (FLOWERS; KELLEY, 2011). However, differences in single-grain eU concentrations and Th/U ratios (Tab. 1) may indicate chemical heterogeneities between grains (GAUTHERON et al., 2013) that might control helium diffusion, and ultimately, increase the scatter in ages depending on the cooling history of the sample (FITZGERALD et al., 2006). Similarly, sample Ang-15 yielded single-grain AHe ages between 91.4 ± 3.4 to 84.8 ± 3.3 Ma characterized by very low dispersion (< 4%) (Tab. 1). This in association with the moderate eU concentrations of their grains (13.3 to 45.4 ppm) may reflect rapid cooling through the Helium Partial Retention Zone (AHePRZ, ~40–80°C) (FARLEY, 2002), also indicating that the cooling rate or residence time within AHePRZ may be an important source for age dispersion (FITZGERALD et al., 2006), although more single-grain data would be helpful to test this point of view. For comparison, the age dispersion of sample Ang-15 is lower than that obtained from measurements in the Durango age standard (9 %) (Tab. 1).

Samples Ang-11 and Ang-13 provided too few grains for a reasonable assessment of AHe age dispersion. However, these samples yielded single-grain ages that are within the range of ages obtained for Ang-12 and Ang-15 (Tab. 1), indicating that the entire dataset are broadly representative of the regional thermal history.

Tab. 1 - AHe data from the Chela Escarpment, southwestern Angolan margin

sample	grain	^{4}He (ncc)	^{238}U (ppm)	^{235}U (ppm)	^{232}Th (ppm)	^{147}Sm (ppm)	Th/U	eU[a] (ppm)	L[b] (µm)	W[c] (µm)	Rs[d] (µm)	T[e]	Raw Age ± UC[f] (Ma)	F_T[g]	Corrected Age ± UC[f] (Ma)
Ang-11	1	248.3	14.5	0.1	40.7	46.9	2.8	24.2	237.2	170.9	94.2	2	82.7 ± 2.0	0.84	98.5 ± 2.4
Ang-11	2	79.0	7.0	0.1	19.4	29.8	2.8	11.7	298.3	173.9	101.0	2	54.5 ± 1.4	0.82	66.5 ± 1.8
													29.1%		
Ang-12	1	222.3	27.3	0.2	11.74	74.2	0.4	30.3	148.1	123.1	65.2	1	59.3 ± 2.0	0.77	77.0 ± 2.6
Ang-12	2	116.9	9.3	0.1	6.3	43.5	0.7	10.8	215.7	142.4	80.3	2	85.9 ± 3.2	0.81	105.6 ± 3.8
Ang-12	3*	2340.2	32.3	0.2	181.2	557.8	5.6	75.1	214.2	140.7	79.5	2	239.0 ± 17.0	0.81	265.6 ± 19.0
Ang-12	4	172.9	12.1	0.1	8.2	37.2	0.7	14.1	242.8	123.7	73.9	2	98.3 ± 3.2	0.80	123.4 ± 4.0
Ang-12	5	137.6	15.8	0.1	12.2	71.4	0.8	18.8	220.1	148.4	83.3	2	58.5 ± 2.1	0.82	71.3 ± 2.6
Ang-12	6	77.7	7.7	0.1	8.0	31.6	1.0	9.7	218.7	125.9	73.3	2	64.3 ± 2.1	0.80	80.8 ± 2.6
Ang-12	7	35.1	5.7	0.0	4.3	40.4	0.8	6.8	188.4	136.1	75.0	1	40.6 ± 1.6	0.81	50.2 ± 2.0
Ang-12	8	242.0	17.6	0.1	13.3	78.1	0.8	20.9	171.7	132.5	71.7	2	92.4 ± 3.3	0.79	116.8 ± 4.2
													29.6%		
Ang-13	1	287.8	20.5	0.1	40.8	-	2.0	30.3	259.6	137.4	81.5	1	73.4 ± 4.2	0.85	86.4 ± 5.0
Ang-15	1	238.8	10.5	0.1	42.0	120.7	4.0	20.5	191.6	123.1	69.9	2	91.4 ± 3.4	0.79	116.3 ± 4.4
Ang-15	2	481.2	37.2	0.3	33.6	22.3	0.9	45.4	241.0	150.4	86.0	2	86.7 ± 1.4	0.83	105.0 ± 1.8
Ang-15	3	151.6	7.0	0.1	26.6	81.1	3.8	13.3	233.4	133.1	77.7	2	88.9 ± 3.4	0.81	110.2 ± 4.2
Ang-15	4	186.2	10.8	0.8	22.9	108.9	2.1	16.2	171.7	143.1	75.8	2	84.8 ± 3.3	0.80	105.8 ± 4.1
													3.2%		
		(cc)	(ng)	(ng)	(ng)	(ng)									
Durango	DUR-1-4-18	3.2E-09	0.16	0.0011	3.07	0.32		—	—	—	—	—	29.7 ± 0.6	—	—
Durango	DUR-2-4-18	2.8E-09	0.12	0.0009	2.69	0.30		—	—	—	—	—	30.1 ± 0.6	—	—
Durango	DUR-3-4-18	5.1E-09	0.22	0.0016	4.15	0.44		—	—	—	—	—	34.8 ± 0.6	—	—
													9.0%		

[a] Effective uranium calculated as [U ppm] + (0.235 * [Th ppm]) (SHUSTER; FLOWERS; FARLEY, 2006). [b] Length and [c] width of the crystal or crystal fragment. [d] Radius of a sphere with the equivalent surface area-to-volume ratio as cylindrical crystal (MEESTERS; DUNAI, 2002), Rs = (3*(RL))/(2*(R+L)) where R = W/2. [e] Number of terminations (tips) identified on crystals, 0 = no termination, 1T = one termination and 2T = two terminations. [f] Estimate uncertaints equal to 2σ analytical error based on error propagated from U, Th, Sm, and He measurements. [g] Correction factor after (FARLEY; WOLF; SILVER, 1996) assuming homogeneous distribution of U and Th within the crystals. Corrected AHe age = raw AHe age/Ft. *single-grain with relative anomalous He, U, Th, and Sm concentrations, and anomalous age. This grain is interpreted as an outlier and it is not computed on thermal modelling

4.2 Thermal History and Denudation of the Chela Escarpment

From base to top of the Chela Escarpment, thermal histories are consistent (Fig. 3). Sample Ang-11 next to the base of the Escarpment (at 777 m) records a pronounced cooling interval at 40 - 0 Ma (from paleotemperatures of ~70°C). Sample Ang-12 from 1,026 m on the Escarpment front records cooling intervals: at 130 - 90 Ma (from paleotemperatures of ~75°C), and a second one at ~15 - 0 Ma (from paleotemperatures of ~50°C). Sample Ang-13 from 1,269 m records a more protacted cooling interval between ~90 – 0 Ma (from paleotemperatures of ~70°C). Finally, sample Ang-15 in the Escarpment summit (at 1,682 m) records an abrupt cooling between ~115 - 90 Ma (from paleotemperatures of ~80°C), which is followed by a period of thermal stability near surface temperatures (<25°C) throughout the Cenozoic (Fig. 3). Taking into account a current surface temperature of 20°C, samples Ang-11 and Ang-12 record Cenozoic cooling rates of ~ 1.3 and 2°C/Ma, respectively, whereas samples Ang-13 and Ang-15 record substantial decrease on Cenozoic cooling rates with values about ~ 0.5 and 0.05°C/Ma, respectively. Overall, thermal histories show a trend in which Cretaceous cooling appears notable towards the escarp summit, in opposition to the Cenozoic cooling that is evident towards the base of the scarp (Fig. 3).

Based on the available thermal histories across the southwestern Angolan margin (GREEN; MACHADO, 2015; SILVA et al., 2019) (Fig. 3), and assuming a regional geothermal gradient of 25°C/km (GREEN; MACHADO, 2015), it is estimated that seawards of the Chela Escarpment summit, a rock overburden removal of up ~ 2 km took place in the Cenozoic, whereas at the top of the escarp Cenozoic denudation has been limited to few tens or hundreds of meters. This interpretation agrees with the preservation of Palaeocene to Eocene lateritic profiles (MACGREGOR, 2013) and remnants of Kalahari Group rocks (HOUBEN et al., 2020) further east of the escarp (Fig. 2), suggesting that low Cenozoic denudation has prevailed at least in parts of the Ancient Plateau. However, we reiterate that lesser and greater amounts of denudation also are possible in view of variations in the geothermal gradient over time and variations in the cooling magnitude within the credible intervals of the thermal histories.

Events of Cenozoic denudation comparable to that reported here have also been recorded at the northwestern Angolan margin (AL-HAJRI; WHITE; FISHWICK,

2009; JACKSON; HUDEC; HEGARTY, 2005; LUNDE et al., 1992; WALGENWITZ; RICHERT; CHARPENTIER, 1992), which also coincide with increasing sedimentation rates into the offshore Angolan basins from the Late Paleogene onwards (LAVIER; STECKLER; BRIGAUD, 2001; MACGREGOR, 2013; SÉRANNE; ANKA, 2005) suggesting a source to sink relationship.

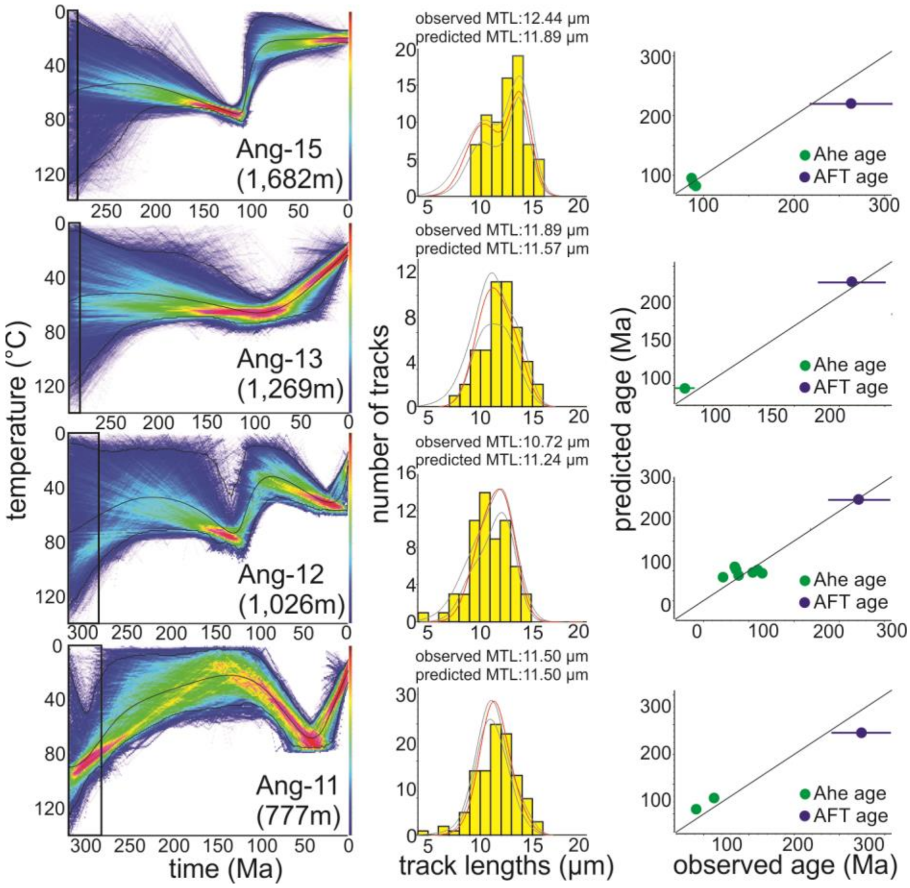

Fig. 3 Thermal history models constrained by both AFT data from (GREEN; MACHADO, 2015) and AHe data from this study. In the left hand side are the time-temperature paths; in the middle are histograms of track length distributions; and in the right hand side the ages predicted by the models are plotted against the measured ages

The existence and the origin of planation surfaces are topics beyond the goal of this work (for more specific works see (BONOW; JAPSEN, 2021; BURKE; GUNNELL, 2008; BURKE; WILKINSON, 2016; GUILLOCHEAU et al., 2015, 2018; JAPSEN et al., 2009, 2018; JAPSEN; CHALMERS, 2022; LIDMAR-BERGSTRÖM; BONOW; JAPSEN, 2013; LINOL et al., 2015; PICART et al., 2020; RÖMER, 2008) and references therein), however, as the Chela Escarpment separates two important planation surfaces described in the literature (BURKE; GUNNELL, 2008; FEIO, 1964; JESSEN, 1936; KING, 1962), we make below some considerations.

At the Chela Escarpment summit, which marks the domain of the Humpata (or the African) surface (Fig. 2c), the denudation-driven cooling event at ~ 100 – 70 Ma (Fig. 3) (GREEN; MACHADO, 2015) matches the period estimated for the initiation of the Humpata (FEIO, 1964) or the African (GUILLOCHEAU et al., 2012, 2018) erosion cycle, as well as the cooling event at ~ 40 – 20 Ma (Fig. 3) (GREEN; MACHADO, 2015; SILVA et al., 2019) recorded over the Serra Abaixo (or Post-African) surface is in agreement with (FEIO, 1964), who based on the simple observation that the Serra Abaixo surface truncates the Maastrichtian one (Fig. 2c), and that the former displays lateral continuity with Miocene deposits onshore, proposed that the erosion phase of the Serra Abaixo cycle likely took place in the Cenozoic with a maximum in the Miocene. In addition, most works converge that the inception of deformation (related to uplift and dissection) of the African surface in many parts of the continent, dates back the period between the Eocene and the Miocene (BURKE; GUNNELL, 2008; GUILLOCHEAU et al., 2018; PARTRIDGE; MAUD, 1987).

4.3 Morphometry of the Drainage Network

The K_{sn} map, encompassing both the coastal and the Cunene river catchments, shows that the highest K_{sn} values predominate from the Chela Escarpment summit to the coast, whereas most of the lowest K_{sn} values dominate the Humpata and the Ancient Plateaus (Fig. 4a). This implies that fluvial incision rates are commonly higher for the coastal rivers in comparison to the interior ones, although the headwaters located near the Chela Escarpment summit, particularly, might show increased K_{sn} values due the occurrence of resistant quartzite (Fig. 4a), which act as a natural barrier to erosion and hence it favours the preservation of steep gradients. This effect can be illustrated by the longitudinal profiles of the Caculuvar (a tributary of the Cunene river) and the coastal rivers, which display steeper gradients towards their headwaters (Fig. 4b).

The χ map of the same region shows highest χ values for rivers draining the Humpata and the Ancient Plateaus, while the lowest χ values mainly characterize the coastal rivers (Fig. 4c). Moreover, the Chela drainage divide (separating the coastal and the Cunene river catchments) is characterized by contrasting cross-divide χ values (Fig. 4c), suggesting that the coastal rivers eroding backwards tend to dissect the Humpata Plateau surface, causing river captures, and the migration of the divide towards the interior. In addition, most of the main rivers show convex upward profiles in the χ plot, where the inflection points roughly mark the separation between the coastal river segments dominated by higher mean K_{sn} values, and the interior river segments dominated by lower mean values (Fig. 4d). Another interesting point is that the main rivers display downstream segments plotting above the steady-state line, and upstream segments plotting below it in the χ plot (Fig. 4d). Assuming that the region has been affected by broad wavelength uplift events (KLÖCKING et al., 2020; WALKER et al., 2016), the river profiles in the χ plot suggest that the Humpata and the Ancient Plateau regions have mostly experienced surface uplift (i.e., when rock uplift is greater than erosion), whereas the Coastal and the Escarpment Zones have been shaped by the landscape dissection (i.e., erosion is greater than rock uplift). The denudation of the Coastal and the Escarpment Zones can be highlighted, for example, by the projection of the χ - z regression line of a relict surface preserved in the χ profile of the Bentiaba river. The intersection of this projection into the elevation axis of the plot points out that ~ 1.5 km of fluvial incision took place downstream of this relict surface, i.e., seaward of the Chela Escarpment (Fig. 4d). This value roughly matches the amount of the Cenozoic denudation derived from the thermochronological data from the same region (GREEN; MACHADO, 2015; SILVA et al., 2019) (Fig. 3).

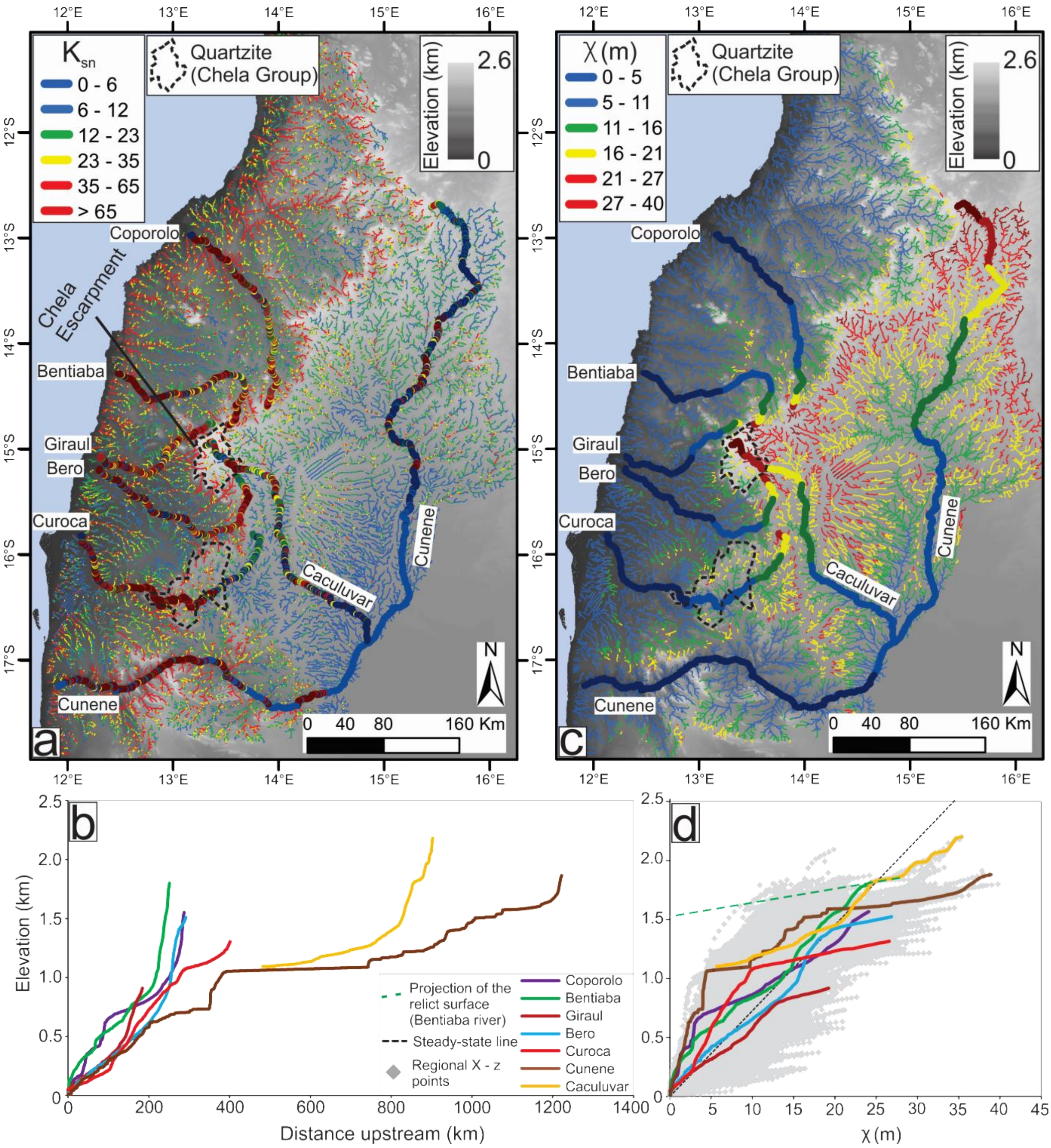

Fig. 4 Morphometric parametres extracted from the drainage network of the Chela Escarpment region and the surroundings by the TopoToolbox 2 (SCHWANGHART; SCHERLER, 2014): a) Regional K_{sn} map from the coastal and the Cunene river catchments with the main rivers highlighted with thick lines. b) Longitudinal profiles of the main rivers where elevation is plotted against the distance from the base level (i.e., the South Atlantic Ocean). c) Regional χ map from the same region with the main rivers highlighted with thick lines. d) χ plot of the main rivers. Remnants of the Chela Group quartzitic rocks were redrawed on the K_{sn} and the χ maps from (LOPES et al., 2016)

4.4 Mechanisms for the Cenozoic Uplift and Denudation

Since the escarpment retreat model was popularized by Lester King (KING, 1953, 1962), subsequent works based on numerical modelling have attempted to decipher the mechanisms underlying the tectonic and the geomorphic evolution of continental margins (BRAUN, 2018; GILCHRIST; KOOI; BEAUMONT, 1994; GILCHRIST; SUMMERFIELD, 1990; KOOI; BEAUMONT, 1994; SACEK; BRAUN; VAN DER BEEK, 2012; TUCKER; SLINGERLAND, 1994; VAN DER BEEK et al., 2002). In this sense, three conceptual models of landscape evolution emerge, each with a distinctive AFT ages pattern. Despite these models originally consider only a major uplift episode related to rifting, we can use them attempting to interpret the thermochronological signature of the southwestern Angolan margin (for a description of the models see (GALLAGHER; BROWN, 1999).

The model of scarp retreat following uplift of the rift shoulder (“uplifted rift flank model”, Fig. 5a) predicts AFT ages equal to the age of rifting near the coast, and older ages towards the interior (Fig. 5d). The model of scarp retreat following the downwarp deformation of the lithosphere during the margin formation (“downwarp model”, Fig. 5b) supposes AFT ages older than rifting, with a trend of AFT age rejuvenation towards the root of the escarpment (Fig. 5d). Finally, the model compelling the downwearing denudation of the rift shoulder from the existence of a drainage divide inland (“pinned divide model”, Fig. 5c) predicts a distribution of AFT ages similar to the uplifted rift flank model, excepting that the former enables some denudation occurring landward of the divide (Fig. 5d).

The available AFT ages from the southwestern Angolan margin fit better the curve of the pinned divide model (Fig. 5d), however, (BURKE; GUNNELL, 2008) demonstrate that the addition of the curve of the downwarp model to the curve of the uplifted rift flank model (as is to be expected if the margin underwent post-rift uplift caused by lithospheric updoming) results in a pattern of AFT ages analogous to that predicted by the pinned divide model. Furthermore, the available AHe ages from the same region are mostly younger than the South Atlantic rifting and thus are distinctive from the AFT ages (Fig. 5d). This supports that the southwestern Angolan margin underwent a post-rift thermal event (or events) capable to partially reset the AHe ages, but without much influence on the AFT ages. Additionaly, the AHe ages approximate the age of rifting near the coast, slightly young towards the root of the Chela Escarpment, and become slightly old towards the Escarpment summit, in a way quite comparable to that presumed by the downwarp model curve (Fig. 5d). This information combined to the fact that the southwestern Angolan margin straddles the southwestern side of the Angola Dome (Fig. 1a,b), strongly suggest that the

Cenozoic denudation of the margin has been triggered by uplifts associated to the Angola Dome growth (FISHWICK; BASTOW, 2011; ROBERTS; WHITE, 2010; WALKER et al., 2016). We reiterate, however, that other tectonic processes such as far-field stresses (COLLI et al., 2014; JAPSEN et al., 2006, 2012) may also have played a role on the reactivation of crustal structures and the uplifts recorded throughout the Angolan margin (GUIRAUD; BUTA-NETO; QUESNE, 2010; HUDEC; JACKSON, 2004).

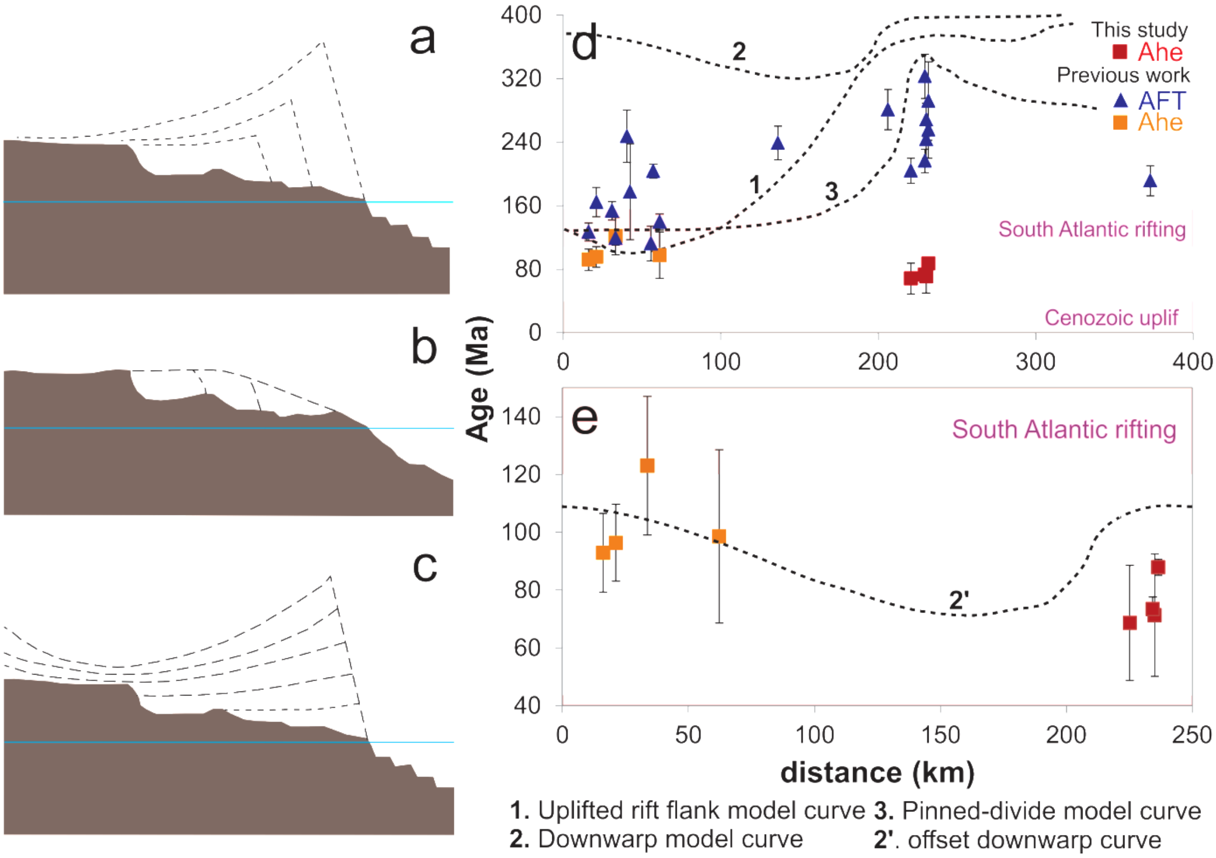

Fig. 5 (a, b, and c) Sketch of the three conceptual models for the landscape evolution at continental margins, redrawed from (GALLAGHER; BROWN, 1999). (d) Expected distributions of the AFT ages from each model are represented by dashed lines (GALLAGHER; BROWN, 1999), whereas symbols represent mean AFT and AHe ages from the southwestern Angolan margin (GREEN; MACHADO, 2015; SILVA et al., 2019) (Tab. 1). e) Detail of the AHe ages roughly fitting the shifted downwarp model curve. See text for discussion

At a global scale, the Eocene - Oligocene boundary marks the onset of periods of major climate cooling (ZACHOS et al., 2001) related to the formation of the Antartica Ice sheet and to the periods of lowering of the sea-level. At the same time, Angola experienced more humid climatic conditions due to the northward migration of the African continent (SCOTESE, 2000; SÉRANNE; ANKA, 2005), as well as the

Angolan margin underwent uplift events that became more pronounced in the Late Paleogene and in the Neogene (GUIRAUD; BUTA-NETO; QUESNE, 2010; LAVIER; STECKLER; BRIGAUD, 2001; ROBERTS; WHITE, 2010; WALKER et al., 2016). These aspects together increased the continental erosion, as also recorded by the thermochronological data (Fig. 3) (GREEN; MACHADO, 2015; JACKSON; HUDEC; HEGARTY, 2005; SILVA et al., 2019), reflecting in the deposition of a thick sedimentary package in depocenters of the Namibe and Kwanza basins, which currently coincide with the Cunene and the Kwanza river mouths, respectively (SÉRANNE; ANKA, 2005).

The Cunene river rises near the apex of the Angola Dome (Fig. 1b), and it flows southwards through the Ancient Plateau when it suddenly inflects westwards entering into falls toward the South Atlantic Ocean (Fig. 4a, c). This trajectory indicates that a Cunene interior (present-day Upper Cunene) was captured by a coastal stream (present-day Lower Cunene) eroding backward (GOUDIE, 2005), but this process is disputed to have occurred during the Eocene (HOUBEN et al., 2020) or Pleistocene times (BUCH, 1997). Nevertheless, the capture of the interior Cunene river in the Cenozoic demonstrates that fluvial incision by the propagation of knickpoints, and escarp retreat processes, also took place in the geological past. In other words, the Cenozoic cooling recorded by the thermal histories (Fig. 3) coupled with the morphometric data (Fig. 4), strongly suggest that these erosive processes commenced in the Late Paleogene, and they have been maintained (not necessarily continuously) until the present day.

It is important to point out that the study area is located few tens of kilometers north of the coastal Namibe desert. It was formed under the influence of the Benguela cold marine current, which started around 10 Ma ago (BUCH, 1997; DIESTER-HAASS et al., 1988) and led to the establishment of hyper-arid conditions in the coastal region from the Pliocene onwards (VAN ZINDEREN BAKKER; MERCER, 1986). Although arid conditions are often ascribed to limited erosion (BURKE; GUNNELL, 2008), these conditions have prevailed more strictly close to the coast, while towards the Chela Escarpment and the Angolan highlands further north, relatively high precipitation rates due to orographic rainfalls (HUNTLEY, 2019) (Fig. 6) have maintained the drainage system and hence the erosion processes.

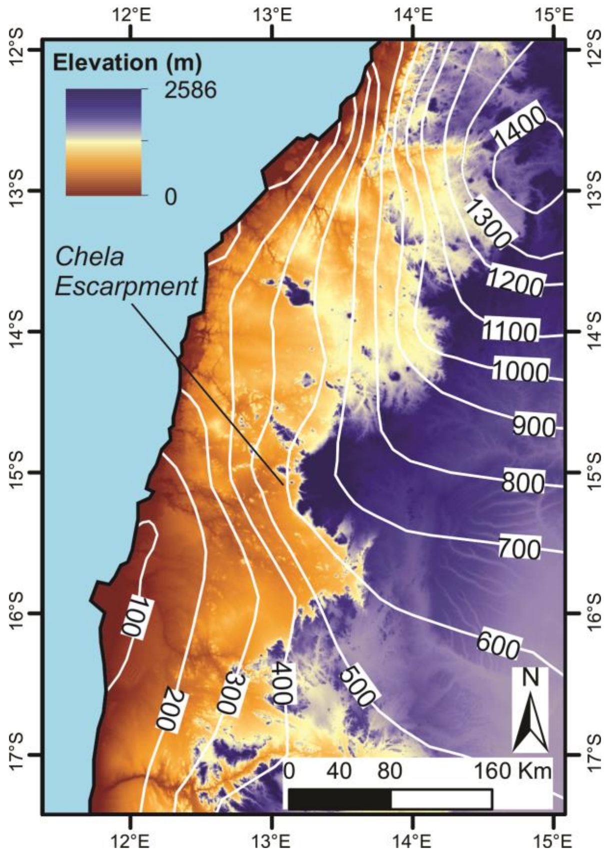

Fig. 6 Elevation map of the southwestern Angolan margin containing isolines of mean annual rainfall (mm), redrawn from (HUNTLEY, 2019)

4.5 The Proposed Model for the Chela Escarpment Formation

The uplifts related to the Angola Dome rise, started at ~ 40 – 20 Ma (BURKE; GUNNELL, 2008; GUILLOCHEAU et al., 2018; ROBERTS; WHITE, 2010), steepened the surface oceanwards, tilted the Maastrichtian to Cenozoic sedimentary strata currently preserved onshore (FEIO, 1964) (Fig. 2c), and caused base-level falls that, in combination with more humid climatic conditions (SÉRANNE; ANKA, 2005), led to the substancial increase of fluvial erosion by the upstream propagation of knickpoints and scarp retreat processes (illustrated in the Fig. 4), also increasing the offshore sedimentation (MACGREGOR, 2013). As steeper surface gradients have been generated at the flanks instead of the apex of the Dome, denudation has become more pronounced oceanward than landward, conditioning for the relative surface uplift of the Humpata (and Ancient) Plateau, at the same time that the Escarpment and Coastal Zones have been formed by the landscape dissection. In this scenario, a paleo erosion surface (Humpata or African surfaces) can be partially preserved over the Humpata Plateau and further inland, as indicated by previous work (BURKE; GUNNELL, 2008; DE PUTTER; RUFFET, 2020; FEIO, 1964; GUILLOCHEAU et al., 2018), but the possibilility for considerable Cenozoic denudation, affecting parts of the Humpata and Ancient Plateaus, may not be precluded. Nevertheless, the Serra Abaixo surface likely results from the rock overburden removal post ~ 40 – 20 Ma (FEIO, 1964; GREEN; MACHADO, 2015; SILVA et al., 2019) (Fig. 3).

It is also important to note that this Cenozoic differential denudation across the region may have been incremented if the coastal rivers initially stripped relatively soft, sedimentary rocks of the Namibe Basin, which likely extended over the basement further inland (FEIO, 1964; GREEN; MACHADO, 2015; SILVA et al., 2019). In addition, the presence of resistant quartzitic rocks, that are currently preserved at the Chela Escarpment (Fig 2b), likely has amplified the relief as lateral variations in rock strength may account for changes in denudation rates and slopes along river profiles (e.g., (PEIFER et al., 2020).

In summary, our model (Fig. 7) is in agreement with previous work with regards the suggestion that the Great Escarpment of Southern Africa is a Late Cenozoic landform, not related to the South Atlantic rifting (BURKE; GUNNELL, 2008; GREEN et al., 2016, 2018; GREEN; MACHADO, 2015; JAPSEN et al., 2012; PICART et al., 2020). Particurlarly, this work brings back the (BURKE; GUNNELL, 2008) theory, in which the Great Escarpment of Southern Africa is the consequence of ~ 1 - 2 km of Late Cenozoic denudation affecting the ocean-facing side of the mantle domes. In addition, numerical models for fluvial erosion have shown that dynamic uplift episodes associated to long wavelength lithospheric updoming and tilting, might induce to substantial drainage reorganization and high-amplitude denudation pulses in time durations less than 30 Myr (BRAUN et al., 2014; DING et al., 2019).

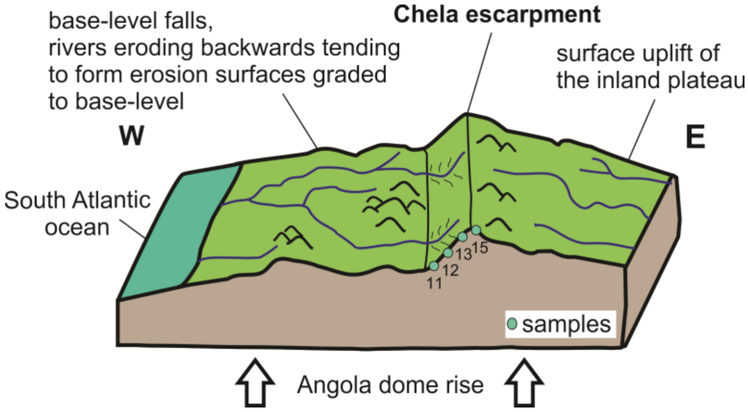

Fig. 7 Schematic representation of the relief formation for the southwestern Angolan margin post ~ 40 – 20 Ma. The rise of the Angola Dome has caused relative surface uplift of the current Humpata Plateau, and a denudation pulse of ~ 2 km of amplitude affecting its seawards side. The removal of rock overburden during this time interval results in the formation of the present-day Chela Escarpment

5 CONCLUSIONS

This work presents new AFT - AHe inverted thermal histories and morphometric data for rivers from the Chela Escarpment region, southwestern margin of Angola, aiming to resolve the timing and possible mechanisms that accounts for the relief development. The new data in combination to previous work support that seaward of the Chela Escarpment summit, a denudation pulse of ~ 2 km in amplitude took place from ~ 40 – 20 Ma onwards, whereas the top of the scarp appears to have undergone relatively low Cenozoic denudation. The distribution pattern of the regional AFT and AHe ages, coupled to the fact the the region lies at the southwestern half of the Angola Dome, suggest that this denudation event has been mainly triggered by uplifts related to the Angola Dome growth. This in combination with relatively humid climatic conditions appears to account for scarp retreat processes induced by rivers eroding backwards, which have dissected the Angola Dome flank. The present work emphasizes that the modern relief of the southwestern Angolan margin, which is marked by the conspicuous Chela Escarpment, appears to be relatively young, mostly shaped during the Cenozoic. This work shows that the (BURKE; GUNNELL, 2008) hypothesis, in which the Great Escarpment of southern Africa is formed by the dissection of the oceanward flank of major mantle domes in the Late Cenozoic, is still alive at least within the Angolan margin context.

References

AL-HAJRI, Y.; WHITE, N.; FISHWICK, S. Scales of transient convective support beneath Africa. **Geology**, v. 37, n. 10, p. 883–886, 2009.

ARAÚJO, A. G.; GUIMARÃES, F. Geologia de Angola. **Notícia explicativa da carta geológica à escala 1:1000000**, p. 137p, 1992.

BABY, G. et al. Solid sedimentation rates history of the Southern African continental margins: Implications for the uplift history of the South African Plateau. **Terra Nova**, v. 32, n. 1, p. 53–65, 2020.

BEERNAERT, F. R. **Republic of Angola Development of a Soil and Terrain Map/Database for Angola**. De Pinte, Belgium: [s.n.].

BEESON, H. W.; MCCOY, S. W.; KEEN-ZEBERT, A. Geometric disequilibrium of river basins produces long-lived transient landscapes. **Earth and Planetary Science Letters**, v. 475, p. 34–43, 2017.

BICCA, M. M. et al. Mesozoic-Cenozoic landscape evolution of NW Mozambique recorded by apatite thermochronology. **Journal of Geodynamics**, v. 125, n. January 2018, p. 48–65, 2019.

BONOW, J. M.; JAPSEN, P. Peneplains and tectonics in north-east greenland after opening of the North-East Atlantic. **GEUS Bulletin**, v. 45, n. 1, p. 1–35, 2021.

BRAUN, J. et al. Rapid erosion of the Southern African Plateau as it climbs over a mantle superswell. **Journal of Geophysical Research: Solid Earth**, v. 119, p. 6093–6112, 2014.

BRAUN, J. A review of numerical modeling studies of passive margin escarpments leading to a new analytical expression for the rate of escarpment migration velocity. **Gondwana Research**, v. 53, p. 209–224, 2018.

BROWN, R. et al. Intracontinental deformation in southern Africa during the Late Cretaceous. **Journal of African Earth Sciences**, v. 100, p. 20–41, 2014.

BROWN, R. W. et al. An Early Cretaceous phase of accelarated erosion on the South-Western margin of Africa: Evidence from apatite fission track analysis and the offshore sedimentary record. **Nucl. Tracks Radiat. Meas.**, v. 17, n. 3, p. 339–350, 1990.

BROWN, R. W. Denudational history along a transect across the Drakensberg Escarpment of southern Africa derived from apatite fission track thermochronology. **Journal of Geophysical Research**, v. 107, n. B12, p. 2350, 2002.

BUCH, M. W. Etosha Pan - The third largest lake in the world? **Madoqua**, v. 20, n. 1, p. 49–64, 1997.

BUMBY, A. J.; GUIRAUD, R. The geodynamic setting of the Phanerozoic basins of Africa. **Journal of African Earth Sciences**, v. 43, n. 1–3, p. 1–12, 2005.

BURKE, K. The African plate. **South African Journal of Geology**, v. 99, n. 4, p. 341–409, 1996.

BURKE, K.; GUNNELL, Y. **The african erosion surface: A Continental-Scale Synthesis of Geomorphology, Tectonics, and Environmental Change over the Past 180 Million Years**. Memoir 201 ed. Boulder, Colorado: Geological Society of

America, 2008.

BURKE, K.; WILKINSON, M. J. Landscape evolution in Africa during the Cenozoic and quaternary—the legacy and limitations of Lester C. King. **Canadian Journal of Earth Sciences**, v. 53, n. 11, p. 1089–1102, 2016.

CASTILLO, M.; MUÑOZ-SALINAS, E.; FERRARI, L. Response of a landscape to tectonics using channel steepness indices (ksn) and OSL: A case of study from the Jalisco Block, Western Mexico. **Geomorphology**, 2014.

CELLI, N. L. et al. African cratonic lithosphere carved by mantle plumes. **Nature Communications**, v. 11, n. 1, 2020.

COCKBURN, H. A. P. et al. Quantifying passive margin denudation and landscape development using a combined fission-track thermochronology and cosmogenic isotope analysis approach. **Earth and Planetary Science Letters**, v. 179, n. 3–4, p. 429–435, 2000.

COLLI, L. et al. Rapid South Atlantic spreading changes and coeval vertical motion in surrounding continents: Evidence for temporal changes of pressure-driven upper mantle flow. **Tectonics**, v. 33, n. 7, p. 1304–1321, 2014.

DE PUTTER, T.; RUFFET, G. Supergene manganese ore records 75 Myr-long Campanian to Pleistocene geodynamic evolution and weathering history of the Central African Great Lakes Region – Tectonics drives, climate assists. **Gondwana Research**, v. 83, p. 96–117, 2020.

DE SOUZA, D. H. et al. Controls on the erosion of the continental margin of southeast Brazil from cosmogenic 10 Be in river sediments. **Geomorphology**, v. 330, p. 163–176, 2019.

DE WAELE, B.; JOHNSON, S. P.; PISAREVSKY, S. A. Palaeoproterozoic to Neoproterozoic growth and evolution of the eastern Congo Craton: Its role in the Rodinia puzzle. **Precambrian Research**, v. 160, n. 1–2, p. 127–141, 2008.

DE WIT, M. C. J. Post-Gondwana drainage and the development of diamond placers in western South Africa. **Economic Geology**, v. 94, n. 5, p. 721–740, 1999.

DE WIT, M. J. The Kalahari Epeirogeny and climate change: Differentiating cause and effect from core to space. **South African Journal of Geology**, v. 110, n. 2–3, p. 367–392, 2007.

DIESTER-HAASS, L. et al. Late Quaternary history of continental climate and the Benguela Current off South West Africa. **Palaeogeography, Palaeoclimatology, Palaeoecology**, v. 65, n. 1–2, p. 81–91, 1988.

DING, X. et al. Drainage and Sedimentary Responses to Dynamic Topography. **Geophysical Research Letters**, v. 46, n. 24, p. 14385–14394, 2019.

DINIZ, A. C. **Características mesológicas de Angola**. Nova Lisboa: Missão de Inquéritos Agrícolas de Angola, 1973.

FARLEY, K. A. (U-Th)/He Dating: Techniques, Calibrations, and Applications. **Reviews in Mineralogy and Geochemistry**, v. 47, n. 1, p. 819–844, 2002.

FARLEY, K. A.; WOLF, R. A.; SILVER, L. T. The effects of long alpha-stopping distances on (U-Th)/He ages. **Geochimica et Cosmochimica Acta**, v. 60, n. 21, p. 4223–4229, 1996.

FEIO, M. A evolução da escadaria de aplanações do sudoeste de Angola. **Garcia da Orla (Lisboa)**, v. 12, n. 2, p. 323–354, 1964.

FISHWICK, S.; BASTOW, I. D. Towards a better understanding of African topography: A review of passive-source seismic studies of the African crust and upper mantle. **Geological Society Special Publication**, v. 357, n. 1, p. 343–371, 2011.

FITZGERALD, P. G. et al. Interpretation of (U-Th)/He single grain ages from slowly cooled crustal terranes: A case study from the Transantarctic Mountains of southern Victoria Land. **Chemical Geology**, v. 225, n. 1–2, p. 91–120, 2006.

FLINT, J. J. Stream Gradient as a Function of Order, Magnitude, and Discharge. **Water Resources Research**, v. 10, n. 5, p. 969–973, 1974.

FLOWERS, R. M.; KELLEY, S. A. Interpreting data dispersion and " inverted" dates in apatite (U-Th)/He and fission-track datasets: An example from the US midcontinent. **Geochimica et Cosmochimica Acta**, v. 75, n. 18, p. 5169–5186, 2011.

FLOWERS, R. M.; SCHOENE, B. (U-Th)/He thermochronometry constraints on unroofing of the eastern Kaapvaal craton and significance for uplift of the southern African plateau. **Geology**, v. 38, n. 9, p. 827–830, 2010.

FORTE, A. M.; WHIPPLE, K. X. Criteria and tools for determining drainage divide stability. **Earth and Planetary Science Letters**, v. 493, p. 102–117, 2018.

FORTE, A. M.; WHIPPLE, K. X. Short communication: The Topographic Analysis Kit (TAK) for TopoToolbox. **Earth Surface Dynamics**, v. 7, n. 1, p. 87–95, 2019.

GALLAGHER, K. et al. Markov chain Monte Carlo (MCMC) sampling methods to determine optimal models, model resolution and model choice for Earth Science problems. **Marine and Petroleum Geology**, v. 26, n. 4, p. 525–535, 2009.

GALLAGHER, K. Transdimensional inverse thermal history modeling for quantitative thermochronology. **Journal of Geophysical Research: Solid Earth**, v. 117, n. 2, p. 1–16, 2012.

GALLAGHER, K.; BROWN, R. Denudation and uplift at passive margins: the record on the Atlantic Margin of southern Africa. **Philosophical Transactions of the Royal Society A: Mathematical, Physical and Engineering Sciences**, v. 357, n. 1753, p. 835–859, 1999.

GAUTHERON, C. et al. Effect of alpha-damage annealing on apatite (U–Th)/He thermochronology. **Chemical Geology**, v. 266, n. 3–4, p. 157–170, 2009.

GAUTHERON, C. et al. Chemical influence on α-recoil damage annealing in apatite: Implications for (U – Th)/He dating. **Chemical Geology**, v. 351, p. 257–267, 2013.

GILCHRIST, A. R.; KOOI, H.; BEAUMONT, C. Post-Gondwana geomorphic evolution of southwestern Africa: Implications for the controls on landscape development from observations and numerical experiments. **J. Geophys. Res.**, v. 99, n. B6, p. 12211–12228, 1994.

GILCHRIST, A. R.; SUMMERFIELD, M. A. Differential denudation and flexural isostasy in formation of rifted-margin upwarps. **Nature**, v. 346, n. 6286, p. 739–742, 1990.

GINDRE-CHANU, L. et al. Diagenetic evolution of aptian evaporites in the Namibe

Basin (south-west Angola). **Sedimentology**, v. 62, n. 1, p. 204–233, 2015.

GINDRE-CHANU, L. et al. Origin and diagenetic evolution of gypsum and microbialitic carbonates in the Late Sag of the Namibe Basin (SW Angola). **Sedimentary Geology**, v. 342, p. 133–153, 2016.

GIRESSE, P.; HOANG, C.-T.; KOUYOUMONTZAKIS, G. Analysis of vertical movements deduced from a geochronological study of marine Pleistocene deposits, southern coast of Angola. **Journal of African Earth Sciences**, v. 2, n. 2, p. 177–187, 1984.

GIULIANI, A. et al. Southwestern Africa on the burner: Pleistocene carbonatite volcanism linked to deep mantle upwelling in Angola. **Geology**, v. 45, n. 11, p. 971–974, 2017.

GOUDIE, A. S. The drainage of Africa since the Cretaceous. **Geomorphology**, v. 67, n. 3–4, p. 437–456, 2005.

GREEN, P. F. et al. Post-breakup burial and exhumation of the southern margin of Africa. **Basin Research**, v. 29, n. 1, p. 1–32, 2016.

GREEN, P. F. et al. Post-breakup burial and exhumation of passive continental margins : Seven propositions to inform geodynamic models. **Gondwana Research**, v. 53, p. 58–81, 2018.

GREEN, P. F.; MACHADO, V. Pre-rift and synrift exhumation, post-rift subsidence and exhumation of the onshore Namibe Margin of Angola revealed from apatite fission track analysis. **Geological Society, London, Special Publications**, v. 438, p. 99–118, 2015.

GUILLOCHEAU, F. et al. Quantification and causes of the terrigeneous sediment budget at the scale of a continental margin: A new method applied to the Namibia-South Africa margin. **Basin Research**, v. 24, n. 1, p. 3–30, 2012.

GUILLOCHEAU, F. et al. Cenozoic Landscape Evolution in and Around the Congo Basin: Constraints from Sediments and Planation Surfaces. In: DE WIT, M. J.; GUILLOCHEAU, F.; DE WIT, M. C. J. (Eds.). . **Geology and Resource Potential of the Congo Basin**. Berlin-Heidelberg: Springer, 2015. p. 1–417.

GUILLOCHEAU, F. et al. Planation surfaces as a record of mantle dynamics: The case example of Africa. **Gondwana Research**, v. 53, p. 82–98, 2018.

GUIRAUD, M.; BUTA-NETO, A.; QUESNE, D. Segmentation and differential post-rift uplift at the Angola margin as recorded by the transform-rifted Benguela and oblique-to-orthogonal-rifted Kwanza basins. **Marine and Petroleum Geology**, v. 27, n. 5, p. 1040–1068, 2010.

HIPONDOKA, M. H. T. **The development and evolution of Etosha Pan, Namibia**. [s.l.] Bayerischen Julius-Maximilians-Universität Würzburg, 2005.

HOLMES, A. **Principles of Physical Geology**. Edinburgh: Thomas Nelson and Sons Limited, 1944.

HOUBEN, G. J. et al. Stacked megafans of the kalahari basin as archives of paleogeography, river capture, and cenozoic paleoclimate of Southwestern Africa. **Journal of Sedimentary Research**, v. 90, n. 9, p. 980–1010, 2020.

HUDEC, M. R.; JACKSON, M. P. A. Regional restoration across the Kwanza Basin, Angola: Salt tectonics triggered by repeated uplift of a metastable passive margin.

AAPG Bulletin, v. 88, n. 7, p. 971–990, 2004.

HUNTLEY, B. J. Angola in Outline: Physiography, Climate and Patterns of Biodiversity. In: HUNTLEY, B. J. et al. (Eds.). . **Biodiversity of Angola: Science & Conservation: A Modern Synthesis**. [s.l.] Springer, 2019. p. 549.

ISBELL, J. L. et al. Glacial paradoxes during the late Paleozoic ice age: Evaluating the equilibrium line altitude as a control on glaciation. **Gondwana Research**, v. 22, n. 1, p. 1–19, 2012.

JACKSON, M. P. A.; HUDEC, M. R.; HEGARTY, K. A. The great West African Tertiary coastal uplift: Fact or fiction? A perspective from the Angolan divergent margin. **Tectonics**, v. 24, n. 6, p. 1–23, 2005.

JAPSEN, P. et al. Elevated, passive continental margins: Long-term highs or Neogene uplifts? New evidence from West Greenland. **Earth and Planetary Science Letters**, v. 248, n. 1–2, p. 315–324, 2006.

JAPSEN, P. et al. Formation, uplift and dissection of planation surfaces at passive continental margins – a new approach. **Earth Surface Processes and Landforms**, v. 34, p. 683–699, 2009.

JAPSEN, P. et al. Elevated, passive continental margins: Not rift shoulders, but expressions of episodic, post-rift burial and exhumation. **Global and Planetary Change**, v. 90–91, p. 73–86, 2012.

JAPSEN, P. et al. Mountains of southernmost Norway: Uplifted miocene peneplains and re-exposed Mesozoic surfaces. **Journal of the Geological Society**, v. 175, n. 5, p. 721–741, 2018.

JAPSEN, P.; CHALMERS, J. A. The Norwegian mountains: the result of multiple episodes of uplift and subsidence. **Geology Today**, v. 38, n. 1, p. 13–19, 2022.

JELSMA, H. A. et al. Preferential distribution along transcontinental corridors of kimberlites and related rocks of Southern Africa. **South African Journal of Geology**, v. 107, n. (1-2), p. 301–324, 2004.

JESSEN, O. **Reisen und forschungen in Angola**. Berlin: Verlag von Dietrich Reimer, 1936.

KETCHAM, R. A. et al. Improved modeling of fission-track annealing in apatite. **American Mineralogist**, v. 92, n. 1999, p. 799–810, 2007.

KING, L. C. Canons of landscape evolution. **Bulletin of the Geological Society of America**, v. 64, p. 721–752, 1953.

KING, L. C. **The Morphology of the Earth: A Study and Synthesis of World Scenery**. London: Oliver and Boyd, 1962.

KING, L. C. Planation remnants upon high lands. **Zeitschrift für Geomorphologie**, v. 20, p. 133–148, 1976.

KIRBY, E.; WHIPPLE, K. X. Expression of active tectonics in erosional landscapes. **Journal of Structural Geology**, v. 44, p. 54–75, 2012.

KLÖCKING, M. et al. A tale of two domes: Neogene to recent volcanism and dynamic uplift of northeast Brazil and southwest Africa. **Earth and Planetary Science Letters**, v. 547, p. 116464, 2020.

KOOI, H.; BEAUMONT, C. Escarpment evolution on high-elevation rifted margins:

Insights derived from a surface processes model that combines diffusion, advection, and reaction. **Journal of Geophysical Research**, v. 99, p. 12191–12209, 1994.

KOUNOV, A. et al. Denudation along the Atlantic passive margin: new insights from apatite fission-track analysis on the western coast of South Africa. **Geological Society, London, Special Publications**, v. 324, n. September, p. 287–306, 2009.

KROB, F. C. et al. **Late Neoproterozoic-to-recent long-term t–T-evolution of the Kaoko and Damara belts in NW Namibia**. [s.l.] Springer Berlin Heidelberg, 2020a. v. 109

KROB, F. C. et al. Application of stratigraphic frameworks and thermochronological data on the Mesozoic SW Gondwana intraplate environment to retrieve the Paraná-Etendeka plume movement. **Gondwana Research**, v. 84, p. 81–110, 2020b.

LAVIER, L. L.; STECKLER, M. S.; BRIGAUD, F. Climatic and tectonic control on the Cenozoic evolution of the West African margin. **Marine Geology**, v. 178, n. 1–4, p. 63–80, 2001.

LETURMY, P.; LUCAZEAU, F.; BRIGAUD, F. Dynamic interactions between the gulf of Guinea passive margin and the Congo River drainage basin: 1. Morphology and mass balance. **Journal of Geophysical Research**, v. 108, n. B8, p. 1–13, 2003.

LIDMAR-BERGSTRÖM, K.; BONOW, J. M.; JAPSEN, P. Stratigraphic Landscape Analysis and geomorphological paradigms: Scandinavia as an example of Phanerozoic uplift and subsidence. **Global and Planetary Change**, v. 100, p. 153–171, 2013.

LINOL, B. et al. Formation and Collapse of the Kalahari Duricrust [’African Surface’] Across the Congo Basin, with Implications for changes in Rates of Cenozoic Off-Shore Sedimentation. **Geology and Resource Potential of the Congo Basin**, n. September, p. 1–417, 2015.

LITHGOW-BERTELLONI, C.; SILVER, P. Dynamic topography, plate driving forces and the African superswell. **Nature**, v. 395, n. September, p. 345–348, 1998.

LOPES, F. C. et al. Morphostructural characterization of the western edge of the Huila Plateau (SW Angola), based on remote sensing techniques. **Journal of African Earth Sciences**, v. 117, p. 114–123, 2016.

LUNDE, G. et al. Tertiary uplift of the Kwanza Basin in Angola. In: CURNELLE, R. (Ed.). . **Géologie Africaine, Colloques de Geologie de Libreville**. [s.l.] Bull. Cent. de Rech. Explor. Product. Elf Aquitaine Mém, 1992. v. 13p. 99–117.

MACGREGOR, D. S. Late Cretaceous – Cenozoic sediment and turbidite reservoir supply to South Atlantic margins. **Geological Society, London, Special Publications**, v. 369, p. 109–128, 2013.

MARGIRIER, A. et al. Climate control on Early Cenozoic denudation of the Namibian margin as deduced from new thermochronological constraints. **Earth and Planetary Science Letters**, v. 527, 2019.

MARQUES, M. M. Esboço das grandes unidades geomorfológicas de Angola (2ª aproximação). **Inst. Inv. Cient. Tropical, Garcia de Orta, Sér. Geol. Lisboa**, v. 2, n. 1, p. 41–43, 1977.

MARSH, J. S.; SWART, R. The Bero Volcanic Complex: Extension of the Paraná-Etendeka Igneous Province into SW Angola. **Journal of Volcanology and**

Geothermal Research, 2016.

MARZOLI, A. et al. Geochronology and petrology of Cretaceous basaltic magmatism in the Kwanza basin (western Angola), and relationships with the Parana-Etendeka continental flood basalt province. **Journal of Geodynamics**, v. 28, n. 4–5, p. 341–356, 1999.

MEESTERS, A. G. C. A.; DUNAI, T. J. Solving the production-diffusion equation for finite diffusion domains of various shapes: Part I. Implications for low-temperature (U-Th)/He thermochronology. **Chemical Geology**, v. 186, n. 3, p. 333–344, 2002.

MEESTERS, A. G. C. A.; DUNAI, T. J. A noniterative solution of the (U-Th)/He age equation. **Geochemistry, Geophysics, Geosystems**, v. 6, n. 4, p. 4–6, 2005.

MILLER, S. R. et al. Neogene rejuvenation of central Appalachian topography: Evidence for differential rock uplift from stream profiles and erosion rates. **Earth and Planetary Science Letters**, v. 369–370, p. 1–12, 2013.

MOORE, A.; BLENKINSOP, T.; COTTERILL, F. Southern African topography and erosion history: Plumes or plate tectonics? **Terra Nova**, v. 21, n. 4, p. 310–315, 2009.

MUDD, S. M. et al. How concave are river channels ? **Earth Surface Dynamics**, v. 6, p. 505–523, 2018.

MVONDO, F.; DAUTEUIL, O.; GUILLOCHEAU, F. The Fish River canyon (Southern Namibia): A record of Cenozoic mantle dynamics? **Comptes Rendus - Geoscience**, v. 343, n. 7, p. 478–485, 2011.

NYBLADE, A. A.; SLEEP, N. H. Long lasting epeirogenic uplift from mantle plumes and the origin of the Southern African Plateau. **Geochemistry, Geophysics, Geosystems**, v. 4, n. 12, p. 1105, 2003.

PARTRIDGE, T. C.; MAUD, R. R. Geomorphic evolution of southern Africa since the Mesozoic. **South African Journal of Geology**, v. 90, n. 2, p. 179–208, 1987.

PEIFER, D. et al. Growing topography due to contrasting rock types in a tectonically dead landscape. **Earth Surface Dynamics**, n. August, p. 1–29, 2020.

PEREIRA, E. et al. New data on the deposition age of the volcano-sedimentary Chela Group and its Eburnean basement: implications to post- Eburnean crustal evolution of the SW of Angola. **Comunicacoes Geologicas**, v. 98, n. 1, p. 29–40, 2011.

PERRON, J. T.; ROYDEN, L. An integral approach to bedrock river profile analysis. **Earth Surface Processes and Landforms**, v. 38, n. 6, p. 570–576, 2013.

PICART, C. et al. Cenozoic deformation of the South African plateau, Namibia: Insights from planation surfaces. **Geomorphology**, v. 350, p. 106922, 2020.

RAAB, M. J. et al. Late Cretaceous reactivation of major crustal shear zones in northern Namibia: Constraints from apatite fission track analysis. **Tectonophysics**, v. 349, n. 1–4, p. 75–92, 2002.

RENNE, P. R. et al. Age of Etendeka flood volcanism and associated intrusions in southwestern Africa. **Geology**, v. 24, n. 7, p. 659–662, 1996.

ROBERTS, G. G.; WHITE, N. Estimating uplift rate histories from river profiles using African examples. **Journal of Geophysical Research: Solid Earth**, v. 115, n. 2, p.

1–24, 2010.

RÖMER, W. Accordant summit heights, summit levels and the origin of the “upper denudation level” in the Serra do Mar (SE-Brazil, São Paulo): A study of hillslope forms and processes. **Geomorphology**, v. 100, n. 3–4, p. 312–327, 2008.

SACEK, V.; BRAUN, J.; VAN DER BEEK, P. The influence of rifting on escarpment migration on high elevation passive continental margins. **Journal of Geophysical Research: Solid Earth**, v. 117, n. 4, p. 1–18, 2012.

SALOMON, E.; PASSCHIER, C.; KOEHN, D. Asymmetric continental deformation during South Atlantic rifting along southern Brazil and Namibia. **Gondwana Research**, v. 51, p. 170–176, 2017.

SCHWANGHART, W.; SCHERLER, D. Short Communication: TopoToolbox 2 - MATLAB-based software for topographic analysis and modeling in Earth surface sciences. **Earth Surface Dynamics**, v. 2, n. 1, p. 1–7, 2014.

SCOTESE, C. R. **Paleomap Project, Climate History**. Disponível em: <http://www.scotese.com/climate.htm>. Acesso em: 5 dez. 2016.

SÉRANNE, M.; ANKA, Z. South Atlantic continental margins of Africa: A comparison of the tectonic vs climate interplay on the evolution of equatorial west Africa and SW Africa margins. **Journal of African Earth Sciences**, v. 43, n. 1–3, p. 283–300, 2005.

SHALER, N. S. Spacing of rivers with reference to hypothesis of baseleveling. **Bulletin of the Geological Society of America**, v. 10, p. 263–276, 1899.

SHUSTER, D. L.; FLOWERS, R. M.; FARLEY, K. A. The influence of natural radiation damage on helium diffusion kinetics in apatite. **Earth and Planetary Science Letters**, v. 249, n. 3–4, p. 148–161, 2006.

SILVA, B. V. et al. Evolution of the Southwestern Angolan Margin: episodic burial and exhumation is more realistic than long-term denudation. **International Journal of Earth Sciences**, v. 108, n. 1, p. 89–113, 2019.

SIQUEIRA-RIBEIRO, M. C. et al. The performance of a new (U+Th)/He thermochronology laboratory at UNESP Rio Claro, Brazil. **Annals of Brazilian Academy of Sciences**, v. 91, n. 1, p. 1–11, 2019.

STANLEY, J. R. **Discerning Erosion patterns and Mantle Sources of Topography Across the Southern African Plateau from the Shallow and Deep Records of Kimberlites**. [s.l.] University of Colorado, Boulder, 2015.

STANLEY, J. R.; FLOWERS, R. M.; BELL, D. B. Erosion patterns and mantle sources of topographic change across the southern African Plateau derived from the shallow and deep records of kimberlites. **Geochemistry, Geophysics, Geosystems**, v. 16, p. 1–22, 2015.

STOCKLI, D. F. Application of Low-Temperature Thermochronometry to Extensional Tectonic Settings. **Reviews in Mineralogy and Geochemistry**, v. 58, n. 1, p. 411–448, 2005.

STRUTH, L. et al. Plateau reduction by drainage divide migration in the Eastern Cordillera of Colombia defined by morphometry and 10Be terrestrial cosmogenic nuclides. **Earth Surface Processes and Landforms**, v. 42, n. 8, p. 1155–1170, 2017.

TINKER, J.; DE WIT, M.; BROWN, R. Mesozoic exhumation of the southern Cape, South Africa, quantified using apatite fission track thermochronology. **Tectonophysics**, v. 455, n. 1–4, p. 77–93, 2008.

TUCKER, G. E.; SLINGERLAND, R. L. Erosional dynamics, flexural isostasy, and long-lived escarpments: A numerical modeling study. **Journal of Geophysical Research: Solid Earth**, v. 99, n. B6, p. 12229–12243, 1994.

VAN DER BEEK, P. et al. Modeling postbreakup landscape development and denudational history across the southeast African (Drakensberg Escarpment) margin. **Journal of Geophysical Research**, v. 107, n. B12, p. 2351, 2002.

VAN ZINDEREN BAKKER, E. M.; MERCER, J. H. Major late Cainozoic climatic events and palaeoenvironmental changes in Africa viewed in a world wide context. **Palaeogeography, Palaeoclimatology, Palaeoecology**, v. 56, n. 3–4, p. 217–235, 1986.

WALGENWITZ, F.; RICHERT, J. P.; CHARPENTIER, P. Southwest African plate margin; thermal history and geodynamical implications. In: **Geologic Evolution of Atlantic Continental Rises**. New York: Van Nostrand Reinhold, 1992. p. 20–45.

WALKER, R. T. et al. Rapid mantle-driven uplift along the Angolan margin in the late Quaternary. **Nature Geoscience**, v. 9, n. 12, p. 909–914, 14 dez. 2016.

WANG, Y. et al. Coupling slope-area analysis, integral approach and statistic tests to steady-state bedrock river profile analysis. **Earth Surface Dynamics**, v. 5, n. 1, p. 145–160, 2017.

WHIPPLE, K. X. et al. Timescales of landscape response to divide migration and drainage capture: Implications for the role of divide mobility in landscape evolution. **Journal of Geophysical Research: Earth Surface**, v. 122, n. 1, p. 248–273, 2017.

WHIPPLE, K. X.; TUCKER, G. E. Dynamics of the stream-power river incision model: Implications for height limits of mountain ranges, landscape response timescales, and research needs. **Journal of Geophysical Research**, v. 104, n. B8, p. 17661–17674, 1999.

WILDMAN, M. et al. Post break-up tectonic inversion across the southwestern cape of South Africa: New insights from apatite and zircon fission track thermochronometry. **Tectonophysics**, v. 654, p. 30–55, 2015.

WILDMAN, M. et al. The chronology and tectonic style of landscape evolution along the elevated Atlantic continental margin of South Africa resolved by joint apatite fission track and (U-Th-Sm)/He thermochronology. **Tectonics**, v. 35, n. 3, p. 511–545, 2016.

WILLETT, S. D. et al. Dynamic reorganization of River Basins. **Science**, v. 343, n. 6175, 2014.

WOBUS, C. et al. Tectonics from topography: Procedures, promise, and pitfalls. **Special Paper of the Geological Society of America**, v. 398, n. 04, p. 55–74, 2006.

ZACHOS, J. et al. Trends, rhythms, and aberrations in global climate 65 Ma to present. **Science**, v. 292, n. 5517, p. 686–693, 2001.

CAPÍTULO 3 - THERMAL HISTORIES OF BASEMENT ROCKS FROM THE NORTHWESTERN ANGOLAN SHIELD, CONGO CRATON: CONSTRAINTS FROM APATITE (U-TH-SM)/HE THERMOCHRONOLOGY

1 INTRODUCTION

Cratons are well-known compartments of the continental lithosphere, characterized by thicker roots and greater resistance to tectonic stresses relative to the surrounding lithospheric components (GROVES; SANTOSH, 2021; JORDAN, 1978). This relative tectonic stability accounts for their typical subdued topography and relief (KOHN; GLEADOW, 2019) as a consequence of a prolonged history of erosional denudation since Precambrian times. Despite this, cratonic blocks accommodates substantial deformation at their margins and internally along pre-existing lithospheric discontinuities, which might control, for example, the ascent of deep magmas and fluids associated to the emplacement of ore deposits (GROVES; SANTOSH, 2021), and episodes of crustal uplift and subsidence that are ultimately related to the redistribution of rock material across the intracratonic environment (MORÓN et al., 2020). Nevertheless, accessing the tectono-thermal history of cratons is central to addressing these geological processes.

Low-temperature thermochronology techniques are based on the accumulation of radiogenic daughter products in minerals, and on the retention of these products as a function of temperature that rocks experienced over time (ENKELMANN; GARVER, 2016). Particularly, the apatite (U-Th-Sm)/He method (AHe) is sensitive to a temperature range of ~ 40 – 80 °C (EHLERS; FARLEY, 2003; FARLEY, 2002), which allows the detection of thermal disturbances within the upper crust, overall representing the cooling of rocks caused by their exhumation from depth (i.e., from higher temperatures) towards the Earth's surface. Therefore, the AHe method has been widely used for interpretation of tectonic and denudation processes occurred at cratonic regions (FLOWERS; SCHOENE, 2010; KASANZU et al., 2016; MACKINTOSH et al., 2017; YI et al., 2009).

In this work, we present new AHe data from basement rocks outcropping at the western portion of the Angolan Shield (Congo Craton) (Fig. 1a, b) with the aim of accessing part of the Phanerozoic tectono-thermal history of the region. This portion of the Angolan Shield hosts important tectonic terrane boundaries (DE CARVALHO et al., 2000; HEILBRON et al., 2008) and fracture zones composed of trans-lithospheric faults, which have focused the location of kimberlite and carbonatite magmatism over time (GIULIANI et al., 2017; JELSMA et al., 2013, 2004; USTINOV et al., 2018) (Fig. 1b). In addition, the study area lies at the northwestern half of the Angola (or Bié) Dome, consisting in a macro-geomorphic landform (of ~ 1000 km wavelength) that dominates the inland topography (AL-HAJRI; WHITE; FISHWICK, 2009; GREEN; MACHADO, 2015; GUILLOCHEAU et al., 2018; ROBERTS; WHITE, 2010) (Fig. 1c). This topographic feature shows physiographic characteristics and geophysical evidence supporting it is likely maintained, at least in part, by dynamic uplift (KLÖCKING et al., 2020), although the timing formation and mechanisms of this remarkable topography are still much debated (CELLI et al., 2020; GUILLOCHEAU et al., 2018; JACKSON; HUDEC; HEGARTY, 2005; KLÖCKING et al., 2020; ROBERTS; WHITE, 2010). Thus, this work looks forward to bring new information into the tectonic and geomorphic histories of this part of the Congo craton.

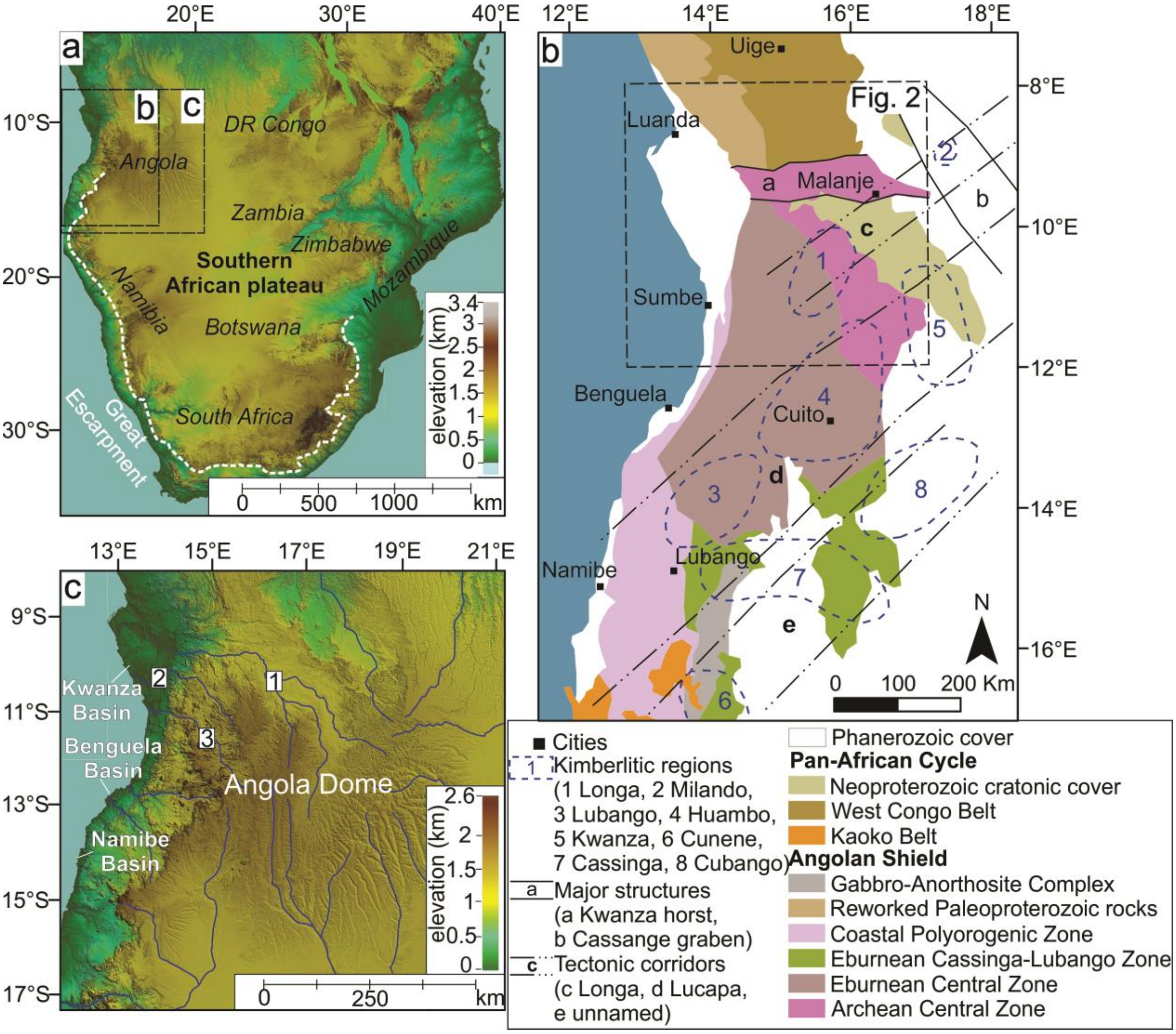

Fig. 1 a) Elevation map of the southern African plateau region showing the encircling Great Escarpment, Coastal Zone, and locations of other figures. b) Simplified tectonic map of the eastern Angolan Shield showing the main tectonic units and basement structures, redrawn from (HEILBRON et al., 2008; USTINOV et al., 2018). c) Elevation map showing the Angola Dome characterized by radial drainage pattern (rivers: 1 Kwanza; 2 Longa; 3 Cuvo) and the location of the coastal Angolan basins

2 REGIONAL SETTING

2.1 Geology

The Angolan Shield in central Angola is divided into the Archean and Eburnean Central Zones, respectively (HEILBRON et al., 2008) (Fig. 1b). The former is mainly composed of Archean granite-gneiss-migmatitic and gabro-anorthosite-charnochytic complexes, and the latter is formed mainly by Paleoproterozoic granite-gneiss and meta-volcano-sedimentary complexes (DE CARVALHO et al., 2000;

HEILBRON et al., 2008) (Fig. 2a). The Angolan Shield is also characterized by major NE-SW tectonic lineaments, hosting along their length regions of carbonatite and kimberlite emplacement (JELSMA et al., 2013, 2004; USTINOV et al., 2018; WHITE; BOORDER; SMITH, 1995) (Fig. 1b, 2a). These alkaline bodies have ages estimated between the Neoproterozoic and Pleistocene (GIULIANI et al., 2017; JELSMA et al., 2013; USTINOV et al., 2018), although only a few bodies were actually dated. At the Longa kimberlitic region (Fig. 1b, 2a), for example, the largest kimberlite body with a surface diameter of ~ 1 km (Lorelei pipe) has a Cretaceous age based on an unpublished paleontological work according information by (USTINOV et al., 2018).

To the north, the Angola Shield is separated from the West Congo Pan-African Mobile Belt (WCPB) by a major E-W trending shear zone known as the Kwanza horst (MCCOURT et al., 2013) (Fig. 1b, 2a). The WCPB is interpreted as an intra-continental rift basin that evolved to a passive margin environment ca. ~ 1.0 – 0.9 Ga, and underwent tectonic inversion during the Pan-African Orogeny ca. ~ 650 - 540 Ma (JELSMA et al., 2013). This event led to the formation of the metasedimentary cover (rift and sag successions) of the West Congo Supergroup (TACK et al., 2001), and red bed sandstones of the Inkisi Group represent a conspicuous cratonic cover that begins to be formed at the end of this orogenic cycle (Fig. 2a). In Angola, the Inkisi Group has a maximum depositional age of ~ 540 Ma estimated by U-Pb zircon dating (JELSMA et al., 2011), as well as the Inkisi rocks reach a thickness of up ~ 3000 m within the intracontinental Congo Basin (LINOL et al., 2015a) (Fig. 2a). In the NW-SE trending Cassange graben (Fig. 1b, 2a) the Inkisi package is overlain unconformably by Carboniferous – Triassic rocks of the Karoo Supergroup (JELSMA et al., 2013; LINOL et al., 2015b), and Jurassic - Cretaceous rocks of the Congo Supergroup outcrop at the surroundings (LINOL et al., 2015c) (Fig. 2a). In the eastern rim of the coastal Kwanza Basin, the Jurassic – Cretaceous strata are also exposed at the surface (Fig. 2a) (JACKSON; HUDEC; HEGARTY, 2005).

Late Cretaceous to Cenozoic rocks of the Kalahari Group reach a thickness of up ~ 60 m (LINOL et al., 2015d) and are most found as minor sedimentary outliers in the study area. These rocks comprise Paleogene conglomerates and silcretized sandstones (Grès Polymorphes Formation), and Neogene unconsolidated sediments (Areias Ocres or Kalahari sands Formation) (LINOL et al., 2015d; THOMAS; SHAW, 1993). The Cenozoic sedimentary cover is also exposed at the inner Kwanza Basin further west (Fig. 2a).

2.2 Geomorphology

The study area lies at the northwestern half of the Angola Dome (Fig. 1c) and is divided, from west to east, into geomorphic zones (DINIZ, 1973; HUNTLEY, 2019) (Fig. 2b): the Coastal Zone is characterized by relatively smooth relief and low elevations below ~ 400 m; the Escarpment Zone consists of a rugged relief domain organized in several steps (small plateaus) with mean elevations below ~ 600 m, but also encompassing part of Angolan Great Escarpment that reaches elevations above ~ 1000 m; the Ancient Plateau comprises a low relief and undulating landscape with mean elevations above ~ 1400 m; the NW-SE trending Malange Plateau reaches elevations between ~ 1000 - 1200 m; the NW-SE trending Cassange Basin comprises a remarkable depression separated from the Malange Plateau by major scarps; and the Congo Peneplain forms a low relief zone bounding the Cassange Basin to the north (Fig. 2b). In more detail, (GUILLOCHEAU et al., 2015) divided the study area into steeped planation surfaces, which from highest to lowest elevations (and also from oldest to youngest ages) correspond to the Upper surface 1 (etchplain), the Upper surface 2 (etchplain) undifferentiated from the Lower surface (pediplain), and the V, W, X, Y and Z surfaces (pediments) (Fig. 2c). The mechanical erosion and weathering phases of the surfaces preserved in the Ancient Plateau are estimated between the Paleocene and Miocene, whereas the erosion phases of the surfaces preserved in the Escarpment and Coastal Zones are estimated from the Miocene to Pliocene (GUILLOCHEAU et al., 2015). Particularly, the Upper surface 1 is within the context of the continent-scale African surface recent revised in (GUILLOCHEAU et al., 2018).

3 APATITE (U-TH-SM)/HE DATA

Apatite (U-Th-Sm)/He data were obtained for 28 single grains from five basement samples, varying in elevation between 1201 m and 1593 m along the northwestern portion of the Ancient plateau (Fig. 2b). All samples are Archean to Paleoproterozoic gneiss derived from outcrops, excepting the Lorelei sample that consists of a gneiss collected from a borehole (provided by CATOCA Sociedade Mineira) crossing the Lorelei kimberlite pipe. Apatite grains were separated by standard concentration techniques and the AHe analysis followed the analytical procedure of (SIQUEIRA-RIBEIRO et al., 2019). The AHe data were acquired at the Department of Geology, São Paulo State University, Rio Claro, Brazil.

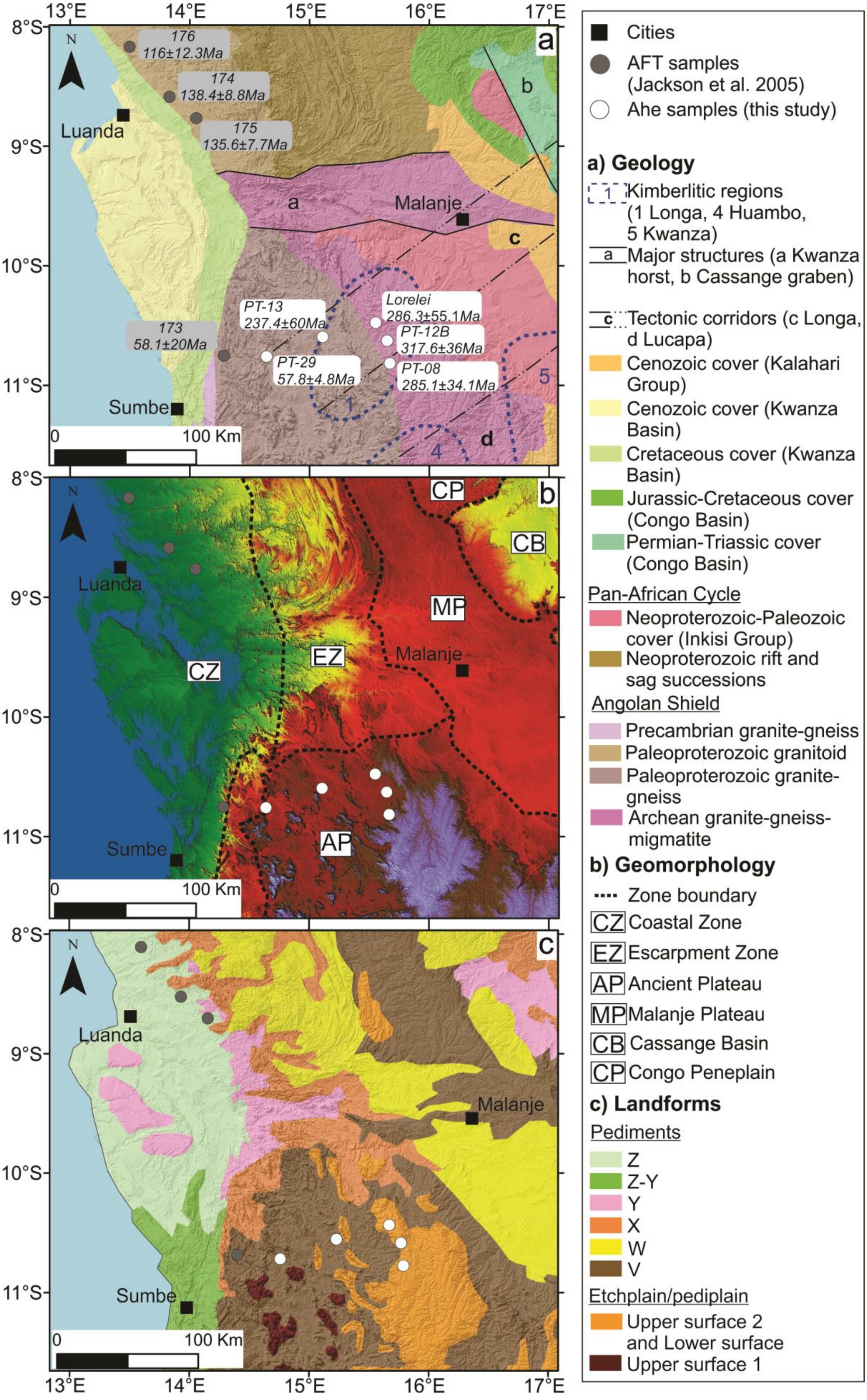
13°E
14°E
15°E
16°E
17°E
8°S
9°S
10°S
11°S
a
b
c
176
116±12.3Ma
174
138.4±8.8Ma
175
135.6±7.7Ma
173
58.1±20Ma
PT-13
237.4±60Ma
PT-29
57.8±4.8Ma
Lorelei
286.3±55.1Ma
PT-12B
317.6±36Ma
PT-08
285.1±34.1Ma
Luanda
Malanje
Sumbe
a
b
c
d
1
4
5
0
100 Km
CP
CB
MP
EZ
CZ
AP
Cities
AFT samples
(Jackson et al. 2005)
Ahe samples (this study)
a) Geology
Kimberlitic regions
(1 Longa, 4 Huambo,
5 Kwanza)
Major structures (a Kwanza
horst, b Cassange graben)
Tectonic corridors (c Longa,
d Lucapa)
Cenozoic cover (Kalahari
Group)
Cenozoic cover (Kwanza
Basin)
Cretaceous cover (Kwanza
Basin)
Jurassic-Cretaceous cover
(Congo Basin)
Permian-Triassic cover
(Congo Basin)
Pan-African Cycle
Neoproterozoic-Paleozoic
cover (Inkisi Group)
Neoproterozoic rift and
sag successions
Angolan Shield
Precambrian granite-gneiss
Paleoproterozoic granitoid
Paleoproterozoic granite-
gneiss
Archean granite-gneiss-
migmatite
b) Geomorphology
Zone boundary
CZ Coastal Zone
EZ Escarpment Zone
AP Ancient Plateau
MP Malanje Plateau
CB Cassange Basin
CP Congo Peneplain
c) Landforms
Pediments
Z
Z-Y
Y
X
W
V
Etchplain/pediplain
Upper surface 2
and Lower surface
Upper surface 1

Fig. 2 a) Simplified geological map of the study area redrawn after (LINOL et al., 2015c), showing the location of Apatite Fission-Track (AFT) ages (pooled or central ages) provided by (JACKSON; HUDEC; HEGARTY, 2005) and AHe ages (mean ± standard deviation) from this study. b) Elevation map and highlight to the geomorphological zones described in (HUNTLEY, 2019). c) Map of landforms redrawn from (GUILLOCHEAU et al., 2015).

Raw single-grain AHe ages, uncorrected for the alpha ejection effect, range from 375.1 ± 11.1 Ma to 52.5 ± 1.9 Ma, whereas the corrected ones vary from 562.8 ± 16.7 Ma to 62.59 ± 2.4 Ma (Tab. 1). The intra-sample age dispersion is low to moderate and vary between 8 and 25 %, similarly to that reported in other cratonic areas (FITZGERALD et al., 2006; FLOWERS; KELLEY, 2011; MORÓN et al., 2020). AHe age dispersion may be associated to a number of causes, including the level of radiation damage, size and morphology, and chemical composition of the single grains, which influence their helium retentivity (BEUCHER et al., 2013; BROWN et al., 2013; FLOWERS et al., 2009; GAUTHERON et al., 2013; REINERS; FARLEY, 2001; SHUSTER; FLOWERS; FARLEY, 2006). The influence of those factors on AHe age dispersion is dependent on the cooling rate or residence time within the Helium Partial Retention Zone (AHePRZ, 40 – 80 °C, (FARLEY, 2002), i.e., the longer the samples spent time at this zone, those factors tend to enhance age dispersion.

Tab. 1 - AHe data from the northwestern Angolan Shield, Ancient Plateau region

sample	grain	^{4}He (ncc)	^{238}U (ppm)	^{235}U (ppm)	^{232}Th (ppm)	^{147}Sm (ppm)	Th/U	eU[a] (ppm)	L[b] (µm)	W[c] (µm)	Rs[d] (µm)	T[e]	Raw Age ± UC[f] (Ma)	F_T[g]	Corrected Age ± UC[f] (Ma)
PT-29	1	252.74	33.24	0.24	5.62	55.37	0.17	34.80	347.27	159.24	97.15	2	64.9 ± 2.2	0.85	76.8 ± 2.6
PT-29	2	143.40	23.58	0.17	2.60	51.64	0.11	24.36	370.23	125.26	80.35	2	52.5 ± 2.0	0.81	64.5 ± 2.4
PT-29	3	120.01	18.97	0.14	2.98	43.37	0.16	19.81	372.56	180.14	108.80	1	54.0 ± 2.0	0.86	62.6 ± 2.4
PT-29	4	226.28	33.16	0.24	5.60	73.24	0.17	34.71	219.07	150.15	83.87	2	58.1 ± 2.0	0.82	70.7 ± 2.4
PT-29	5	298.85	41.63	0.30	5.54	61.92	0.13	43.23	260.57	131.89	78.94	1	61.9 ± 1.9	0.81	76.4 ± 2.4
PT-29	6	251.45	38.97	0.28	4.65	79.03	0.12	40.34	264.9	139.06	82.61	1	55.6 ± 2.0	0.82	67.9 ± 2.4
													8.3%		
PT-08	2	2808.50	98.64	0.72	8.34	73.10	0.08	101.32	264.74	133.18	79.81	2	245.5 ± 6.4	0.81	302.3 ± 7.8
PT-08	3	1463.19	41.25	0.30	19.67	153.78	0.48	46.17	256.69	87.61	56.13	2	274.4 ± 10.4	0.73	374.4 ± 14.4
PT-08	4	4034.10	132.53	0.96	18.91	77.12	0.14	137.94	235.16	149.99	85.29	2	259.0 ± 5.6	0.82	314.3 ± 6.8
PT-08	5	4738.54	132.94	0.96	21.98	84.51	0.17	139.07	293.56	106.48	67.60	2	300.5 ± 6.6	0.78	386.2 ± 8.6
PT-08	6	3138.04	99.08	0.72	24.36	65.61	0.25	105.52	318.36	145.42	88.79	2	263.2 ± 5.8	0.83	316.7 ± 7.0
PT-08	7	5170.44	134.17	0.97	21.24	74.01	0.16	140.13	264.75	127.55	77.09	2	324.9 ± 7.0	0.81	403.4 ± 8.6
PT-08	8	3324.11	112.14	0.81	23.23	75.08	0.21	118.41	316.88	139.69	85.85	2	248.8 ± 5.6	0.83	301.4 ± 6.8
PT-08	9	5020.39	126.06	0.91	22.96	76.62	0.18	132.37	256.69	146.64	85.55	2	333.6 ± 7.2	0.82	404.5 ± 8.8
PT-08	10	3263.57	87.36	0.63	10.83	89.15	0.12	90.53	281.72	108.63	68.30	2	316.5 ± 8.8	0.78	405.6 ± 11.2
													12.0%		
Lorelei	1	1054.90	32.46	0.24	14.49	118.64	0.45	36.10	142.7	97.86	54.65	2	253.5 ± 9.0	0.73	349.4 ± 12.4
Lorelei	2	1005.34	25.87	0.19	7.79	103.46	0.30	27.89	162.05	78.97	47.62	2	310.1 ± 12.3	0.69	452.7 ± 18.0
Lorelei	3	843.90	22.80	0.17	2.89	68.94	0.13	23.65	128.75	88.77	49.51	2	308.8 ± 19.8	0.70	443.0 ± 28.4
Lorelei	4	8076.72	177.11	1.28	38.93	254.17	0.22	187.54	125.71	78.76	44.98	2	375.1 ± 11.1	0.67	562.8 ± 16.7
Lorelei	5	1210.44	35.66	0.26	1.06	117.71	0.03	36.16	179.35	115.95	65.72	2	289.3 ± 27.9	0.77	374.9 ± 36.1
Lorelei	6	656.26	15.14	0.11	24.17	88.01	1.60	20.93	259.55	104.74	65.37	2	270.0 ± 9.6	0.77	350.5 ± 12.5

Lorelei	7	992.74	38.60	0.28	3.32	150.59	0.09	39.66	201.34	91.23	55.78	2	197.5 ± 11.4	0.73	270.1 ± 15.6
													19.2%		
PT-12B	1	3249.21	72.54	0.53	11.15	40.54	0.15	75.69	145.62	145.62	72.81	2	343.1 ± 8.5	0.75	459.8 ± 11.4
PT-12B	2	5409.73	140.53	1.02	30.17	83.95	0.21	148.64	141.57	109.72	59.31	2	292.2 ± 6.2	0.75	391.1 ± 8.3
													11.3%		
PT 13	2	600.89	23.40	0.17	0.42	25.01	0.02	23.67	278.42	174.28	99.55	2	204.6 ± 30.3	0.85	240.9 ± 35.7
PT 13	3	1223.27	39.40	0.29	9.93	23.49	0.25	42.02	223.34	127.8	74.53	2	235.0 ± 5.2	0.80	294.2 ± 6.5
PT 13	5	5094.79	122.61	0.89	12.70	71.96	0.10	126.49	213.91	136.43	77.58	2	322.4 ± 7.5	0.81	399.6 ± 9.3
PT 13	6	427.35	17.98	0.13	1.35	16.10	0.08	18.42	225.43	178.16	95.77	1	187.5 ± 8.9	0.84	222.3 ± 10.5
													25.3%		
		(cc)	(ng)	(ng)	(ng)	(ng)									
Durango	DUR-1-4-18	1.41E-09	0.07	0.0005	1.36	0.14	20.38	—	—	—	—	—	32.9 ± 0.6	—	—
Durango	DUR-2-4-18	1.58E-09	0.07	0.0005	1.50	0.14	20.88	—	—	—	—	—	33.5 ± 0.6	—	—
Durango	DUR-3-4-18	1.54E-09	0.08	0.0006	1.50	0.17	19.45	—	—	—	—	—	32.2 ± 0.6	—	—
Durango	DUR-4-4-18	1.21E-09	0.06	0.0004	1.13	0.11	19.99	—	—	—	—	—	33.6 ± 0.6	—	—
Durango	DUR-5-4-18	1.67E-09	0.07	0.0005	1.61	0.18	21.97	—	—	—	—	—	33.1 ± 0.6	—	—
													1.7%		

(a) Effective uranium calculated as [U ppm] + (0.235 * [Th ppm]) (SHUSTER; FLOWERS; FARLEY, 2006). (b) Length and (c) width of the crystal or crystal fragment. (d) Radius of a sphere with the equivalent surface area-to volume ratio as cylindrical crystal (MEESTERS; DUNAI, 2002), Rs = (3*(RL))/(2*(R+L)) where R = W/2. (e) Number of terminations (tips) identified on crystals, 0 = no termination, 1T = one termination, and 2T = two terminations. (f) Estimate uncertainty equal to 2σ analytical error in the AHe ages based on U, Th, Sm, and He measurements. (g) Correction factor for alpha-ejection (FARLEY; WOLF; SILVER, 1996) assuming a homogeneous distribution of U and Th within the crystals. Corrected AHe age = raw AHe age/Ft. The percentage of age dispersion of each sample is quoted below their raw ages

In the plots AHe age versus effective uranium (eU) (Fig. 3), samples PT-29 and PT-13 show weak and strong positive correlations, respectively, whereas in the plots AHe age versus spherical radius (Rs) (Fig. 3), only samples Lorelei and PT-13 show negative correlations. Grain morphology (BEUCHER et al., 2013; BROWN et al., 2013) does not appear to be a major source of age dispersion in the sample PT-29, where grains with one broken tip (i.e., that preserve only one termination – 1T) were also analysed. However, the 1T fragments appear to disrupt the AHe age – Rs relationship in this sample (Fig. 3).

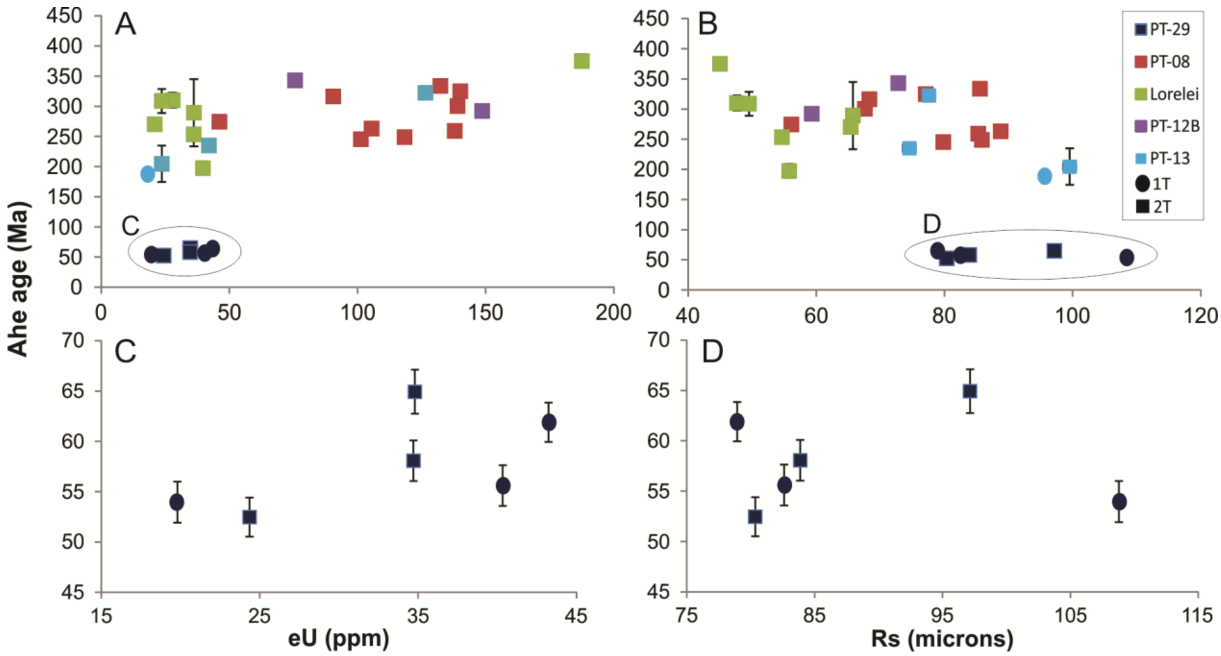

Fig. 3 a) Correlation between single-grain AHe age and eU, and b) correlation between AHe age and Rs. c) Detail of the AHe age – eU, and d) AHe age – Rs correlations in the sample PT-29, where 1T fragments were also analysed

Nevertheless, other causes for intra-sample AHe age dispersion, such as the presence of inclusions (VERMEESCH et al., 2007), neighbouring minerals (SPIEGEL et al., 2009), or grain boundary phases (MURRAY; ORME; REINERS, 2014) rich in uranium and thorium, which all these introduce foreign helium into the grains, a priori, may be discarded as primary sources of age dispersion because most of the analysed grains are relatively high eU (Tab. 1, Fig. 3), and therefore, they are less sensitive to these factors (MORÓN et al., 2020). In summary, most of the intra-sample scatter in the AHe ages may be roughly explained in terms of the cooling rate of the samples through the AHePRZ, i.e., AHe age dispersion appears to most reflect the thermal histories of the samples, which are outlined further below.

4 THERMAL HISTORIES FROM THE NORTHWESTERN ANGOLAN SHIELD

4.1 Thermal Modelling Strategy

The Bayesian trans-dimensional Markov Chain Monte Carlo (MCMC) approach of the QTQt software (GALLAGHER, 2012) uses the inversion strategy, in which the unknown model parameters are extracted from the data by sampling within a defined model space, i.e., the MCMC sampling aims to find a set of acceptable thermal histories (time-temperature simulations) that best fit the data, and express these histories solutions in terms of the posterior probability distribution. The Bayesian structure utilises the prior probability density function of the model (i.e., represent initial information parameters of the model such as geological constraints, etc.) and utilises a likelihood function that estimates the probability of determined parameter model in fitting the data. Thus, the likelihood function improves the prior distribution to generate the posterior one (GALLAGHER, 2012).

The process of generating a set of acceptable thermal histories involves successive iterations, where in each of them a new model is produced by random modification of the current (former) model (i.e., Markov Chain mean that a new model is generated conditional to the prior model; (GALLAGHER et al., 2009), and based on an acceptance criterion the MCMC decides for utilising either the former or the new proposed model. Therefore, each iteration provides only one model that may compose the posterior distribution. The MCMC starts the process from an initial model randomly sampled from the model space and the following sampled models tend to be less complex (i.e., the time-temperature curve tend to show less deflexions and nodes) and best fitting the observed data (i.e., the likelihood function values are increased) (GALLAGHER, 2012; GALLAGHER et al., 2009). Thus, the posterior probability distribution is effectively estimated after discarding a set of initial thermal history models provided during the “burn-in” period, and by considering the range of models generated during the “post burn-in” period. The latter is considered to be the period where the likelihood values do not significantly change with increasing the number of iterations, i.e., the likelihood function can no longer improve the current models (GALLAGHER, 2012; GALLAGHER et al., 2009).

So far, the thermal history of the northern Angolan plateau was obtained in terms of time-temperature simulations, by inversion of the all single-grain AHe data (age, eU concentration, grain morphology and size) in each sample. The helium diffusion model of (GAUTHERON et al., 2009) was used for 2T grains, whereas the approach of (BROWN et al., 2013) was utilised for 1T fragments. The MCMC was applied with 100.000 iterations as burn-in and another 100.000 ones as post-burn in period. The time-temperature simulations were interpreted in terms of their expected model, which consists of an average of the models sampled during the post burn-in stage (GALLAGHER, 2012).

4.2 Thermal History Constraints and Results

Prior time-temperature constraints (i.e., t-T boxes within the model space where simulations must pass) (Fig. 4) were established based on available geological information. A first t-T constraint of 0 – 140 °C at 600 – 480 Ma permits that samples reached shallow crustal depths during the Pan-African Orogeny, taking into account that red bed sandstones of the Inkisi Group overlain the basement further northeast of the analysed samples (Fig. 2a). The second imposed constraint of 0 – 140 °C at 340 – 260 Ma permits that the basement rocks reached shallow crustal depths at the onset of the Karoo Supergroup deposition, as Permian-Triassic Karoo rocks are preserved at the Cassange Graben (Fig. 2a). A third constraint of 0 – 30 °C at 56 – 20 Ma represents that the basement was near surface temperatures at the deposition of the Grès Polimorphes sediments during the Paleogene. An additional constraint of 0 – 140 °C at 130 – 70 Ma was exclusively applied to the Lorelei sample to test a possible thermal effect of the kimberlite eruption on this sample. Finally, a current surface temperature of 0 – 30 °C was chosen for the present-day basement.

Thermal histories from samples Lorelei, PT-08, and PT-13 require temperatures of ~ 10 - 80 °C at ~ 580 – 540 Ma, from which a heating interval is observed. These samples reach peak temperatures of 60 – 110 °C at 340 – 280 Ma, from which a rapid cooling (samples Lorelei and PT-08) or a more protracted cooling (sample PT-13) occurs (Fig. 4). Sample PT-12B supports relatively high temperatures of ~ 110 °C at 520 – 500 Ma followed by a cooling interval until ~ 300 Ma, however, this sample yielded only two apatite grains and hence its thermal history is poorly constrained relatively to the other samples (Fig. 4). On the other hand, sample PT-29 shows a distinctive thermal history supporting a cooling event at ~ 90 – 50 Ma from peak temperatures about ~ 100 °C. All samples require the maintenance of temperatures below ~ 30 °C after their major cooling intervals (Fig. 4).

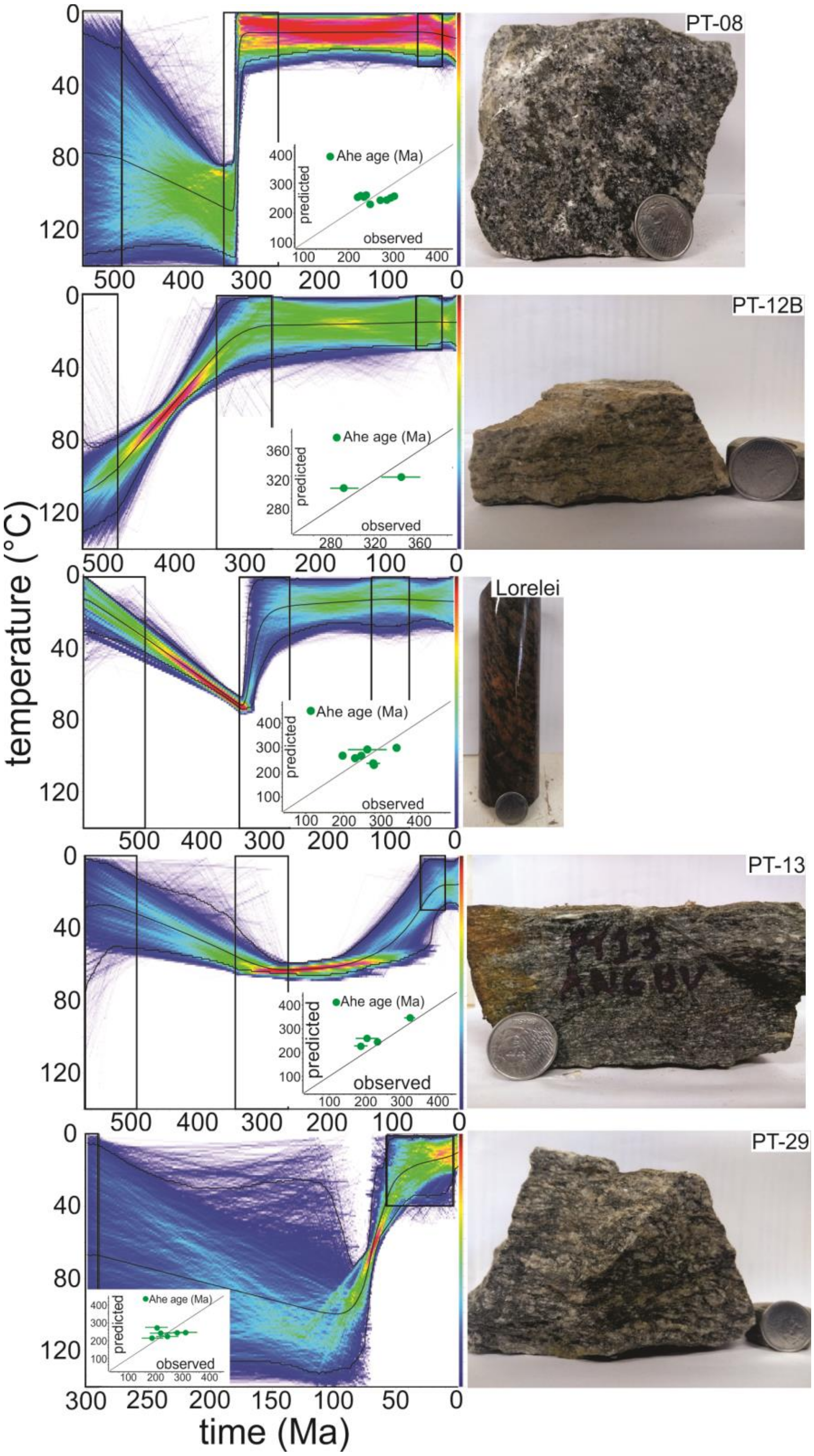

Fig. 4 AHe thermal history models (left hand side) and the analysed basement samples from the Angolan Shield, collected in the northwestern Ancient plateau (right hand side). The expected model (average of the posterior distribution) is the central black line, and the 95 % credible interval is bounded by the two peripheral black lines; black boxes are t-T geological constraints where models should pass, and the probability of samples have experienced any t-T condition in the past, increase from blue to red colours in the plots. The ages predicted by the models are also plotted against the measured ages

The low intra-sample AHe age dispersion (<20 %, Tab. 1) for most samples supports that they experienced relatively rapid cooling through AHePRZ, i.e., in the Carboniferous-Permian (samples Lorelei and PT-08) and in the Late Cretaceous (sample PT-29), respectively. By contrast, the more dispersive ages of sample PT-13 (>20 %, Tab. 1) indicate more prolonged cooling within the AHePRZ in comparison to the other samples. These data aspects are in agreement with the inferred thermal histories (Fig. 4).

5 CONTRIBUTIONS TO DENUDATION HISTORY OF THE NORTHWESTERN ANGOLAN SHIELD: GEOLOGICAL AND GEOMORPHOLOGICAL IMPLICATIONS

5.1 Cambrian - Carboniferous Basement Burial

The heating interval commencing by ~ 580 – 540 Ma (Fig. 4) roughly coincides with the onset of the deposition of the Inkisi Group, which outcrops few tens of kilometres farther northeast of the analysed samples (Fig. 2a). Thus, we consider that the Inkisi rocks likely extended across much of the Angolan Shield to the west, and this is consistent with the propositions of (LINOL et al., 2015a) that the Inkisi Group covered a wider area forming the foreland of the West Congo Belt (Fig. 5). In Angola, the Inkisi Group rocks were formed possibly before ~ 320 Ma (MIYOUNA et al., 2018) and after ~ 540 Ma (JELSMA et al., 2011). Thus, assuming that the peak Carboniferous – Permian temperatures of ~ 60 – 110 °C (Fig. 4) are most ascribed to the burial by the Inkisi cover, it is estimated an overburden of ~ 1.5 – 4.5 km across the area, assuming regional geothermal gradients of 20 - 30 °C/km (GREEN; MACHADO, 2015; JACKSON; HUDEC; HEGARTY, 2005).

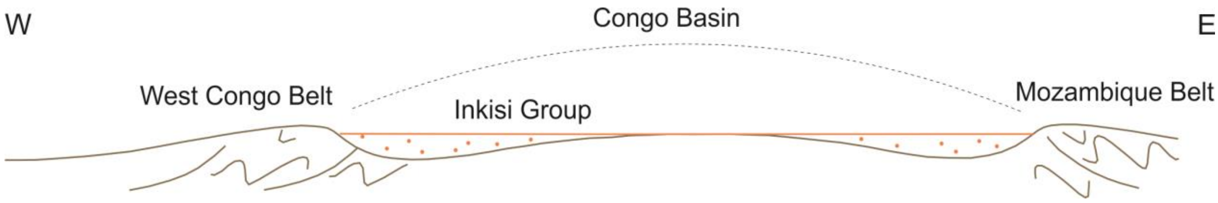

Fig. 5 Simplified transect showing the Neoproterozoic – Paleozoic Inkisi Group filling the foreland domain of the WCPB, redrawn from (LINOL et al., 2015a)

5.2 Carboniferous - Permian Basement Denudation

The Carboniferous – Permian subsequent cooling event starting ca. ~ 340 – 280 Ma (Fig. 4) appears to record the removal of most of the Inkisi overburden from the northwestern Angolan Shield. This is consistent with the observations of (JACKSON; HUDEC; HEGARTY, 2005) that the Neoproterozoic cover occurs mainly as minor outliers south of the Kwanza horst, indicating that most of the original cover was removed by erosion. In addition, similar episodes of accelerated basement cooling have been reported in other parts of Africa (GREEN; MACHADO, 2015; KASANZU, 2017; KASANZU et al., 2016; KROB et al., 2020; MACKINTOSH et al., 2017) and in South America (BORBA; VIGNOL-LELARGE; MIZUSAKI, 2002; DORANTI-TIRITAN et al., 2014; FONSECA et al., 2020; MACHADO et al., 2020; RIBEIRO et al., 2005), which are, in a general sense, ascribed to crustal uplift and denudation resulted from the intra-plate stresses generated by the Western Gondwana orogenies, associated to the Pangea Supercontinent assembly (VEEVERS, 2004) (Fig. 6a). Furthermore, the Carboniferous – Permian basement cooling event also overlaps with major glaciation episodes affecting the Gondwanaland (DÁVILA et al., 2021; ISBELL et al., 2012) (Fig. 6b), supporting that this cooling event may be also associated with denudation driven by glacial dynamics (GREEN; MACHADO, 2015; KASANZU et al., 2016; VEEVERS, 2004). Sediments produced during that time were possibly deposited into the Gondwanan intracontinental basins (Fig. 6c), as suggested, for example, by synchronous subsidence episodes affecting the Parana and Congo basins through Carboniferous – Permian times (LINOL et al., 2015a; MILANI; DE WIT, 2008). However, it is important to highlight that a more complete sediment provenance analysis is required to address these questions (ALESSANDRETTI; WARREN, 2022), and this is beyond the scope of this work.

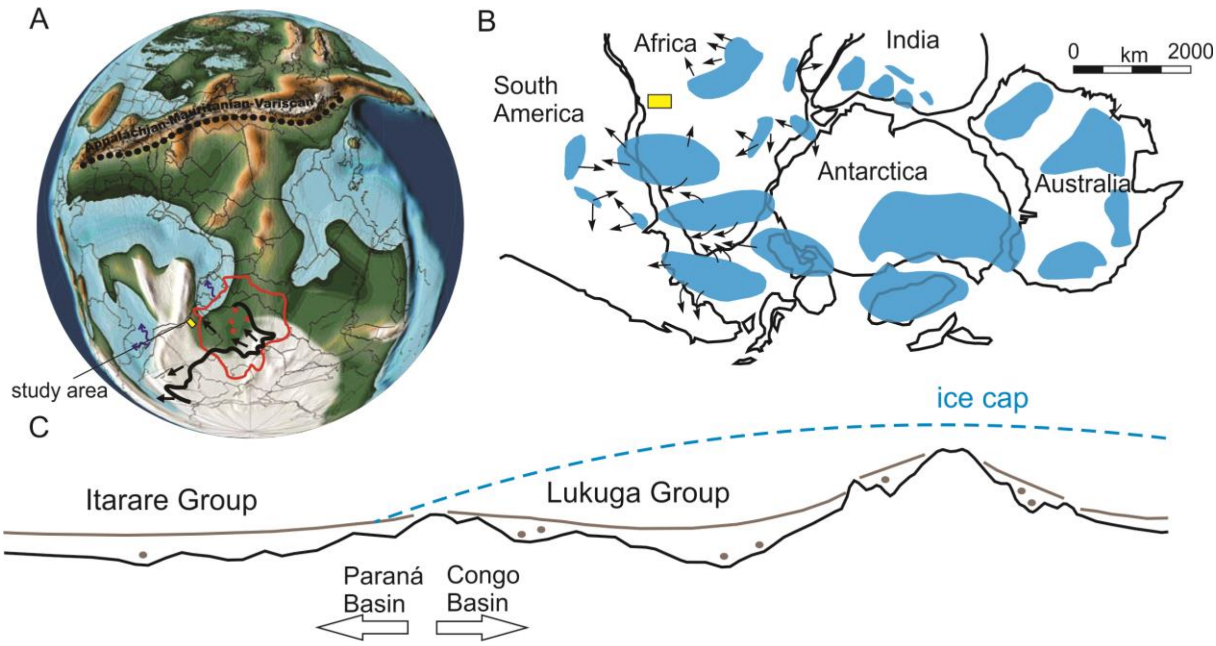

Fig. 6 a) Paleogeographic reconstruction for the Late Carboniferous (Pennsylvanian) (after (LINOL et al., 2015a) showing the Variscan Orogeny in the north (dotted black line), the boundary of the Congo Basin (red line), fluvio-marine and glacial flow directions (blue and black arrows), and a major ice cap covering most of the southern hemisphere. b) Another paleogeographic reconstruction for the Pennsylvanian – Early Permian times (modified from (ISBELL et al., 2012) showing ice sheets (blue) and flow directions (arrows). c) Simplified transect showing Carboniferous to Early Permian glacial – periglacial deposits from the Paraná and Congo Basins (LINOL et al., 2015a). The yellow boxes indicate the approximate location of the study area.

Another relevant point regards the fact that sample Lorelei (collected at the contact with the Lorelei kimberlite pipe) does not show any evident heating likely induced by the kimberlite emplacement. For a while, it is interpreted here that if some thermal disturbance occurred, it was minimal.

5.3 Late Cretaceous - Paleocene Basement Denudation

The Late Cretaceous – Paleocene cooling ca. ~ 90 – 50 Ma (Fig. 4) may correspond to a second important phase of uplift and denudation affecting parts of the northwestern Angolan Shield. Similar denudation events have also been interpreted in the Kwanza (JACKSON; HUDEC; HEGARTY, 2005) and Namibe (GREEN; MACHADO, 2015) margins (Fig. 1c, 2a). Assuming regional geothermal gradients of 20 – 30 °C (GREEN; MACHADO, 2015; JACKSON; HUDEC; HEGARTY, 2005), this Late Cretaceous – Paleocene cooling event records the removal of ca. ~ 2.6 – 4 km of rock section from this part of the Angolan Shield.

As mentioned earlier, the Late Cretaceous marks the onset of large-scale denudation episodes in the southern African plateau, which led to the increase in sedimentation rates into the marginal basins related to the development of thick depocenters (BABY et al., 2020; BRAUN et al., 2014; GUILLOCHEAU et al., 2012; MACGREGOR, 2013). Reactivation of ancient basement structures and crustal uplift at that time would be consequence of far-field compressional stresses (GUIRAUD; BOSWORTH, 1997) and/or the result of mantle plumes activity beneath the African plate (BRAUN et al., 2014; O'CONNOR et al., 2018). In Angola, the Late Cretaceous uplift caused the tilt of the margin triggering raft tectonics (i.e., salt movement offshore) in the Kwanza Basin (CRAMEZ; JACKSON, 2000). However, the Late Cretaceous – Paleocene interval is marked by the prevalence of low sedimentation rates and the overall starvation of the Angolan marginal basins (MACGREGOR, 2013), excepting for the development of a major depocenter in the offshore Kwanza Basin, which coincides with the present-day Kwanza river mouth (LETURMY; LUCAZEAU; BRIGAUD, 2003) (Fig. 7). The Kwanza river currently flows northwards across the Angola Dome, until it deflects in the direction of the South Atlantic Ocean (Fig. 1c). So far, it is proposed here that parts of the northwestern Angolan Shield were potential source areas for the sediments deposited into the Kwanza Basin during the Late Cretaceous – Paleocene denudation event.

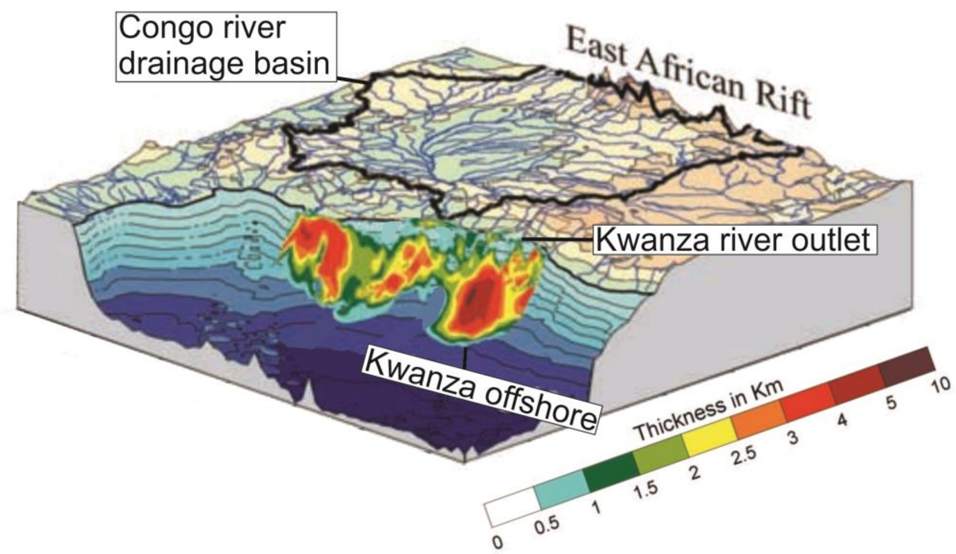

Fig. 7 Late Cretaceous – Paleocene sediment accumulation along the western African margin, with emphasis on the offshore Kwanza Basin and the Kwanza river outlet, redrawn from (LETURMY; LUCAZEAU; BRIGAUD, 2003)

5.4 Late Cenozoic Differential Denudation between the Coastal Zone and the Ancient Plateau

It is interesting to note that the AHe thermal histories presented here do not support substantial Cenozoic cooling, indicating that samples have been maintained near surface temperatures (< 40 °C, Fig. 4) and the amplitude of the Cenozoic denudation in the area has been low (likely below ~ 1 km). Despite this, this portion of the Ancient plateau and margin has experienced high amplitude Late Cenozoic (i.e., since ~ 40–30 Ma) uplifts as supported by a number of works (AL-HAJRI; WHITE; FISHWICK, 2009; GUILLOCHEAU et al., 2018; GUIRAUD; BUTA-NETO; QUESNE, 2010; HUDEC; JACKSON, 2002, 2004; JACKSON; HUDEC; HEGARTY, 2005; LETURMY; LUCAZEAU; BRIGAUD, 2003; LUNDE et al., 1992; ROBERTS; WHITE, 2010; WALKER et al., 2016). These uplifts are particularly associated to the second phase of raft tectonics in the Kwanza Basin (CRAMEZ; JACKSON, 2000; SPATHOPOULOS, 1996), to the truncation of marine strata offshore (AL-HAJRI; WHITE; FISHWICK, 2009), to the warping and elevation of marine strata, paleodeltas, and paleovalleys onshore (GUIRAUD; BUTA-NETO; QUESNE, 2010; WALKER et al., 2016), and they likely account for the convex long profiles of rivers that drain the Ancient Plateau (GUIRAUD; BUTA-NETO; QUESNE, 2010; LETURMY; LUCAZEAU; BRIGAUD, 2003; ROBERTS; WHITE, 2010). Late Cenozoic uplift of the Ancient plateau is also suggested by the increase in the terrigenous sedimentation rates into the Kwanza Basin in the Oligocene, with a dramatic increase in the Mid to Late Miocene around ~ 20 Ma (MACGREGOR, 2013; SÉRANNE; ANKA, 2005) that is also illustrated by a decrease in the sediment maturity offshore (MACHADO, 2007). The later event is consistent with a major Oligocene-Miocene unconformity offshore Angola, separating carbonate strata from overlapping siliciclastic strata (JACKSON; HUDEC; HEGARTY, 2005; ROBERTS; WHITE, 2010). In addition, substantial Cenozoic denudation of the eastern rim of the Kwanza Basin is also evidenced by the exposition of older stratigraphic levels (Cretaceous) whose width and deep of incision suggest that denudation was quite uniform along the basin rim (Fig. 2a), and it was related to values from ~ 600 to 2000 m depending on the assumed geometry of the basin edge (HUDEC; JACKSON, 2002, 2004; JACKSON; HUDEC; HEGARTY, 2005). Most of this denudation likely took place post ~ 40 Ma considering that Eocene strata outcrops seaward, but are lacking at the eastern basin rim. These stratigraphic information used in combination with vitrinite reflectance (LUNDE et al., 1992; MACHADO, 2007) and AFT data (JACKSON; HUDEC; HEGARTY, 2005; MACHADO, 2007) indicate that ~ 1500 – 2000 m (or more) of Oligocene to Miocene denudation took place in the eastern basin rim and the adjacent Precambrian basement. By the presented above, the most probable scenario is that differential Oligocene to Miocene denudation has taken place between the Coastal Zone (Kwanza margin) and the Ancient Plateau. This relatively higher Oligocene to Miocene denudation detected at the Coastal Zone matches with its present-day low elevation in comparison to the Ancient plateau characterized by high elevation (Fig. 1c). Therefore, it is reasonable to think that most of the relief created between these two zones has been formed through the Late Cenozoic times.

It is important to note that at this portion of the Ancient plateau occur remnants of etchplains preserved at elevations of ~ 1600 m. The Late Cretaceous-Paleocene cooling recorded in the sample PT-29 (Fig. 4) temporally overlap with the erosion phase estimated for the development of the Upper surface 1 (GUILLOCHEAU et al., 2015), however, most samples yielded only Carboniferous-Permian cooling (Fig. 4) that is much older than the erosion phases of both Upper 1 and 2 surfaces (GUILLOCHEAU et al., 2015). This suggest that at least the Upper surface 2 was developed under low amounts of Cenozoic denudation that is outside the AHe method sensitivity, and therefore, prudence must be taken in interpreting the origin of these planation surfaces by means of thermochronology. Nevertheless, at the Coastal Zone (Fig. 2b) the preserved planation surfaces (GUILLOCHEAU et al., 2015) (Fig 2c), as well as the vitrinite reflectance and AFT data (JACKSON; HUDEC; HEGARTY, 2005; LUNDE et al., 1992; MACHADO, 2007) converge that denudation events post ~ 40–30 Ma occurred in the Coastal Zone.

In summary, while there is no more quantitative data across the region, the AHe data presented here in combination with previous work suggest that not only the regional topography is post ~ 40–30 Ma (BURKE; GUNNELL, 2008; GUILLOCHEAU et al., 2018; ROBERTS; WHITE, 2010), but at least part of the relief between the Coastal Zone and the Ancient Plateau has been formed at this time. This is in close agreement to works suggesting that the Great Escarpment is not a rift-related feature, but rather, it formed much later during Cenozoic times as has been proposed for the Namibe margin further south (GREEN; MACHADO, 2015), other parts of southern Africa (BURKE; GUNNELL, 2008; GREEN et al., 2016; PICART et al., 2020), and worldwide (GREEN et al., 2017; JAPSEN et al., 2006, 2012). In addition, if the Angola Dome has been formed by dynamic uplifts since ~ 40–10 Ma (BURKE; GUNNELL, 2008; GUILLOCHEAU et al., 2018; ROBERTS; WHITE, 2010), the model of (BURKE; GUNNELL, 2008) in which the African Great Escarpment has developed by the dissection of some dome flanks since ~ 30 Ma, is consistent with the data and discussions presented here.

References

AL-HAJRI, Y.; WHITE, N.; FISHWICK, S. Scales of transient convective support beneath Africa. **Geology**, v. 37, n. 10, p. 883–886, 2009.

ALESSANDRETTI, L.; WARREN, L. V. Comments on "Devonian to Permian post-orogenic denudation of the Brasília Belt of West Gondwana: Insights from apatite fission track thermochronology" by Fonseca et al. (2020). **Journal of Geodynamics**, v. 149, n. August 2021, p. 101892, 2022.

BABY, G. et al. Solid sedimentation rates history of the Southern African continental margins: Implications for the uplift history of the South African Plateau. **Terra Nova**, v. 32, n. 1, p. 53–65, 2020.

BEUCHER, R. et al. Natural age dispersion arising from the analysis of broken crystals: Part II. Practical application to apatite (U-Th)/He thermochronometry. **Geochimica et Cosmochimica Acta**, v. 120, p. 395–416, 2013.

BORBA, A. W.; VIGNOL-LELARGE, M. L. M.; MIZUSAKI, A. M. P. Uplift and denudation of the Caçapava do Sul granitoids (southern Brazil) during Late Paleozoic and Mesozoic: Constraints from apatite fission-tract data. **Journal of South American Earth Sciences**, v. 15, n. 6, p. 683–692, 2002.

BRAUN, J. et al. Rapid erosion of the Southern African Plateau as it climbs over a mantle superswell. **Journal of Geophysical Research: Solid Earth**, v. 119, p. 6093–6112, 2014.

BROWN, R. W. et al. Natural age dispersion arising from the analysis of broken crystals . Part I : Theoretical basis and implications for the apatite (U – Th)/ He thermochronometer. **Geochimica et Cosmochimica Acta**, p. 478–497, 2013.

BURKE, K.; GUNNELL, Y. **The african erosion surface: A Continental-Scale Synthesis of Geomorphology, Tectonics, and Environmental Change over the Past 180 Million Years**. Memoir 201 ed. Boulder, Colorado: Geological Society of America, 2008.

CELLI, N. L. et al. The upper mantle beneath the South Atlantic Ocean, South America and Africa from waveform tomography with massive data sets. **Geophysical Journal International**, v. 221, n. 1, p. 178–204, 2020.

CRAMEZ, C.; JACKSON, M. P. A. Superposed deformation straddling the continental-oceanic transition in deep-water Angola. **Marine and Petroleum Geology**, v. 17, n. 10, p. 1095–1109, 2000.

DÁVILA, F. M. et al. Effects of uplift on Carboniferous exhumation and mountain glaciations in pericratonic areas of SW Gondwana, central Argentina. **Tectonics**, 2021.

DE CARVALHO, H. et al. Geochronological review of the Precambrian in western Angola: Links with Brazil. **Journal of African Earth Sciences**, v. 31, n. 2, p. 383–402, 2000.

DINIZ, A. C. **Características mesológicas de Angola**. Nova Lisboa: Missão de Inquéritos Agrícolas de Angola, 1973.

DORANTI-TIRITAN, C. et al. Evolução do relevo da região do planalto de Poços de Caldas (Sp/Mg) baseada em dados de termocronologia de baixa temperatura e modelagem termocinemática 3D. **Revista Brasileira de Geomorfologia**, v. 15, n. 2, 2014.

EHLERS, T. A.; FARLEY, K. A. Apatite (U-Th)/He thermochronometry: Methods and applications to problems in tectonic and surface processes. **Earth and Planetary Science Letters**, v. 206, n. 1–2, p. 1–14, 2003.

ENKELMANN, E.; GARVER, J. I. Low-temperature thermochronology applied to ancient settings. **Journal of Geodynamics**, v. 93, p. 17–30, 2016.

FARLEY, K. A. (U-Th)/He Dating: Techniques, Calibrations, and Applications. **Reviews in Mineralogy and Geochemistry**, v. 47, n. 1, p. 819–844, 2002.

FARLEY, K. A.; WOLF, R. A.; SILVER, L. T. The effects of long alpha-stopping distances on (U-Th)/He ages. **Geochimica et Cosmochimica Acta**, v. 60, n. 21, p. 4223–4229, 1996.

FITZGERALD, P. G. et al. Interpretation of (U-Th)/He single grain ages from slowly cooled crustal terranes: A case study from the Transantarctic Mountains of southern Victoria Land. **Chemical Geology**, v. 225, n. 1–2, p. 91–120, 2006.

FLOWERS, R. M. et al. Apatite (U-Th)/He thermochronometry using a radiation damage accumulation and annealing model. **Geochimica et Cosmochimica Acta**, v. 73, n. 8, p. 2347–2365, 2009.

FLOWERS, R. M.; KELLEY, S. A. Interpreting data dispersion and “ inverted” dates in apatite (U-Th)/He and fission-track datasets: An example from the US midcontinent. **Geochimica et Cosmochimica Acta**, v. 75, n. 18, p. 5169–5186, 2011.

FLOWERS, R. M.; SCHOENE, B. (U-Th)/He thermochronometry constraints on unroofing of the eastern Kaapvaal craton and significance for uplift of the southern African plateau. **Geology**, v. 38, n. 9, p. 827–830, 2010.

FONSECA, A. C. et al. Devonian to Permian post-orogenic denudation of the Brasília Belt of West Gondwana: insights from apatite fission track thermochronology. **Journal of Geodynamics**, v. 137, n. March, 2020.

GALLAGHER, K. et al. Markov chain Monte Carlo (MCMC) sampling methods to determine optimal models, model resolution and model choice for Earth Science problems. **Marine and Petroleum Geology**, v. 26, n. 4, p. 525–535, 2009.

GALLAGHER, K. Transdimensional inverse thermal history modeling for quantitative thermochronology. **Journal of Geophysical Research: Solid Earth**, v. 117, n. 2, p. 1–16, 2012.

GAUTHERON, C. et al. Effect of alpha-damage annealing on apatite (U–Th)/He thermochronology. **Chemical Geology**, v. 266, n. 3–4, p. 157–170, 2009.

GAUTHERON, C. et al. Chemical influence on α-recoil damage annealing in apatite: Implications for (U – Th)/He dating. **Chemical Geology**, v. 351, p. 257–267, 2013.

GIULIANI, A. et al. Southwestern Africa on the burner: Pleistocene carbonatite volcanism linked to deep mantle upwelling in Angola. **Geology**, v. 45, n. 11, p. 971–974, 2017.

GREEN, P. F. et al. Post-breakup burial and exhumation of the southern margin of Africa. **Basin Research**, v. 29, n. 1, p. 1–32, 2016.

GREEN, P. F. et al. Post-breakup burial and exhumation of passive continental margins : Seven propositions to inform geodynamic models. **Gondwana Research**, 2017.

GREEN, P. F.; MACHADO, V. Pre-rift and synrift exhumation, post-rift subsidence and exhumation of the onshore Namibe Margin of Angola revealed from apatite fission track analysis. **Geological Society, London, Special Publications**, v. 438, p. 99–118, 2015.

GROVES, D. I.; SANTOSH, M. Craton and thick lithosphere margins: The sites of giant mineral deposits and mineral provinces. **Gondwana Research**, v. 100, p. 195–222, 2021.

GUILLOCHEAU, F. et al. Quantification and causes of the terrigeneous sediment budget at the scale of a continental margin: A new method applied to the Namibia-South Africa margin. **Basin Research**, v. 24, n. 1, p. 3–30, 2012.

GUILLOCHEAU, F. et al. Cenozoic Landscape Evolution in and Around the Congo Basin: Constraints from Sediments and Planation Surfaces. In: DE WIT, M. J.; GUILLOCHEAU, F.; DE WIT, M. C. J. (Eds.). . **Geology and Resource Potential of the Congo Basin**. Berlin-Heidelberg: Springer, 2015. p. 1–417.

GUILLOCHEAU, F. et al. Planation surfaces as a record of mantle dynamics: The case example of Africa. **Gondwana Research**, v. 53, p. 82–98, 2018.

GUIRAUD, M.; BUTA-NETO, A.; QUESNE, D. Segmentation and differential post-rift uplift at the Angola margin as recorded by the transform-rifted Benguela and oblique-to-orthogonal-rifted Kwanza basins. **Marine and Petroleum Geology**, v. 27, n. 5, p. 1040–1068, 2010.

GUIRAUD, R.; BOSWORTH, W. Senonian basin inversion and rejuvenation of rifting in Africa and Arabia: synthesis and implications to plate-scale tectonics. **Tectonophysics**, v. 282, n. 1–4, p. 39–82, 1997.

HEILBRON, M. et al. Correlation of Neoproterozoic terrane between te Ribeira Belt, SE Brazil and its African countepart: comparative tectonic evolution and open questions. **Geological Society, London, Special Publications**, v. 294, n. 1, p. 2011–237, 2008.

HUDEC, M. R.; JACKSON, M. P. A. Structural segmentation, inversion, and salt tectonics on a passive margin: Evolution of the Inner Kwanza Basin, Angola. **Bulletin of the Geological Society of America**, v. 114, n. 10, p. 1222–1244, 2002.

HUDEC, M. R.; JACKSON, M. P. A. Regional restoration across the Kwanza Basin, Angola: Salt tectonics triggered by repeated uplift of a metastable passive margin. **AAPG Bulletin**, v. 88, n. 7, p. 971–990, 2004.

HUNTLEY, B. J. Angola in Outline: Physiography, Climate and Patterns of Biodiversity. In: HUNTLEY, B. J. et al. (Eds.). . **Biodiversity of Angola: Science & Conservation: A Modern Synthesis**. [s.l.] Springer, 2019. p. 549.

ISBELL, J. L. et al. Glacial paradoxes during the late Paleozoic ice age: Evaluating the equilibrium line altitude as a control on glaciation. **Gondwana Research**, v. 22, n. 1, p. 1–19, 2012.

JACKSON, M. P. A.; HUDEC, M. R.; HEGARTY, K. A. The great West African Tertiary coastal uplift: Fact or fiction? A perspective from the Angolan divergent margin. **Tectonics**, v. 24, n. 6, p. 1–23, 2005.

JAPSEN, P. et al. Elevated, passive continental margins: Long-term highs or Neogene uplifts? New evidence from West Greenland. **Earth and Planetary Science Letters**, v. 248, n. 1–2, p. 315–324, 2006.

JAPSEN, P. et al. Elevated, passive continental margins: Not rift shoulders, but expressions of episodic, post-rift burial and exhumation. **Global and Planetary Change**, v. 90–91, p. 73–86, 2012.

JELSMA, H. et al. **Kimberlites from Central Angola: A Case Study of Exploration Findings**. (D. G. Pearson et al., Eds.)International Kimberlite Conference 10. **Anais**...Bangalore, India: Springer, 2013

JELSMA, H. A. et al. Preferential distribution along transcontinental corridors of kimberlites and related rocks of Southern Africa. **South African Journal of Geology**, v. 107, n. (1-2), p. 301–324, 2004.

JELSMA, H. A. et al. SHRIMP U-Pb zircon geochronology of basement rocks of the Angolan Shield, western Angola. **23rd Colloquium of African Geology.**, n. January, p. 203, 2011.

JORDAN, T. H. Composition and development of the continental tectosphere. **Nature**, v. 274, p. 544–548, 1978.

KASANZU, C. H. et al. From source to sink in central Gondwana: Exhumation of the Precambrian basement rocks of Tanzania and sediment accumulation in the adjacent Congo basin. **Tectonics**, v. 35, n. 9, 2016.

KASANZU, C. H. Apatite fission track and (U-Th)/He thermochronology from the Archean Tanzania Craton: Contributions to cooling histories of Tanzanian basement rocks. **Geoscience Frontiers**, v. 8, n. 5, p. 999–1007, 2017.

KLÖCKING, M. et al. A tale of two domes: Neogene to recent volcanism and dynamic uplift of northeast Brazil and southwest Africa. **Earth and Planetary Science Letters**, v. 547, p. 116464, 2020.

KOHN, B.; GLEADOW, A. Application of Low-Temperature Thermochronology to Craton Evolution. In: MALUSÀ, M. G.; FITZGERALD, P. G. (Eds.). . **Fission-track thermochronology and its application to geology**. Switzerland: Springer, 2019. p. 393.

KROB, F. C. et al. **Late Neoproterozoic-to-recent long-term t–T-evolution of the Kaoko and Damara belts in NW Namibia**. [s.l.] Springer Berlin Heidelberg, 2020. v. 109

LETURMY, P.; LUCAZEAU, F.; BRIGAUD, F. Dynamic interactions between the gulf of Guinea passive margin and the Congo River drainage basin: 1. Morphology and mass balance. **Journal of Geophysical Research**, v. 108, n. B8, p. 1–13, 2003.

LINOL, B. et al. Multiphase Phanerozoic Subsidence and Uplift History Recorded in the Congo Basin: A Complex Successor Basin. In: DE WIT, M. J.; GUILLOCHEAU, F.; DE WIT, M. C. J. (Eds.). . **Geology and Resource Potential of the Congo Basin**. Verlag Berlin Heidelberg: Springer, 2015a. p. 1–417.

LINOL, B. et al. Paleogeography and Tectono-Stratigraphy of Carboniferous-Permian and Triassic ‘Karoo-Like’ Sequences of the Congo Basin. In: DE WIT, M. J.; GUILLOCHEAU, F.; DE WIT, M. C. J. (Eds.). . **Geology and Resource Potential of the Congo Basin. Regional Geology Reviews**. Verlag Berlin Heidelberg: Springer, 2015b. p. 1–417.

LINOL, B. et al. Facies Analyses, Chronostratigraphy and Paleo-Environmental Reconstructions of Jurassic to Cretaceous Sequences of the Congo Basin. In: DE WIT, M. J.; GUILLOCHEAU, F.; DE WIT, M. C. J. (Eds.). . **Geology and Resource Potential of the Congo Basin, Regional Geology Reviews**. Berlin-Heidelberg: Springer, 2015c. p. 417.

LINOL, B. et al. Formation and Collapse of the Kalahari Duricrust [’African Surface’] Across the Congo Basin, with Implications for changes in Rates of Cenozoic Off-Shore Sedimentation. **Geology and Resource Potential of the Congo Basin**, n. September, p. 1–417, 2015d.

LUNDE, G. et al. Tertiary uplift of the Kwanza Basin in Angola. In: CURNELLE, R. (Ed.). . **Géologie Africaine, Colloques de Geologie de Libreville**. [s.l.] Bull. Cent. de Rech. Explor. Product. Elf Aquitaine Mém, 1992. v. 13p. 99–117.

MACGREGOR, D. S. Late Cretaceous – Cenozoic sediment and turbidite reservoir supply to South Atlantic margins. **Geological Society, London, Special Publications**, v. 369, p. 109–128, 2013.

MACHADO, J. P. S. L. et al. Low-temperature thermochronology of the South Atlantic margin along Uruguay and its relation to tectonic events in West Gondwana. **Tectonophysics**, v. 784, p. 228439, 2020.

MACHADO, V. A. G. **Sand provenance, diagenesis and hydrocarbon charge hystory of the Kwanza Basin, Angola**. [s.l.] University of Aberdeen, 2007.

MACKINTOSH, V. et al. Phanerozoic Morphotectonic Evolution of the Zimbabwe Craton: Unexpected Outcomes From a Multiple Low-Temperature Thermochronology Study. **Tectonics**, v. 36, n. 10, p. 2044–2067, 2017.

MCCOURT, S. et al. New U-Pb SHRIMP ages from the Lubango region, SW Angola: insights into the Palaeoproterozoic evolution of the Angolan Shield, southern Congo Craton, Africa. **Journal of the Geological Society**, v. 170, n. 2, p. 353–363, 2013.

MEESTERS, A. G. C. A.; DUNAI, T. J. Solving the production-diffusion equation for finite diffusion domains of various shapes: Part I. Implications for low-temperature (U-Th)/He thermochronology. **Chemical Geology**, v. 186, n. 3, p. 333–344, 2002.

MILANI, E. J.; DE WIT, M. J. Correlations between the classic Paraná and Cape–Karoo sequences of South America and southern Africa and their basin infills flanking the Gondwanides: du Toit revisited. **Geological Society, London, Special Publications**, v. 294, p. 319–342, 2008.

MIYOUNA, T. et al. Strike-slip deformation in the Inkisi Formation, Brazzaville, Republic of Congo. **Cogent Geoscience**, v. 4, n. 1, p. 1542762, 2018.

MORÓN, S. et al. Denuding a Craton: Thermochronology Record of Phanerozoic Unroofing From the Pilbara Craton, Australia. **Tectonics**, v. 39, n. 9, 2020.

MURRAY, K. E.; ORME, D. A.; REINERS, P. W. Effects of U-Th-rich grain boundary phases on apatite helium ages. **Chemical Geology**, v. 390, p. 135–151, 2014.

O’CONNOR, J. et al. Hotspot tracks in the South Atlantic located above bands of fast flowing asthenosphere driven by waning pulsations from the African LLSVP. **Gondwana Research**, v. 53, p. 197–208, 2018.

PICART, C. et al. Cenozoic deformation of the South African plateau, Namibia: Insights from planation surfaces. **Geomorphology**, v. 350, p. 106922, 2020.

REINERS, P. W.; FARLEY, K. A. Influence of crystal size on apatite (U-Th)/He thermochronology: An example from the Bighorn Mountains, Wyoming. **Earth and Planetary Science Letters**, v. 188, n. 3–4, p. 413–420, 2001.

RIBEIRO, L. F. B. et al. Thermotectonic and fault dynamic analysis of Precambrian basement and tectonic constraints with the Parana basin. **Radiation Measurements**, v. 39, n. 6, p. 669–673, 2005.

ROBERTS, G. G.; WHITE, N. Estimating uplift rate histories from river profiles using African examples. **Journal of Geophysical Research: Solid Earth**, v. 115, n. 2, p. 1–24, 2010.

SÉRANNE, M.; ANKA, Z. South Atlantic continental margins of Africa: A comparison of the tectonic vs climate interplay on the evolution of equatorial west Africa and SW Africa margins. **Journal of African Earth Sciences**, v. 43, n. 1–3, p. 283–300, 2005.

SHUSTER, D. L.; FLOWERS, R. M.; FARLEY, K. A. The influence of natural radiation damage on helium diffusion kinetics in apatite. **Earth and Planetary Science Letters**, v. 249, n. 3–4, p. 148–161, 2006.

SIQUEIRA-RIBEIRO, M. C. et al. The performance of a new (U+Th)/He thermochronology laboratory at UNESP Rio Claro, Brazil. **Annals of Brazilian Academy of Sciences**, v. 91, n. 1, p. 1–11, 2019.

SPATHOPOULOS, F. An insight on salt tectonics in the Angola Basin, South Atlantic. **Geological Society Special Publication**, v. 100, n. 100, p. 153–174, 1996.

SPIEGEL, C. et al. Apatite (U-Th-Sm)/He thermochronology of rapidly cooled samples: The effect of He implantation. **Earth and Planetary Science Letters**, v. 285, n. 1–2, p. 105–114, 2009.

TACK, L. et al. Early Neoproterozoic magmatism (1000-910 Ma) of the Zadinian and Mayumbian groups (Bas-Congo): Onset of Rodinia rifting at the western edge of the Congo craton. **Precambrian Research**, v. 110, n. 1–4, p. 277–306, 2001.

THOMAS, D. S. G.; SHAW, P. A. **The evolution and characteristics of the Kalahari, southern AfricaJournal of Arid Environments**, 1993.

USTINOV, V. N. et al. Kimberlites distribution in Angola and prospective areas for new discoveries. **Mineralogy and Petrology**, v. 112, p. 383–396, 2018.

VEEVERS, J. J. Gondwanaland from 650-500 Ma assembly through 320 Ma merger in Pangea to 185-100 Ma breakup: Supercontinental tectonics via stratigraphy and radiometric dating. **Earth-Science Reviews**, v. 68, n. 1–2, p. 1–132, 2004.

VERMEESCH, P. et al. a -Emitting mineral inclusions in apatite , their effect on (U – Th)/ He ages , and how to reduce it. **Geochimica et Cosmochimica Acta**, v. 71, n. 7, p. 1737–1746, 2007.

WALKER, R. T. et al. Rapid mantle-driven uplift along the Angolan margin in the late Quaternary. **Nature Geoscience**, v. 9, n. 12, p. 909–914, 14 dez. 2016.

WHITE, S. H.; BOORDER, H. DE; SMITH, C. B. Structural controls of kimberlite and lamproite emplacement. **Journal of Geoquemical Exploration**, v. 53, p. 245–264, 1995.

YI, Y. et al. A fission-track and (U-Th)/He thermochronometric study of the northern margin of the South China Sea: An example of a complex passive margin. **Tectonophysics**, v. 474, n. 3–4, p. 584–594, 2009.

CAPÍTULO 4 - ZIRCON FISSION-TRACK AGES OF KIMBERLITES RECORD NEOPROTEROZOIC AND PALEOGENE THERMAL REACTIVATIONS IN THE ANGOLAN SHIELD, CONGO CRATON

1 INTRODUCTION

Kimberlites are ultrabasic, K-rich rocks formed by the rapid, near surface emplacement of magmas that ascend from deep reservoirs in the Earth's mantle, making these rocks an invaluable source of information regarding the thermal state, composition, and evolution of the underlying asthenosphere and/or lithosphere through which they cross (GIULIANI; PEARSON, 2019). So far, determining the age of kimberlite volcanism at Cratons is advantageous in interpreting geodynamic processes, such as those related to deep (plate tectonics, mantle convection) or surface (denudation, weathering) setting (STANLEY; FLOWERS; BELL, 2015, 2013).

The near-surface emplacement of kimberlite magmas usually forms diatremes infilled with volcaniclastic material, which contain abundant magmaclasts and occasionally mantle and/or crustal basement xenoliths (MITCHELL; GIULIANI; O'BRIEN, 2019). These deposits are often altered by deuteric (i.e., late magmatic) and/or hydrothermal (i.e., external water) fluids that account for the extensive replacement of their original mineralogy by serpentine and carbonate (MITCHELL; GIULIANI; O'BRIEN, 2019; SCOTT SMITH et al., 2018), while later weathering led to the formation of a set of clay minerals and also secondary carbonate (MITCHELL, 1986). Despite it is suggested that the formation of diatremes and volcaniclastic deposits is dominated by moderate to low temperatures, based on analysis of surficial xenoliths and the preservation of carbonatised wood (MITCHELL, 1986; VAN OTTERLOO; CAS, 2016), the bounded limits for temperature and time duration of the processes governing the formation of volcaniclastic deposits are, however, poorly constrained.

Dating volcaniclastic kimberlite is challenging because most deposits lack enough amounts of datable minerals crystallized directly from the magma (e.g., perovskite for the U-Pb method), or these minerals are affected by alteration (e.g., phlogopite for Rb-Sr and $^{40}Ar/^{39}Ar$ methods) (HEAMAN; PHILLIPS; PEARSON, 2019). As an alternative, the zircon (U-Th-Sm)/He and fission-track methods have lower closure temperatures, respectively of ~ 180 - 200 °C (REINERS, 2005) and 180 – 360 °C (BERNET, 2009; RAHN et al., 2004; TAGAMI; SHIMADA, 1996; ZAUN; WAGNER, 1985), than more routinely used methods, which enables dating crustal zircon crystals (xenocrysts), which are resistant to alteration and might be totally reset by the emplacement temperatures when they entrain into the volcaniclastic deposits. Those techniques have been successfully employed in reproducing the emplacement ages of various kimberlites (BLACKBURN et al., 2008; BLACKBURN; STOCKLI; WALKER, 2007; HAGGERTY; RABER; NAESER, 1983; MCINNES et al., 2009; STANLEY; FLOWERS, 2016), however, these methods continue being little utilised for this purpose.

This work provides new electron microprobe zircon fission-track (EP-FT) data from kimberlites of the Longa headwaters, Angolan Shield. The advantage of the EP-FT technique (DIAS et al., 2017; GOMBOSI; GARVER; BALDWIN, 2014) is the possibility for dating zircon crystals with high levels of radiation damage, which are more sensitive to detect low-temperature thermal events in comparison to such poor-damaged zircon (GARVER; KAMP, 2002). The region shows conspicuous characteristics as follows: a) most of their kimberlite bodies lack any radiometric data and their rocks are strongly altered; b) kimberlite bodies outcrop near the apex of a long-wavelength dome structure (Angola Dome), which cause is attributed to dynamic uplift (ROBERTS; WHITE, 2010), and c) the region shows evidence for loss of cratonic root along the time (CELLI et al., 2020). Nevertheless, determine the age of the kimberlite volcanism in the Longa region is key to better constraint how those processes mutually interact and drive its tectonic and geomorphological evolution.

2 GEOLOGICAL SETTING

The study area lies at the western part of the Angolan Shield, Congo Craton (DE WAELE; JOHNSON; PISAREVSKY, 2008), nearby the boundary between the Central Shield Zone and the Central Eburnean Zone (DE CARVALHO et al., 2000) (Fig 1). According to (DE CARVALHO et al., 2000) the Central Shield Zone is most composed of Archean granite-gneiss-migmatitic complexes with U-Pb ages of 2.68 Ga +- 5 Ma (DELHAL; LEDENT; PASTELS, 1975) recalculated by (CAHEN et al., 1984), and Rb-Sr ages of 2.52 Ga +- 36 Ma, which intrude the Archean gabbro-anorthosite-charnochytic complex with U-Pb ages of 2.82 Ga (CAHEN et al., 1984).

The Central Eburnean Zone is primarily composed of Paleoproterozoic granite-gneiss complexes with Rb-Sr ages around 2.2 Ga (TORQUATO et al., 1979) and meta-volcano-sedimentary sequences with a metamorphic peak age of 2.1 Ga (CAHEN et al., 1984).

To the north, the Angolan Shield is separated from the West Congolian Pan-African Mobile Belt (WCPB) by a major E-W trending shear zone known as the Kwanza Horst (MCCOURT et al., 2013) (Fig. 1). The WCPB is interpreted as an intra-continental rift basin that evolved to passive margin environment at 1.0 – 0.9 Ga, and underwent tectonic inversion during the Pan-African orogenesis at 650 - 540 Ma (JELSMA et al., 2013). This event led to the formation of the metasedimentary cover of the West Congo Supergroup (TACK et al., 2001), which to the east of the study area, outcrops as red bed sandstones of the Inkisi Group with a maximum depositional age estimated at ~ 540 Ma (JELSMA et al., 2011). Further east, Karoo rocks (Late Carboniferous-Triassic) infill the NW-SE trending Cassange Graben (JELSMA et al., 2013) (Fig. 1).

A 2000 km long, NE-SW tectonic lineament known as the Lucapa corridor (BOORDER, 1982), transect the Angolan territory and it occurs few tens of kilometres south of the area (Fig. 1). This lineament is thought to be reactivated in the Cretaceous during rifting and opening of the South Atlantic Ocean, controlling the emplacement of carbonatites and kimberlite pipes and dykes across the Angolan Shield at that time (BOORDER, 1982; JELSMA et al., 2004; WHITE; BOORDER; SMITH, 1995).

Remnants of Paleogene conglomerates and silcretized sandstones of the Grès Polymorphes Fm. (GUILLOCHEAU et al., 2015) (Fig. 2) outcrop at interfluves or valleys of some important rivers, such as the Cunene, Cubango, and Gango. Those silicified sandstones, containing kimberlitic ilmenite, can also be found at the surface of some kimberlite pipes, and this is interpreted as evidence of a younger, Middle Paleogene, kimberlitic magmatism at the Angolan Shield, coeval with the silicification of the polymorph sandstones (CHAMBEL; CAETANO; CORREIA, 2014; MONFORTE, 1988).

Lateritic profiles containing iron duricrust form a stripped etchplain at elevations of ~ 1600 m, which in places, truncates the Grès Polymorphes sandstones, the kimberlite pipes, and the Precambrian basement rocks. This surface corresponds to the Upper Planation Surface 2 preserved across the northwestern

Ancient Plateau, in which incision due regional uplift and later weathering probably occurred between Middle Eocene and Late Oligocene at ~ 45 - 29 Ma (GUILLOCHEAU et al., 2015). The Neogene sedimentary cover is represented by sands of the Areias Ocres Fm. (ARAÚJO; GUIMARÃES, 1992), equivalent in southern Africa to the Kalahari sands (HADDON; MCCARTHY, 2005; LINOL et al., 2015) and by alluvial gravels, sands, and clays that locally form diamond placer deposits.

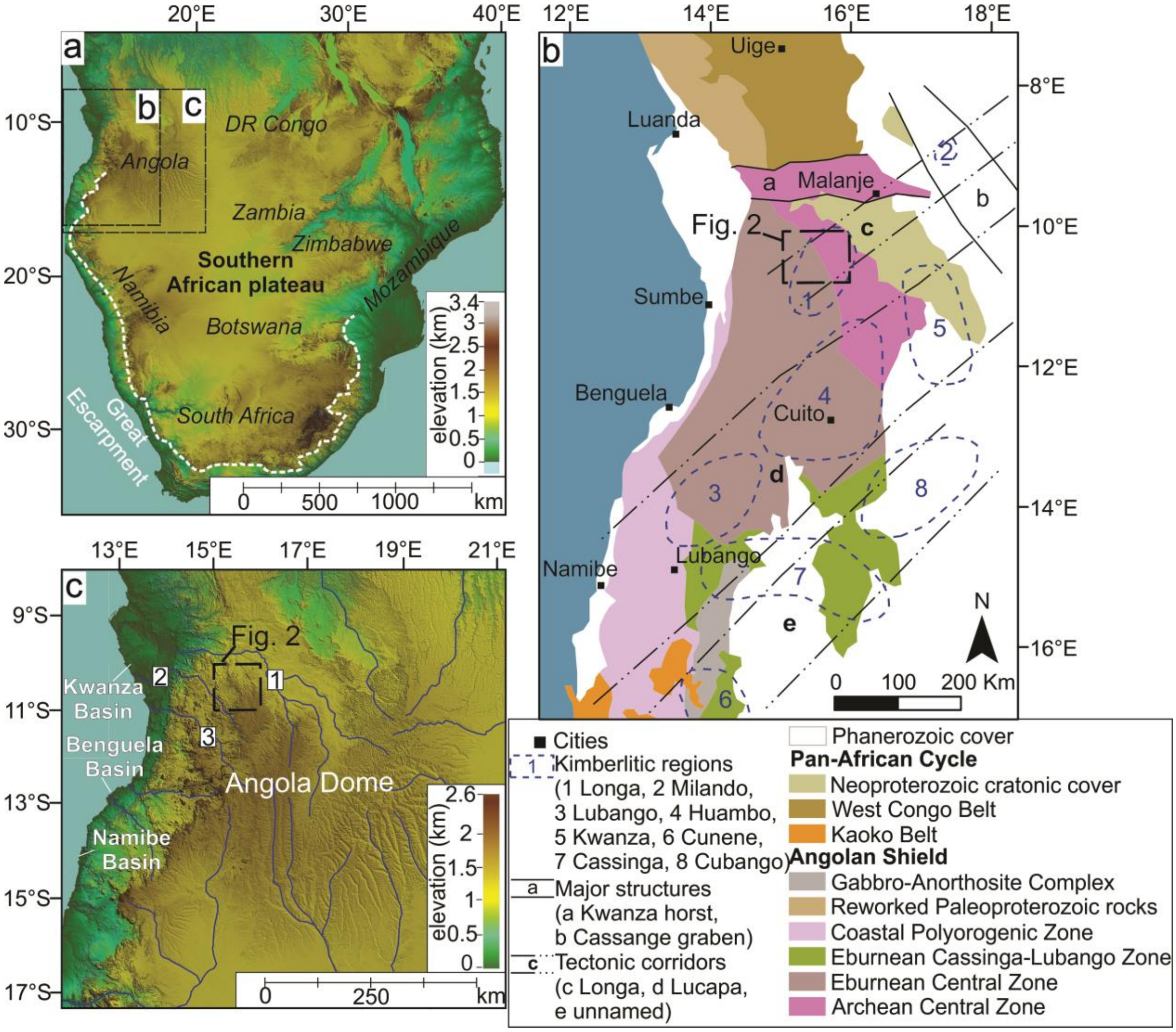

Fig. 1 a) Elevation map of the southern African plateau region showing the encircling Great Escarpment, Coastal Zone, and locations of the Fig. 1b, 1c. b) Simplified tectonic map of the eastern Angolan Shield showing the main tectonic units and basement structures, redrawn from (Heilbron et al., 2008; Ustinov et al., 2018). Location of Fig. 2 is also indicated. c) Elevation map showing the Angola Dome characterized by radial drainage pattern (rivers: 1 Kwanza; 2 Longa; 3 Cuvo) and the location of the coastal Angolan basins and Fig. 2

2.1 Kimberlites from the Longa Headwaters

The Longa region located in the West-Central Angola hosts more than 25 known kimberlite pipes distributed into the Gango (northern) and the Quitubia (southern) kimberlitic fields (USTINOV et al., 2018). At the surface, the pipes show elliptical to rounded contours ranging in size from 1 to 125 ha, and are intruded into Archean to Paleoproterozoic gneisses and granitoids (Catoca internal report).

Pipes are preserved on the lateritic plateau at ~ 1600 m of elevation, and can also be found towards the incised valleys of regional rivers between ~ 1300 and 1500 m of elevation. The Lorelei pipe, representing the first group, is the largest pipe of the area (125 ha in size) and preserves crater facies sediments ~ 235 m thick. A Cretaceous age is estimated for this pipe according to an unpublished Paleontological study (USTINOV et al., 2018). On the other hand, pipes of the second group are more eroded and occur below the main lateritic plateau, some still preserving crater-fill sediments (e.g., QTB-014 pipe) or preserving diatreme facies rocks at the surface, mainly represented by pyroclastic and coherent kimberlites (e.g., Tchiandongo pipe) (Catoca internal report). A variety of centimetre- to metre-size, mantle- and crustal-derived xenoliths can be encountered within the pipes, including eclogite, lherzolite, gneiss, granite, sandstone, and siltstone (Catoca internal report). The presence of those sedimentary rocks infilling some pipes, suggests there was a more continuous sedimentary cover across the region at the time of the kimberlite eruptions, which was later eroded.

A number of pipes discovered at the Longa region is proved to be diamantiferous (even with a low diamond grade, e.g., the Lorelei pipe), or with possible potential for diamonds according to the kimberlite indicator minerals (KIMs) analysis, which also indicates that most of the kimberlitic melts were generated between ~ 70 and 150 km deep in the Earth’s mantle (USTINOV et al., 2018). However, the knowledge regarding diamond metallogeny of the Longa kimberlitic region is not straightforward (CHAMBEL; CAETANO; CORREIA, 2014).

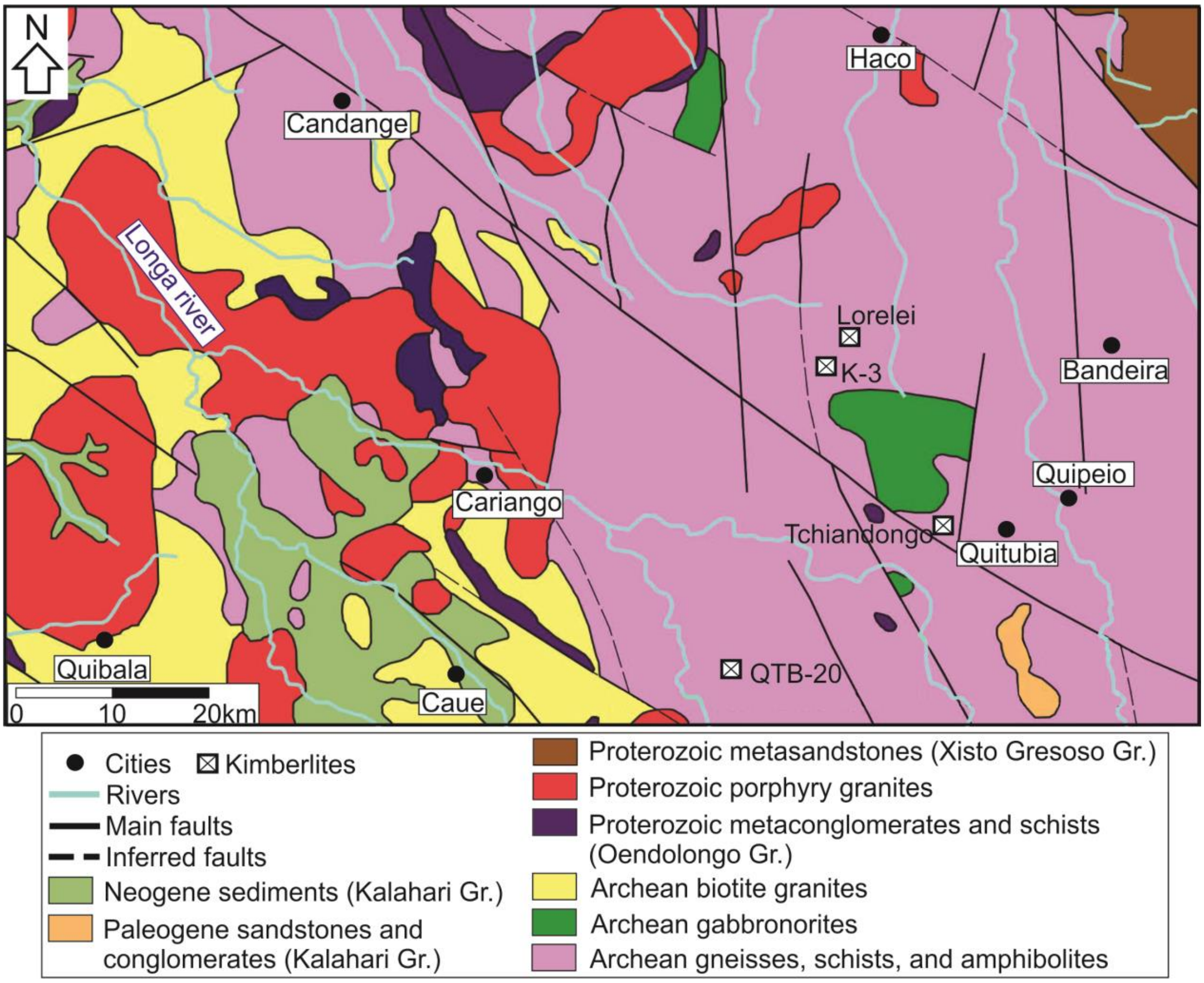

Fig. 2 Geological map from the Longa kimberlitic region redrawn from (ARAÚJO; GUIMARÃES, 1992), with the approximate location of the kimberlite pipes analysed in this study

3 SAMPLES AND METHODS

Outcrop samples of volcaniclastic kimberlite were collected from the Tchiandongo and the QTB-020 pipes, whereas a heavy mineral concentrate was obtained from the K-3 pipe. Samples were previously analysed by optical microscopy and powder X-ray diffraction (XRD) for a basic recognition of their mineralogy, in order to establish a range of temperature associated to their formation. After that, zircon grains were recovered from the samples and from the heavy mineral concentrates for EP-FT analysis.

3.1 Petrography

Samples were analysed macroscopically and further microscopically under an optical microscope. They were described in terms of alteration, structure, texture, and components (compound clasts, crystals, and interstitial matrix), following the recommendations of (SCOTT SMITH et al., 2013, 2018). For magmaclasts (i.e., material formed near surface, by fluidal fragmentation of the former melt during the kimberlite emplacement) it was utilised the terminology of (WEBB; HETMAN, 2021). Powder XRD analyses were carried out at the Soil Mineralogy Laboratory (ARGILAB) of the Luiz de Queiroz College of Agriculture, University of São Paulo (ESALQ-USP). The diffractometer (RIGAKU) utilized a CuKα radiation of 0.1540562 nm, and was operated at 30 kV and 15 mA, with a Ni filter for Kβ suppression, and a NaI scintillator coupled with a Be window for detection. The angular range of the analyses was 3° - 60 º2θ, step of 0.02 º2θ s^{-1} or less.

3.2 Zircon Fission-Track Dating

3.2.1 Background

The method is based on counting fission-tracks (radioactive defects formed from the spontaneous fission of ^{238}U, equivalent to daughter nuclides) and in estimating the ratio between the number of spontaneous tracks and the amount of ^{238}U (parent nuclides) on a delimited volume of the zircon grain. Among the approaches utilized, the external detector method (EDM) has been commonly used to stablish this ratio, but require irradiation of the grains in a nuclear reactor to induce fission of ^{235}U and generation of induced tracks imprinted on the detector (poor-U mica) coupled to the grains (the amount of induced tracks mirrors the amount of ^{238}U, taking into account that the $^{235}U/^{238}U$ ratio is constant). On the other hand, techniques that directly measure ^{238}U and avoid the need of irradiation have been increasingly employed. The EP-FT method, for example, is based on counting fission-tracks over a backscattering image (BSE) of the zircon single-grains, and on the measurement of the uranium concentration in a single-point within the track counting area, under an electron microprobe (GOMBOSI; GARVER; BALDWIN, 2014). Zircon grains may be dated once they are polished, to expose the internal surface of the grain, and chemically etched, to make the tracks large enough to be visible at the BSE images.

3.2.2 Closure temperature of the zircon fission-track system

A zircon fission-track age results from the relationship between the production of fission-tracks within the mineral lattice, and the annealing of them (partial or total) when they are heated over the geological time. Despite there is consensus that track annealing kinetics in zircon (i.e., the rate at which a track is shortened) is dependent of temperature, cooling rate, and the level of the radiation damage of the grains (produced by the radioactive decay of U and Th), the wide range of chemical compositions and degree of crystallinity in natural zircon grains, result in discrepancies on the estimation of the closure temperature (Tc) of the zircon fission-track system, which ranges from ca. ~ 180 – 360 °C (BERNET, 2009; HASEBE et al., 2003; RAHN et al., 2004; TAGAMI et al., 1998; TAGAMI; SHIMADA, 1996; YAMADA et al., 1995; ZAUN; WAGNER, 1985). In this sense, high-damaged zircon grains, characterized by strong colours (from red to black) and high uranium concentrations, yield zircon fission-track Tc lower than the low-damaged ones that are colourless to light coloured and low uranium (GARVER; KAMP, 2002; GORDON GASTIL; DELISLE; MORGAN, 1967). This property of the method system may be used to gain additional information regarding the thermal history of rocks.

3.2.3 Analysis

Zircon grains were separated using rock crushing, panning, magnetic separation, and heavy liquid steps carried out at Department of Geology, São Paulo State University (Unesp), Rio Claro, Brazil. Zircon crystals were observed under binocular glass, and then grouped according their size, colour, and shape (Tab. 1) before being embedded in separated Teflon by using a hot plate at ~ 330 °C. Teflon mounts were polished to expose the internal surface of the grains, and then chemically etched between 1 and 9 hours in an eutectic solution of KOH:NaOH, and heated in an oven at ~ 230 – 240 °C for tracks revelation (GLEADOW; HURFORD; QUAIFE, 1976). After etching, zircon grains were analysed at the Electron

Microprobe laboratory of Department of Geology (Unesp) in which they were imaged under a backscatter detector utilizing a 10 nA current. A centre point on each single grain, within an area of homogeneous track density, was selected for determination of uranium [U] concentration through wavelength dispersive spectroscopy (WDS) (Fig. 3). Run conditions were a diameter beam of 10 μm, a current of 300 nA, an accelerating voltage of 25 keV, and a counting time of 300 s on the peak and 150 s on the background. The BSE images were later imported into the ImageJ software (SCHNEIDER; RASBAND; ELICEIRI, 2012) for counting the fission-tracks and calculating their track counting areas (Fig. 3). For zircon EP-FT age determinations, a mean Z value of 4302 ± 1674 (1σ) was used based on measurements of 14 zircon grains from the Fish Canyon Tuff age standard. All the procedure described above as well as the calculation of the zircon EP-FT ages followed the equations published in (GOMBOSI; GARVER; BALDWIN, 2014).

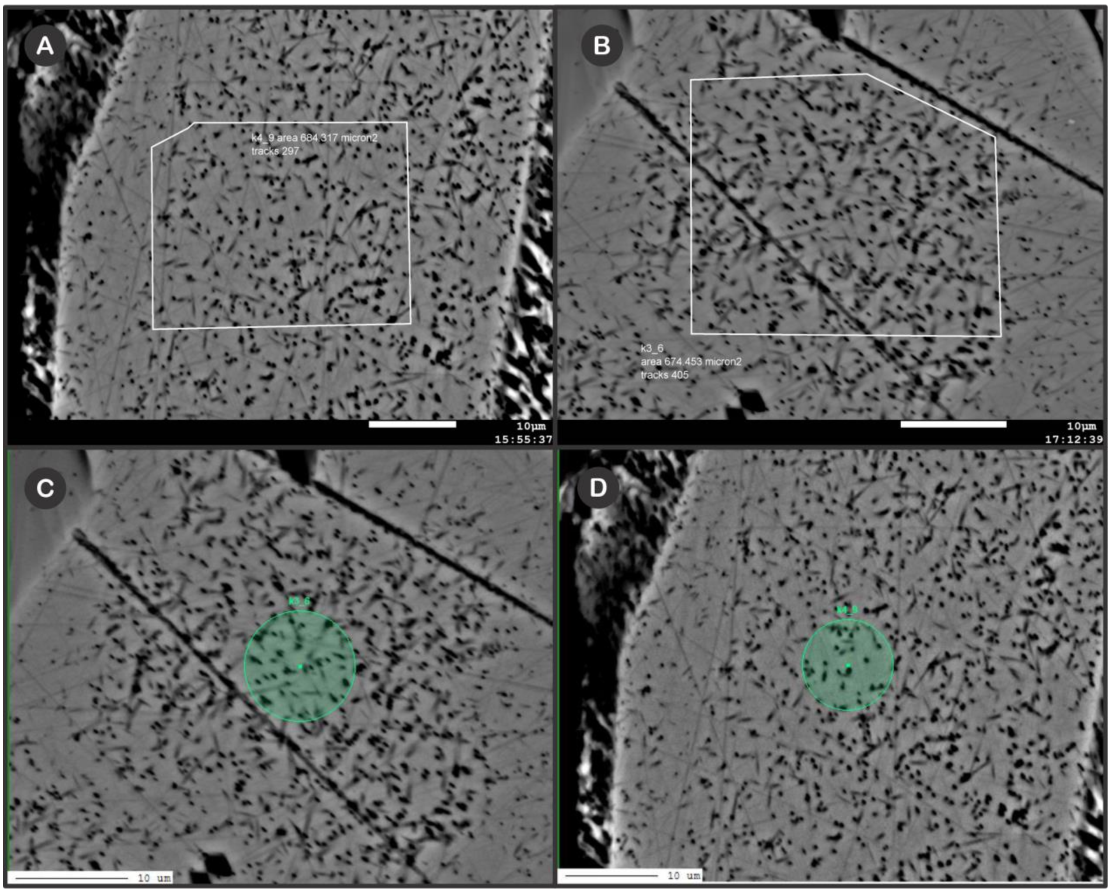

Fig. 3 a) and b) BSE images showing the fission-track counting areas in two different zircon crystals; c) and d) the location and size of the spot utilised for uranium determinations in these crystals

4 RESULTS

4.1 Petrography

4.1.1 Tchiandongo kimberlite

The analysed sample shows a strong to intense degree of alteration, where the primary mineralogy is pervasively pseudomorphed or replaced by serpentine and carbonate minerals (and in a minor extent by chlorite and talc) in response to deuteric (i.e., late magmatic fluids) and/or hydrothermal (i.e., circulation of hot, external water) processes. The rock is also moderately weathered as supported by the pervasive replacement of serpentine by clay minerals, likely from the smectite group (Fig. 4). Sample is massive in appearance, poorly sorted, and shows an inequigranular texture mainly characterized by micro to small macroxenoliths (~ 5 modal %), olivine macrocrysts and microcrysts (15 – 50 modal %), and magmaclasts with different sizes (15 – 50 modal %) set in a fine-grained interclast matrix, usually optically unresolved due the sample alteration.

Microxenoliths (< 16 mm) comprise angular to subrounded granitoid and gneiss basement clasts, as well as are mantle derived material. All small macroxenoliths (16 – 24 mm) encountered in the sample are serpentinised mantle clasts (Fig. 4). One micro autolith (< 16 mm) shows an elongated and amoeboid shape, and is composed of an aggregate of phlogopite crystals, some of which poiquilitic and enclosing opaque minerals.

Super fine to fine (0.2 – 1.8 mm) magmaclasts are the dominant constituent of the sample and are basically represented by two types of melt-bearing pyroclasts. The first one is the most abundant, spherical to subspherical in shape (regular to irregular), being either cored (preserves a kernel of single olivine or xenolith) or uncored (preserves olivine crystals set in a finer-grained, well to poorly crystalline groundmass); they also may be either poorly (1 – 10 %) or highly vesicular (> 10 %), and are usually enclosed by thin, cryptocrystalline to poorly crystalline rims showing sharp to diffuse margins (Fig. 5a, b). The second one is lesser abundant, typically melt-rich, amoeboid to curvilinear in shape, and consists of olivine crystals set in a dark, cryptocrystalline groundmass. When recognizable, groundmass minerals are phlogopite, serpentine, spinel, and perovskite (Fig. 5b). A larger magmaclast (Fig. 5c) shows an elongated shape similar to the “ovoid-shaped” magmaclast described by (SCOTT SMITH, 2008), which is typical of extrusive volcanism.

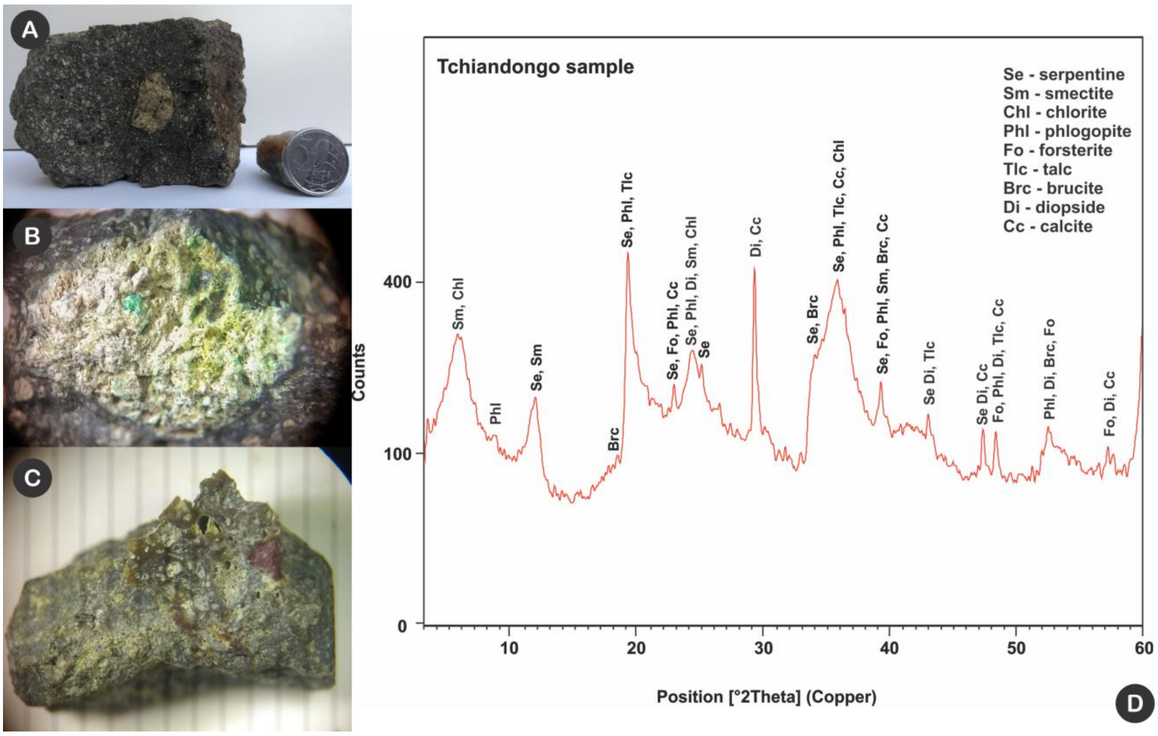

Fig. 4 Tchiandongo sample: a) volcaniclastic kimberlite with a serpentinised mantle xenolith in the centre; b) serpentinised mantle xenolith with chrome diopside (green); c) pyrope garnet (red). d) XRD pattern from the volcaniclastic kimberlite

Crystals are represented by anhedral, fine to medium (1 – 3 mm) olivine macrocrysts, and subedral to euhedral, super fine to very fine (< 1 mm) olivine microcrysts. Both macrocrystic and microcrystic olivine grains usually compose the kernel of melt-bearing pyroclasts (Fig. 5d), suggesting that they might be, at least in part, xenocrysts (i.e., mantle-derived) and phenocrysts (i.e., crystallised from the kimberlite magma), respectively. Fine to coarse (2 – 6 mm) pyrope garnet and chrome diopside macrocrysts are rare, and occur either in the kimberlite mass or within mantle xenoliths (Fig. 4).

The interstitial matrix of the rock, when recognizable, consists of a mixture of ultra to very fine (< 0.1 – 0.7 mm) phyllosilicates (Fig. 5e) and carbonate, the later often filling voids between clasts (Fig. 5f). The phyllosilicate assemblage is identified as serpentine, phlogopite, smectite, chlorite, talc and brucite in the XRD pattern (Fig. 4). Diopside is recognized as microlites forming fringes around magmaclasts, as well it is suggested in the XRD pattern (Fig. 4). The interstitial matrix also contains minor amounts of typical groundmass minerals, such as perovskite and spinel. Following the scheme of (SCOTT SMITH et al., 2013, 2018) the analysed rock sample may be described as a very micro to small macroxenolith-poor, super fine to medium olivine-rich, super fine to fine melt-bearing pyroclast-rich, volcaniclastic kimberlite (VK).

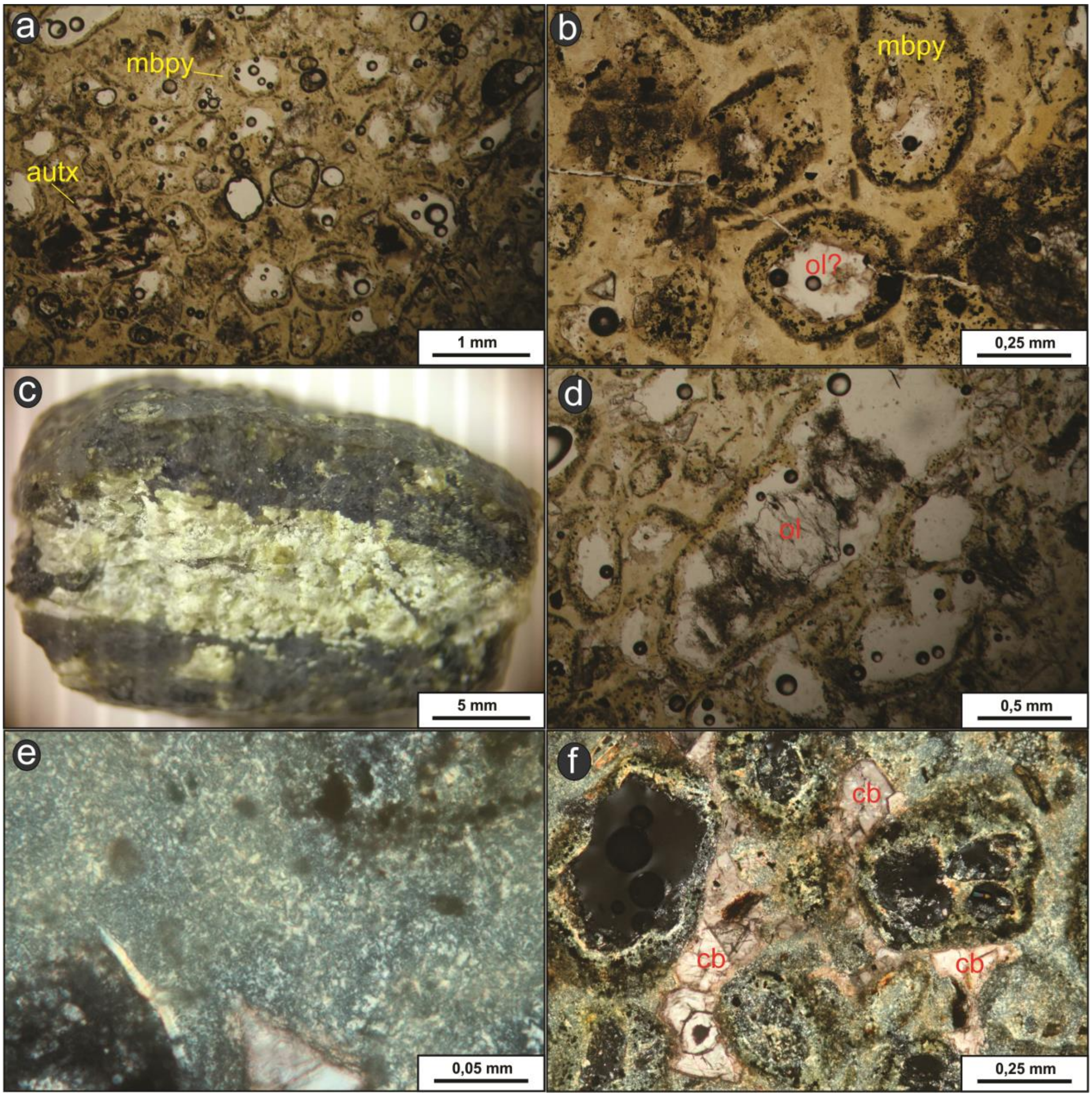

Fig. 5 Images of the VK sample from the Tchiandongo kimberlite. a) Photograph in plane polarized light (PPL) showing abundant melt-bearing pyroclasts (mbpy) and an autolith (autx). b) Photograph in PPL showing melt-bearing pyroclasts containing typical cryptocrystalline rims, fine-grained groundmass with perovskite, magnetite, and spinel, and internal holes (white) possibly corresponding to kernels of olivine. c) Photograph in PPL showing a preserved olivine crystal (ol). d) Photograph in cross polarized light (XPL) showing the interstitial matrix most composed of fine to very fine phyllosilicates (serpentine and chlorite). e) Photograph in XPL showing the interstitial carbonate (cb). f) Photograph of a magmaclast similar to the “ovoid-shaped” described by (SCOTT SMITH, 2008). Discussions in the text

4.1.2 QTB-20 kimberlite

The analysed rock sample shows petrographic and XRD pattern broadly similar to the Tchiandongo one, excepting with regard to xenoliths contents. The sample shows a strong to intense degree of alteration, resulting from either deuteric/hydrothermal (serpentinisation and carbonatisation) or weathering (clay and oxide substitutions) processes (Fig. 6). Sample is massive, poorly sorted, inequigranular, and composed of microxenoliths (< 16 mm, ~ 5 modal %), fine to medium pseudomorphs of olivine macrocrysts and microcrysts (1 – 3 mm, 15 – 50 modal %), and fine to medium melt-bearing pyroclasts (0.2 – 1.8 mm, 15 – 50 modal %) set in a fine-grained interclast matrix (< 0.1 – 0.7 mm) usually hard to resolve under the optical microscope. Matrix minerals include serpentine, carbonate, phlogopite, smectite, chlorite, talc, brucite, microlitic diopside, and minor spinel and perovskite (Fig. 6).

The analysed sample lacks mantle xenoliths (although they are commonly described in boreholes, according to the Catoca internal report), but yield angular to subrounded basement microxenoliths that occasionally contain thin selvages of dark (cryptocrystalline), solidified former melt. The analysed rock sample is described here as a very microxenolith-poor, super fine to medium olivine-rich, super fine to fine melt-bearing pyroclast-rich, VK.

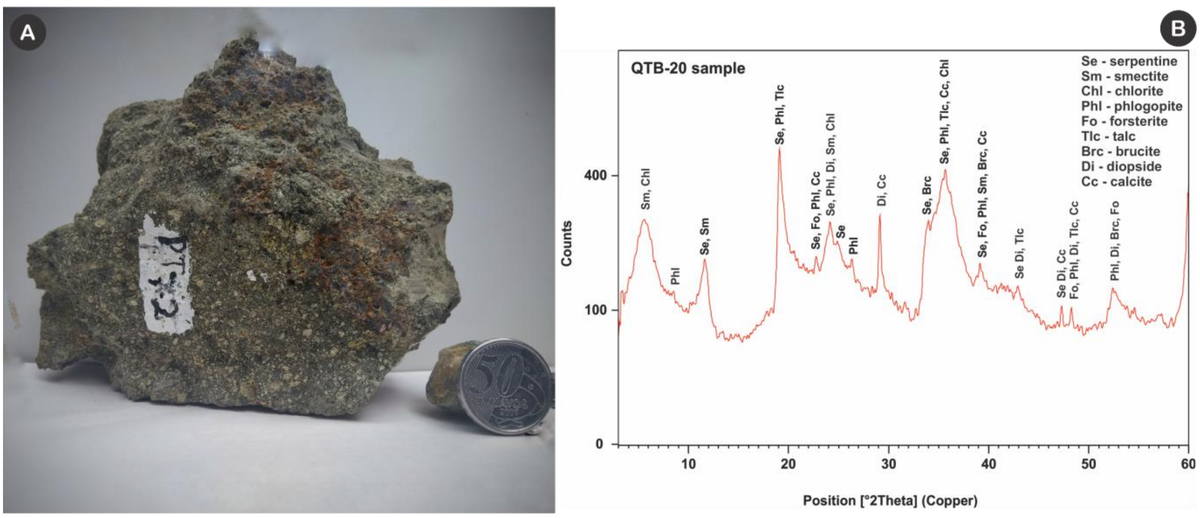

Fig. 6 QTB-20 sample: a) altered VK and b) its XRD pattern

4.2 Electron Microprobe Zircon Fission-Track Data

4.2.1 Z factor and Fish Canyon Tuff age standard

The Fish Canyon Tuff age standard yielded single, zircon EP-FT grain ages between 38.8 ± 10.14 Ma and 18.6 ± 4.43 Ma that define a single age population (sample pass the $P(\chi)^2 > 0.05$) (GALBRAITH, 2005) and a central age of 28.7 ± 2.1 (1σ) (Fig. 7). The obtained central age agree with a previous K/Ar sanidine age of 28.305 ± 0.072 Ma (2σ) (RENNE et al., 2010), as well as with a previous EP-FT age of 26.8 ± 2.5 Ma (2σ) (GOMBOSI; GARVER; BALDWIN, 2014). These demonstrate that the Z factor was correctly applied on calculation of the EP-FT ages.

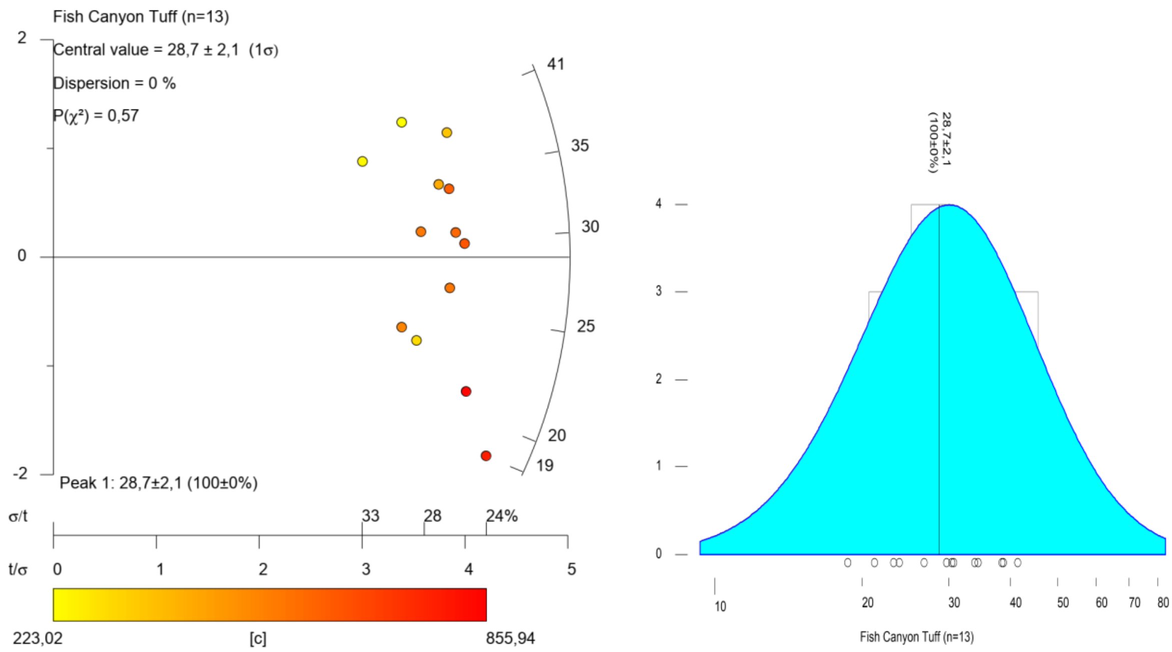

Fig. 7 (left hand side) Radial plot showing the single-grain zircon EP-FT ages from the Fish Canyon Tuff age standard, colours represent the uranium concentrations of the dated grains; (right hand side) Kernel density estimate (KDE) showing the frequency of the single-grain zircon ages (vertical) along the time axis (horizontal) plus a Gaussian curve representing the ages distribution. Radial plot and KDE generated in the RadialPlotter software (VERMEESCH, 2009)

4.2.2 Tchiandongo kimberlite

The volcaniclastic rock yielded distinct zircon populations, varying in colour and shape (Fig. 8). Zircon crystals are typically prismatic, although rounded ones are also observed. Colourless, pale pink, pale yellow and pale brown zircon crystals are commonly translucent (clear), and provided areas with well-developed tracks (~ 1 micron width) after ~ 5 - 10 hours of chemical etching. On the other hand, the ones characterized by strong red colours, frosted to opaque, did not provide visible tracks. These zircon crystals had their surfaces corroded and became dark with less than ~ 3 hours of etching. The analysed zircon crystals are typically crustal-derived xenocrysts, given their physical properties and uranium concentrations (> 100 ppm, Tab. 1).

The sample provided single zircon EP-FT ages between 1283.1 ± 544.3 Ma and 26.8 ± 6.8 Ma (Tab. 1) that fail the $P(\chi^2)$ test (Fig. 8), indicating that ages do not fully conform to a Poissonian distribution. This behaviour likely arises from the existence of more than one single age population in the sample (i.e., as a result of distinct provenance areas or distinct thermal events), as observed in the radial plot that clearly shows a cluster of older ages (peaks in 595 ± 68 and 297 ± 36 Ma), visually separated from an younger one (peak in 49.4 ± 4 Ma) (Fig. 8). Therefore, the defined central age of 207 ± 45 Ma (1σ) only represent an intermediate value between multiple age populations.

Tab. 1 - Summary of the zircon fission-track data from the Tchiandongo kimberlite

Zircon grain	ρ_s (cm²)	Ns	^{238}U (ppm)	Uncertainty ^{238}U (%)	Age (Myr)	Uncertainty (Myr)
1	4.3×10^7	144	257	15	358.9	96.7
2	3.1×10^7	50	2595	1	26.8	6.8
3	3.8×10^7	176	333	12	248.8	62.5
4	7.3×10^7	241	299	13	522.6	132.4
5	6.3×10^7	168	326	12	415.8	105.4
6	1.4×10^7	57	701	6	44.3	11.2
7	7.7×10^7	212	2648	1	65.0	14.3
8	3.3×10^7	255	143	26	497.0	168.9
9	7.2×10^7	295	200	18	760.1	216.2
10	2.0×10^7	209	936	4	47.0	10.5
11	4.4×10^6	62	176	21	55.4	17.9
12	6.0×10^7	117	369	11	355.1	89.2
13	6.1×10^7	221	217	17	600.7	167.8
14	7.1×10^7	252	192	19	773.1	225.1
15	6.6×10^7	193	104	36	1283.1	544.3
16	7.2×10^7	229	279	13	553.9	142.2
17	7.2×10^7	208	452	8	344.4	81.0
18	8.7×10^7	162	282	14	651.9	170.0
19	8.0×10^7	228	225	17	751.8	207.1
20	6.4×10^7	172	2866	1	49.4	11.0

21	7.6×10^7	136	595	7	277.9	65.3
22	8.3×10^7	240	367	10	488.7	117.9
23	5.0×10^7	213	417	9	264.6	62.9
24	3.5×10^7	130	379	10	205.4	50.6
25	3.8×10^6	56	233	16	36.1	10.7
26	3.4×10^6	61	225	16	33.7	9.9
27	1.6×10^7	53	363	11	99.7	27.1
28	9.4×10^6	153	323	12	64.4	16.3

Note. ρ_S: density of spontaneous tracks; Ns: number of spontaneous tracks. Fission-track ages were calculated using a Z value of 4302 ± 1674 (1σ). Uncertainties in ages are quoted as 2σ. All the calculations follow (GOMBOSI; GARVER; BALDWIN, 2014).

The uranium concentrations of the dated crystals vary greatly, between 104.9 to 2886.9 ppm and show a conspicuous relationship with ages. All U-richest zircon grains fall within the younger age population, whereas the U-poorer crystals belong to both the younger and the older age populations (Fig. 8).

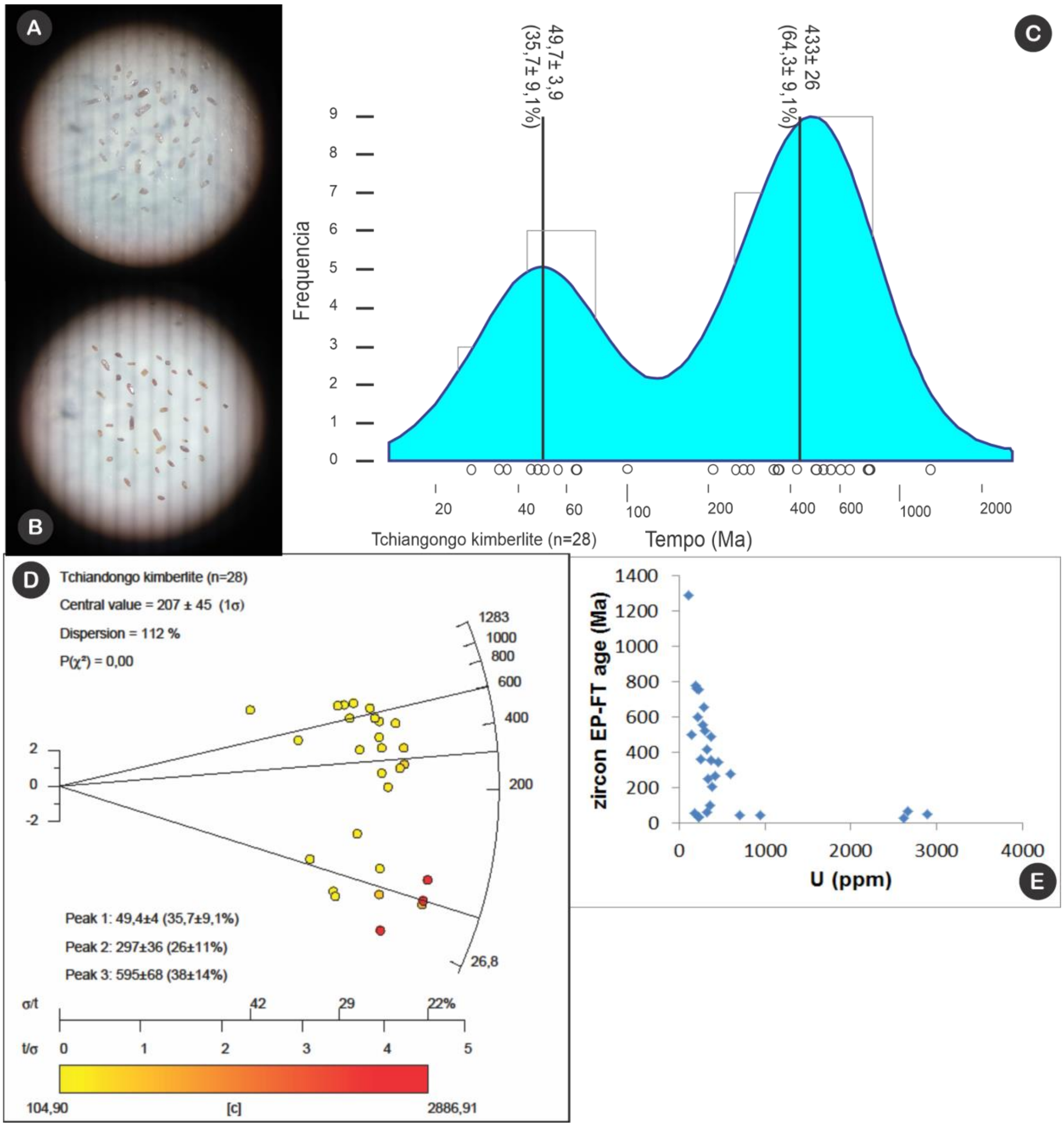

Fig. 8 Tchiandongo sample: a) and b) Selected zircon crystals under the binocular microscope; c) KDE showing the frequency (vertical) of the single-grain zircon EP-FT ages along the time axis (horizontal) and the two age peaks; d) radial plot showing the distribution of the single-grain ages into visually distinct two age groups (colours represent the uranium concentrations of the dated grains); and e) Single-grain ages plotted against uranium concentrations showing a roughly "boomerang" pattern. Radial plot and KDE generated in the RadialPlotter software (VERMEESCH, 2009)

4.2.3 QTB-20 kimberlite

The analysed zircon crystals are prismatic to rounded in shape and the colourless, pale pink and pale brown, usually translucent ones, yielded areas with well-developed tracks after ~ 8 hour of chemical etching. By contrast, zircon crystals characterized by strong yellow, brown, green, and red colours, frosted to opaque in appearance, had their surfaces fully consumed with less than ~ 2 hours and 20 minutes of etching. The characteristics and the uranium contents of the zircon grains (> 170 ppm, Fig. 9, Tab. 2) support they are crustal xenocrysts.

Tab. 2 - Summary of the zircon fission-track data from the QTB-20 kimberlite

Zircon grain	ρ_s (cm²)	Ns	^{238}U (ppm)	Uncertainty ^{238}U (%)	Age (Myr)	Uncertainty (Myr)
1	7.0×10^7	265	449	9	339.0	79.5
2	9.1×10^7	345	311	12	623.3	155.2
3	6.8×10^7	319	291	14	503.3	128.3
4	9.5×10^7	284	282	14	714.4	183.6
5	4.1×10^7	164	282	14	316.5	82.9
6	8.0×10^7	134	272	14	627.3	166.1
7	1.3×10^8	232	394	10	677.6	162.1
8	7.4×10^7	395	2734	1	60.1	12.9
9	1.1×10^8	437	302	12	743.7	184.1
10	8.5×10^7	318	444	9	415.1	96.6
11	8.7×10^7	221	377	10	495.5	119.6
12	7.2×10^7	217	288	13	536.6	136.8
13	8.1×10^7	264	236	16	722.3	192.9
14	2.4×10^7	325	2311	1	23.5	5.1
15	5.0×10^7	270	2937	1	38.1	8.3
16	6.0×10^6	67	173	21	76.7	24.7
17	1.1×10^7	60	1062	4	23.4	5.8
18	9.2×10^6	109	499	8	40.9	9.9
19	4.3×10^6	55	384	10	24.7	6.6
20	3.0×10^7	102	334	11	197.5	50.9
21	4.8×10^6	72	311	12	34.4	9.3
22	7.4×10^7	207	262	14	601.6	158.2
23	6.1×10^7	250	239	16	545.0	147.0
24	1.7×10^7	133	1848	2	20.7	4.7

Note. ρ_s: density of spontaneous tracks; Ns: number of spontaneous tracks. Fission-track ages were calculated using a Z value of 4302 ± 1674 (1σ). Uncertainties in ages are quoted as 2σ. All the calculations follow (GOMBOSI; GARVER; BALDWIN, 2014).

Single-grain EP-FT ages vary from 743.7 ± 184.1 to 20.7 ± 4.7 Ma, and are distributed into two distinct age populations with well-defined peaks in 506 ± 33 and 33.5 ± 2.7 Ma, respectively (Fig. 9). As a result, the sample fails the P(χ²) test and the central age value of 185 ± 51 (1σ) Ma is solely an intermediate value between those age populations (Fig. 9) and should not be used on further interpretations.

The dated zircon crystals yielded uranium concentrations from 174.5 to 2958.3 ppm, in which the U-richest crystals exclusively fall into the younger age population, whereas the U-poorer crystals fall into both the younger and the older populations (Fig. 9).

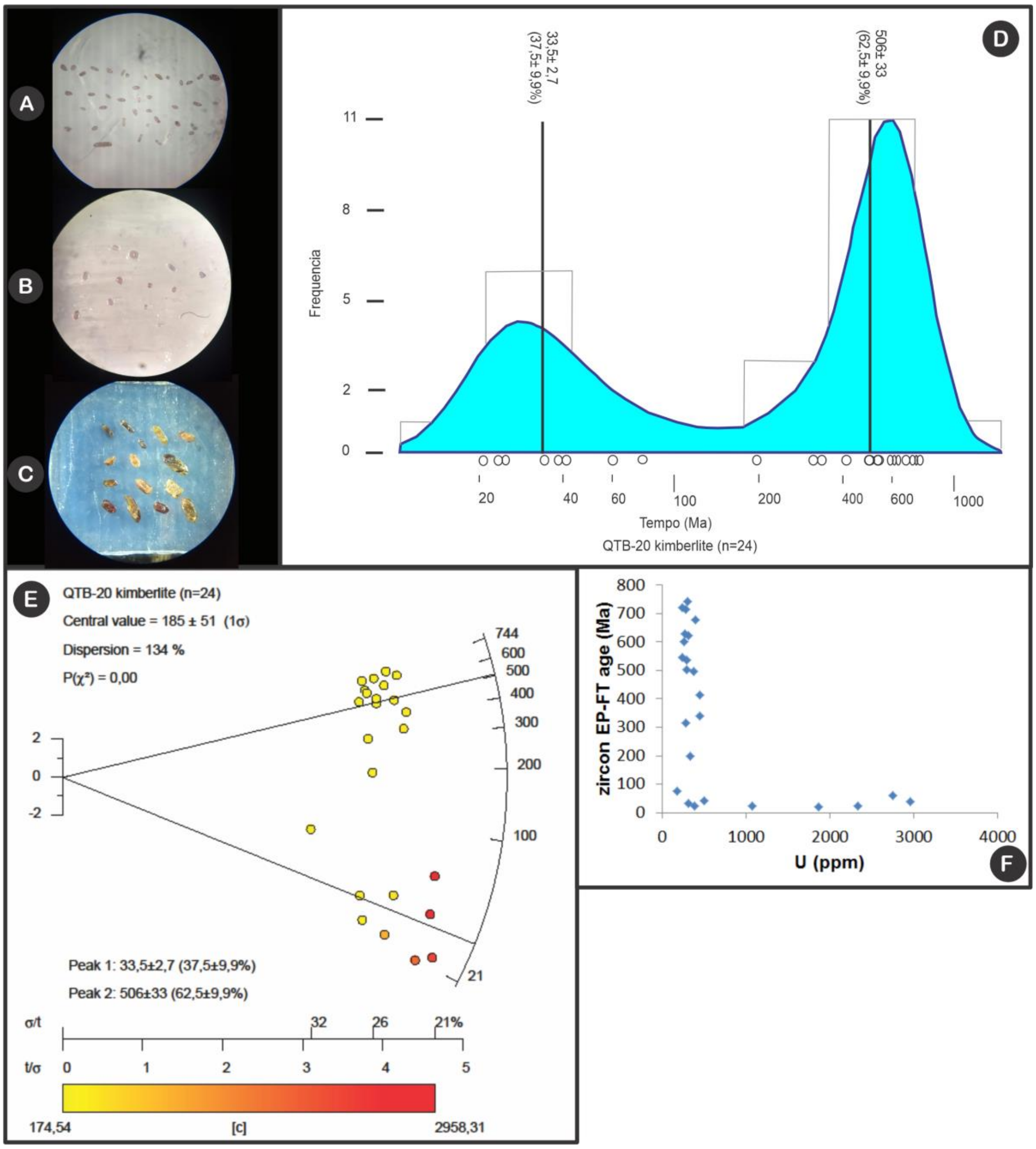

Fig. 9 QTB-20 sample: a), b), and c) Selected zircon crystals under the binocular microscope; d) KDE showing the frequency (vertical) of the single-grain zircon EP-FT ages along the time axis (horizontal) and the two age peaks; e) radial plot showing the distribution of the single-grain ages into visually distinct two age groups (colours represent the uranium concentrations of the dated grains); and f) Single-grain ages plotted against uranium concentrations. Radial plot and KDE generated in the RadialPlotter software (VERMEESCH, 2009)

4.2.4 K-3 kimberlite

Zircon grains recovered from the heavy mineral concentrate are prismatic to rounded in shape, and the ones that provided the best areas with tracks enough large are colourless, pale pink, and pale yellow coloured, as well as translucent in appearance. The crystals marked by strong yellow, brown, and red colours, frosted to opaque, did not provide good visible tracks, excepting in rare areas within some frosted crystals where the tracks emerged. Well-developed tracks became evident in the analysed grains after ~ 5 hours of chemical etching. The characteristics coupled with the uranium contents (> 90 ppm, Fig. 10, Tab. 3) point out that most of the recovered zircon grains consist of crustal xenocrysts.

Single-grain, zircon EP-FT ages vary between 1099.5 ± 435.0 and 28.0 ± 6.2 Ma and the age distribution fails the P(χ^2) test (Fig. 10). This behaviour is easily explained by the occurrence of two unambiguous age populations with well-defined peaks in 614.0 ± 51.0 Ma and in 41.0 ± 3.2 Ma, respectively (Fig. 10). As discussed above, the central age value of 252.0 ± 70.0 (1σ) obtained for this sample (Fig. 10) do not represent the ages distribution.

Tab. 3 - Summary of the zircon fission-track data from the K-3 kimberlite

Zircon grain	ρ_s (cm²)	Ns	^{238}U (ppm)	Uncertainty ^{238}U (%)	Age (Myr)	Uncertainty (Myr)
1	2.5×10^7	151	119	32	454.1	177.7
2	2.8×10^7	221	2228	1	28.0	6.2
3	4.0×10^7	340	219	17	399.4	109.9
4	5.4×10^7	602	2489	1	48.3	10.3
5	7.0×10^7	353	3125	1	49.9	10.8
6	4.7×10^7	238	105	35	920.3	378.6
7	6.0×10^7	405	164	23	771.3	241.2
8	4.8×10^7	156	230	17	445.3	124.0
9	4.3×10^7	446	139	27	661.4	225.6
10	5.8×10^7	303	108	33	1099.5	435.0
11	4.5×10^7	258	201	19	484.3	138.7
12	4.9×10^7	499	140	26	742.5	250.7
13	5.4×10^7	179	2329	1	51.4	11.4
14	4.0×10^7	31	328	11	27.4	8.2
15	4.3×10^7	297	2927	1	33.0	7.2
16	4.9×10^7	306	115	33	890.7	349.5
17	4.7×10^7	331	2567	1	41.2	8.9
18	5.5×10^7	225	295	13	402.8	102.1
19	2.4×10^7	150	91	41	571.5	266.8
20	4.1×10^7	217	132	27	663.5	232.2
21	7.2×10^7	251	3175	1	50.7	11.1
22	5.5×10^7	185	125	30	907.9	335.6
23	5.1×10^7	368	124	30	858.9	317.1
24	6.2×10^7	184	164	22	791.6	249.7

Note. ρ_s: density of spontaneous tracks; Ns: number of spontaneous tracks. Fission-track ages were calculated using a Z value of 4302 ± 1674 (1σ). Uncertainties in ages are quoted as 2σ. All the calculations follow (GOMBOSI; GARVER; BALDWIN, 2014).

This sample best demonstrates that the obtained zircon EP-FT ages are strong controlled by the uranium content of the single crystals. All the U-richer crystals fall into the young age population, whereas almost all the U-poorer crystals (excepting only one grain) define the older age component of the sample (Fig. 10).

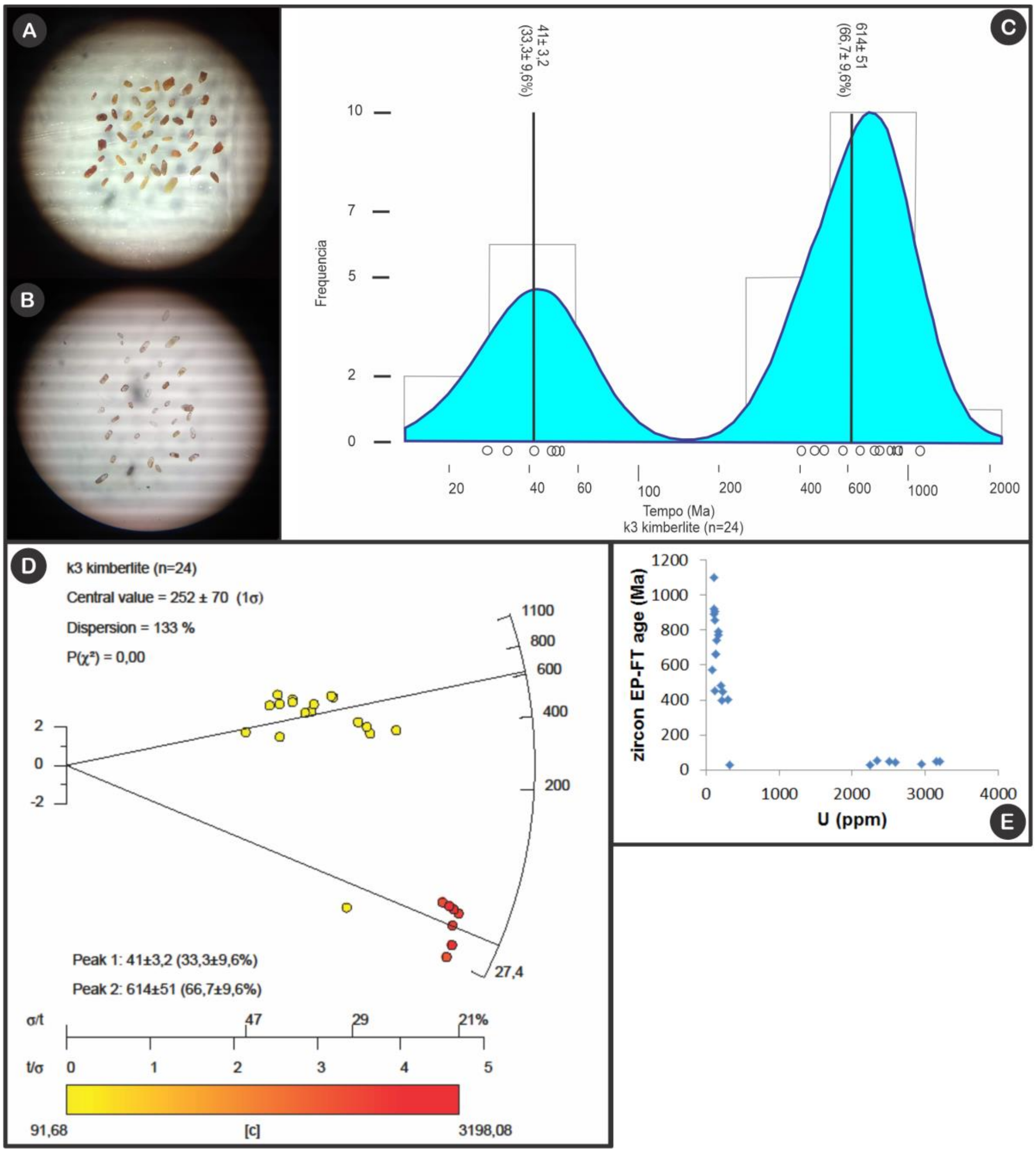

Fig. 10 K-3 sample: a) and b) Selected zircon crystals under the binocular microscope; c) KDE showing the frequency (vertical) of the single-grain zircon EP-FT ages along the time axis (horizontal) and the two age peaks; d) radial plot showing the distribution of the single-grain ages into visually distinct two age groups (colours represent the uranium concentrations of the dated grains); and e) Single-grain ages plotted against uranium concentrations showing that grains > 2000 ppm U define the young age component, whereas almost all grains < 500 ppm define the old age component of the sample. Radial plot and KDE generated in the RadialPlotter software (VERMEESCH, 2009)

5 DISCUSSION

5.1 Heat Duration and Emplacement Temperatures of the VK Samples

From the petrographic and XRD analyses, the Tchiandongo and QTB-20 samples are quite similar regarding textural and mineralogical characteristics. The pervasive serpentinisation and carbonatisation, as well as the presence of chlorite, talc, and smectite (Fig. 4, 6), support that the rocks were intensively altered by deuteric and/or hydrothermal processes, which likely drove the temperature of formation of the deposit.

Previous works indicate that serpentinisation in volcaniclastic deposits may occur in a range of ~ 130 - 600 °C, where reactions involving olivine replacements start at higher temperatures, possibly with stabilization of antigorite (500 - 600 °C, (EVANS, 1977), monticellite (> 400 °C, (HAYMAN; CAS; JOHNSON, 2009), and magnetite and chromite (> 350 °C, (BARNES, 2000; HAYMAN; CAS; JOHNSON, 2009), undergoing lower temperatures with stabilization of lizardite and chrysotile (300 – 400 °C, (EVANS, 2004; STRIPP et al., 2006), microlitic diopside (< 370 °C, (HAYMAN; CAS; JOHNSON, 2009), talc, brucite (< 350 °C, (FROST; BEARD, 2007), and smectites (saponite in ~ 20 – 270 °C, (HAYMAN; CAS; JOHNSON, 2009; NIMIS et al., 2004). In the analysed samples, serpentine is associated with magnetite and chromite, suggesting reactions at temperatures > 350 °C. On the other hand, the occurrence of brucite suggests temperatures < 350 °C, as well as the occurrence of smectite (Fig. 4, 6), which usually replaces the serpentine, suggests later temperatures between < 270 °C. Thus, it is suggested here that the VK samples were driven by temperatures below ~ 500 – 600 °C in the course of their formation.

VK deposits are considered of fast cooling considering geological time scales, in agreement with the fast ascent (hours to days) and near-surface emplacement of kimberlite magmas (NASDALA et al., 2014). Assuming cooling rates well above 100 °C/Myr, natural zircon crystals with some content of radiation damage would need temperatures above ~ 260 °C for the total reset of the zircon fission-track system (REINERS; BRANDON, 2006). Maintaining these high cooling rates and closure temperatures, zircon crystals would need to be undergone a heat interval shorter than ~ 1 Myr (REINERS; BRANDON, 2006). (NASDALA et al., 2014) analysing radiation-damaged zircon xenocrysts found in kimberlites from the Siberian Craton, conclude that the xenocrysts were derived from the Upper crust (< 12 km depth) and they did not experience more than few days at temperatures higher than ~ 500 – 600 °C during eruptions, otherwise, the radiation damage would be annealed from the lattice of the crystals.

In summary, it is speculated here that the main stage of serpentinisation of the VK samples took place in temperatures between ~ 260 and 500 °C, associated to a heat duration in a period from several days to up ~ 1 Myr. These conditions may explain the preservation of damage and the resetting of the EP-FT ages in some zircon crystals, as well as support that such deposits experienced very rapid cooling at geological time spans (AFANASYEV et al., 2014; NASDALA et al., 2014; PESLIER; WOODLAND; WOLFF, 2008).

5.2 Meaning of the Electron Microprobe Zircon Fission-Track Ages

Zircon EP-FT ages fall into two age groups, defined by Neoproterozoic and Paleogene age peaks, respectively (Fig. 8, 9, 10). This pattern of zircon fission-track ages has been recognized in volcanic rocks (YANG et al., 1995), including kimberlites (HAGGERTY; RABER; NAESER, 1983; NAESER, 1971), where the younger age peak roughly matches the age of the volcanism (also determined by other radiometric methods), while the older age peak represent inherited zircon ages. These two age groups are further discussed below.

5.2.1 Neoproterozoic zircon EP-FT ages

QTB-20 and K-3 samples yielded low age dispersion characterized by well-defined age peaks in the Neoproterozoic, whereas the Tchiandongo sample yielded more scattered ages (Fig. 8, 9, 10, Tab. 1, 2, 3). This age pattern indicates a regional thermal event in the Neoproterozoic; however, such event is unlikely to correspond the time of the kimberlite eruptions.

The region has underwent major exhumation of the basement during the Pan-African Orogeny in the Neoproterozoic (DE WAELE; JOHNSON; PISAREVSKY, 2008; MONIÉ et al., 2012), associated with the exposure of the metamorphic rocks of the West Congo Belt (Fig. 1 for location). The basement rocks also experienced km-scale erosion in the Paleozoic, related to uplifts caused by far-field stresses propagated from the margins of the Gondwana (e.g., Variscan and Gondwanides orogenies), as well as related to glacial dynamics, as correlative sedimentary rocks (Karoo Supergroup) are preserved at the Cassange Graben (CATUNEANU et al., 2005; JELSMA et al., 2013) (Fig. 1b). In the Cretaceous, km-scale erosion of the basement also took place in many parts of the southern African plateau, including the Lucapa corridor in Angola (JELSMA et al., 2004). Finally, events of surface uplift and erosion of the basement have occurred at the Angolan margin and interior throughout the Middle to Late Cenozoic (AL-HAJRI; WHITE; FISHWICK, 2009; DA SILVA et al., 2019; GREEN; MACHADO, 2015; GUIRAUD; BUTA-NETO; QUESNE, 2010; JACKSON; HUDEC; HEGARTY, 2005; LAVIER; STECKLER; BRIGAUD, 2001; LUNDE et al., 1992; ROBERTS; WHITE, 2010). Most of the Grès Polimorphs Fm. is thought to be removed from the Ancient Plateau ever since (HADDON, 2005).

In addition, new apatite (U-Th-Sm)/He data from the basement around the studied pipes reveal major erosion driven cooling in the Carboniferous – Permian and in the Late Cretaceous-Paleocene, respectively, whereas near-surface temperatures have prevailed in the Cenozoic (chapter 3). All the information above supports that the Longa region experienced several kilometres of erosion from the Neoproterozoic to the Cretaceous, whereas erosion has been of small magnitude in the Cenozoic. This is in line with textural and mineralogical features of the VK samples suggesting they are part of the diatreme or crater infill, as supported by the magmaclasts (Fig. 5a, b, c). Crater-fill sediments are also recognized in some pipes from boreholes (Catoca, internal report), showing that they have undergone limited erosion. In other words, it is unlikely that the VK analysed here are Neoproterozoic in age and they have survived all these major pulses of erosion.

Nevertheless, the Neoproterozoic age peaks represent inherited zircon ages, which record the last time the crystals were deep in the crust at temperatures of ~ 180 – 300 °C, from which they were exhumed (GARVER et al., 2005). However, the analysed crystals were probably affected by some degree of partial reset during the kimberlite volcanism, which is more visible in the Tchiandongo sample where the older age group shows more scattering (Fig. 8). This occurs because crystals with various concentrations of radiation damage can provide distinctive zircon fission-track ages when they are subjected to the same thermal event (GARVER et al., 2005).

5.2.2 Paleogene zircon EP-FT ages

Tchiandongo and K-3 samples yielded age peaks in the Eocene, and the QTB-20 sample provided an age peak in the Eocene – Oligocene transition (Fig. 8, 9, 10, Tab. 1, 2, 3). These age peaks are interpreted here as being the ages of the kimberlites, and the arguments are as follows: These ages do not reflect regional denudation as discussed above, as these ages would be compatible with ~ 8 – 12 km of denudation since the Paleogene, which is unrealistic from the geodynamic point of view. Angola is far away from any convergent plate boundary and the highest values of basement uplift in the Cenozoic stay between ~ 3 – 4 km (JACKSON; HUDEC; HEGARTY, 2005). In addition, most of the Cenozoic uplift is related to the growth of the Angola Dome; thus, only a part of the uplift may be converted into any amount of denudation.

Furthermore, the Paleogene age peaks probably do not express thermal events (hydrothermalism) occurred much later, unrelated to the kimberlite eruptions. The main phase of serpentinisation likely took place during or soon after kimberlite emplacement, while geothermal gradients were high enough and the volcaniclastic deposit preserved porosity for the percolation of deuteric and/or hydrothermal fluids (AFANASYEV et al., 2014; SPARKS, 2013). The presence of brucite in the VK samples (Fig. 4, 6) suggests that serpentinisation reactions may have involved an increase of rock volume, which causes cementation and closure of the pore spaces as the geothermal gradient decreases (STRIPP et al., 2006). Therefore, if there was a much later hydrothermal event, unrelated to the kimberlite pipe formation, it took place along fractures onto rocks without enough porosity (massive) and this event would not have the same efficiency in resetting the fission-track system in the zircon grains. This interpretation is consistent with a growing set of works that has interpreted post-emplacement hydrothermalism or erosion in kimberlite bodies from thermochronometers of lower closure temperatures, such as apatite fission-track and (U-Th-Sm)/He (BLACKBURN et al., 2008; LARSON; AMINI, 1981).

The existence of sandstones and mudstones xenoliths in the QTB-20 pipe suggests that there were pre-existing sedimentary rocks, or at least they were contemporaneous to the eruption. Similar rocks outcrop ~ 10 km eastwards of the pipe and are remnants of the Paleogene Grès Polymorphes Fm. (GUILLOCHEAU et al., 2015) (Fig. 2). Taking into consideration the Longa region lacks any evidence for the existence of older, similar rocks, at least part of the xenoliths mentioned above may be Paleogene in age, and this interpretation strongly agrees to the zircon EP-FT ages of the QTB-20 sample.

5.3 Tectonic and Geomorphological Implications

From a geotectonic point of view, diamondiferous kimberlites reveal the existence of thick lithosphere (at least of ~ 150 km) at the time of their eruptions (WHITE; BOORDER; SMITH, 1995). Diamonds are stable at the root of thick cratons where physicochemical conditions of pressure and temperature are suitable (HAGGERTY, 1999) (Fig. 11). However, recent geophysical data indicate a present-day lithosphere thickness less than ~ 120 – 100 km underneath the Angolan Shield (CELLI et al., 2020; GLOBIG et al., 2016) (Fig. 11), and this has been interpreted as evidence for loss of cratonic root since the Cretaceous, considering that the last kimberlite volcanism hitherto known in Angola was Cretaceous in age (CELLI et al., 2020; KLÖCKING et al., 2020). The recognition of diamondiferous (and with potential for diamonds, Catoca internal report), Paleogene kimberlites at the Longa region strongly suggests that most of the removal of the cratonic root has taken place from the Paleogene onwards, although significant lithospheric thinning may also have occurred in the Cretaceous as indicated by previous works (CELLI et al., 2020; KLÖCKING et al., 2020).

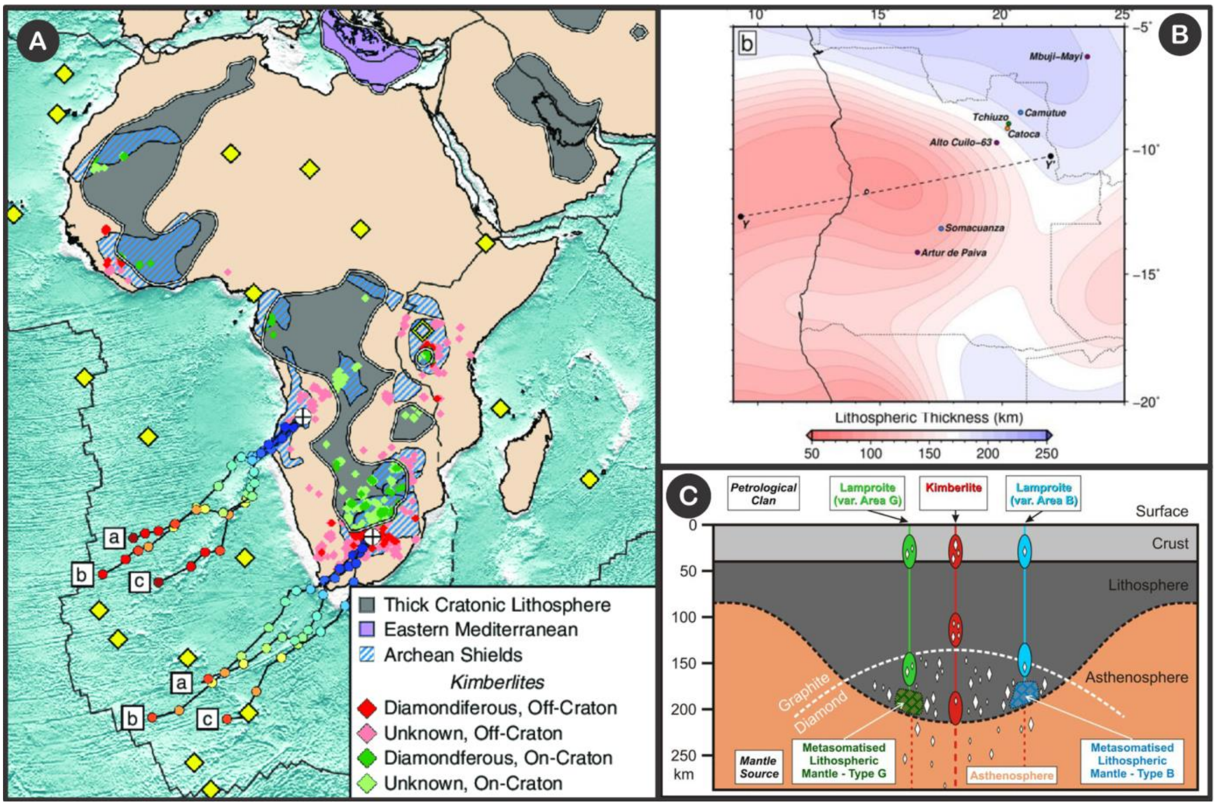

Fig. 10 a) Map of Africa showing areas of Archean Shields, areas with remnants of thick cratonic root, and spatial distribution of kimberlites. In the Angolan Shield (crossed white circle at the centre) thick lithosphere is lacking (after (CELLI et al., 2020); b) Detail of the lithosphere beneath the Angolan Shield showing thickness < 100 km at the centre where the Longa headwaters are (after (CELLI et al., 2020); and c) Sketch showing the stability of diamonds at the root of a thick craton and the zones where kimberlite and related melts may be formed (SCOTT SMITH, 2017)

The understanding of the underlying specific mechanisms behind the loss of the cratonic root is beyond the scope of this work, however, kimberlite volcanism might indicate thermochemical changes and partial melting processes within the Earth’s mantle (STANLEY; FLOWERS; BELL, 2015), which are often linked to deep mantle plumes (HAGGERTY, 1994, 1999; TORSVIK et al., 2010); as an effect of slab material transported into the mantle by subduction processes (HELMSTAEDT; GURNEY, 1984); as a consequence tectonic stresses in cratons related to plate dynamics (JELSMA et al., 2009), or as a combination or the predominance of each of these mechanisms (GIULIANI; PEARSON, 2019). As discussed in (CELLI et al., 2020), the influence of subduction processes a priori can be discarded because the last subduction event was related to the Pan-African Orogeny; thus, it is hard to connect this mechanism as the trigger for the Paleogene kimberlite volcanism in Angola. Moreover, although tectonics plays a hole in bringing kimberlite melts to the

Earth's surface, far-field stresses alone may not account for the remarkable loss of the cratonic root beneath the Angolan Shield. In summary, the Paleogene kimberlites in Angola at least link partial melting in the deep Earth's mantle, lithospheric erosion, the onset of dynamic uplifts associated with the formation of the Angola Dome, and the onset of erosion pulses across both the Angolan margin and interior (see chapters 2 and 3 and references therein). In the same way that (STANLEY; FLOWERS; BELL, 2013) claim that the Cretaceous kimberlite volcanism in South Africa is coevally linked to lithospheric thinning and surface erosion, it is proposed here that this link also exists in Angola since the Paleogene, long after the Cretaceous rifting and opening of the South Atlantic Ocean. Furthermore, the recent discovery of Pleistocene, mantle-derived carbonatite at the Catanga complex (GIULIANI et al., 2017), about ~ 200 km further southwest of the Longa region, combined with the fast Quaternary uplift of the Angolan margin (GIRESSE; HOANG; KOUYOUMONTZAKIS, 1984; WALKER et al., 2016), suggest that the deep mantle has been the motor for the ongoing growth of the Angola Dome.

6 CONCLUSION

To characterize and to establish the age of kimberlite rocks from the Longa headwaters, on the northwestern sector of the Angolan Shield, this work has combined petrography, XRD analyses, and the recent-developed electron microprobe zircon fission-track technique.

The rocks consist of volcaniclastic kimberlite, largely affected by deuteric/hydrothermal and weathering processes. Zircon crystals marked by different colours and uranium concentrations yielded consistently two unambiguous age groups in each of the analysed samples, associated with major age peaks in the Neoproterozoic and in the Paleogene. The Neoproterozoic age peaks appear to represent zircon crystals non to partially reset by the volcanism, which seems to preserve a history of exhumation of the crust related to the Pan-African Orogeny, whereas the Paleogene age peaks likely represent zircon crystals entirely reset by the volcanism and therefore, are representative of the kimberlite eruptions. The highest uranium zircon crystals persistently define the younger age component in each sample, demonstrating the capability of the technique in using high-damaged zircon crystals to constraint the time of the relatively low-temperature emplacement of the volcaniclastic rocks. In addition, based on the rock mineralogy and the physical characteristics of the encountered zircon grains, the data suggest that the rocks underwent temperatures of ~ 260 – 500 °C during an interval less than 1 Myr of heating duration.

This work proposes the existence of a kimberlitic volcanism episode in the Angolan Shield in the Paleogene. The close spatial-temporal relationship between this volcanism with lithospheric erosion indicates that deep Earth's processes have been the motor for dynamic uplifts and major denudation events across the Angolan margin, as well it places new constraints on the geomorphic age of the Angola Dome.

References

AFANASYEV, A. A. et al. Hydrothermal alteration of kimberlite by convective flows of external water. **Contributions to Mineralogy and Petrology**, v. 168, n. 1, p. 1–17, 2014.

AL-HAJRI, Y.; WHITE, N.; FISHWICK, S. Scales of transient convective support beneath Africa. **Geology**, v. 37, n. 10, p. 883–886, 2009.

ARAÚJO, A. G.; GUIMARÃES, F. Geologia de Angola. **Notícia explicativa da carta geológica à escala 1:1000000**, p. 137p, 1992.

BARNES, S. J. Chromite in komatiites, II. Modification during greenschist to mid-amphibolite facies metamorphism. **Journal of Petrology**, v. 41, n. 3, p. 387–409, 2000.

BERNET, M. A field-based estimate of the zircon fission-track closure temperature. **Chemical Geology**, v. 259, n. 3–4, p. 181–189, 2009.

BLACKBURN, T. J. et al. (U-Th)/He dating of kimberlites-A case study from north-eastern Kansas. **Earth and Planetary Science Letters**, p. 111–120, 2008.

BLACKBURN, T. J.; STOCKLI, D. F.; WALKER, J. D. Magnetite (U-Th)/He dating and its application to the geochronology of intermediate to mafic volcanic rocks. **Earth and Planetary Science Letters**, v. 259, n. 3–4, p. 360–371, 2007.

BOORDER, H. DE. Deep-reaching fracture zones in the crystalline basement surrounding the West Congo System and their control of mineralization in Angola and Gabon. **Geoexploration**, v. 20, n. 3–4, p. 259–273, 1982.

CAHEN, L. et al. **The geochronology and evolution of Africa**. Oxford: Clarendon Press, 1984.

CATUNEANU, O. et al. The Karoo basins of south-central Africa. **Journal of African Earth Sciences**, v. 43, n. 1–3, p. 211–253, 2005.

CELLI, N. L. et al. African cratonic lithosphere carved by mantle plumes. **Nature Communications**, v. 11, n. 1, 2020.

CHAMBEL, L.; CAETANO, L.; CORREIA, A. **Kimberlite Provinces of Angola: a map**. Disponível em: <https://sinese.org/econgeo/maps/.>. Acesso em: 8 dez. 2021.

DA SILVA, B. V. et al. Evolution of the Southwestern Angolan Margin: episodic burial and exhumation is more realistic than long-term denudation. **International Journal of Earth Sciences**, v. 108, n. 1, p. 89–113, 2019.

DE CARVALHO, H. et al. Geochronological review of the Precambrian in western Angola: Links with Brazil. **Journal of African Earth Sciences**, v. 31, n. 2, p. 383–402, 2000.

DE WAELE, B.; JOHNSON, S. P.; PISAREVSKY, S. A. Palaeoproterozoic to Neoproterozoic growth and evolution of the eastern Congo Craton: Its role in the Rodinia puzzle. **Precambrian Research**, v. 160, n. 1–2, p. 127–141, 2008.

DELHAL, J.; LEDENT, D.; PASTELS, P. L'âge du Complexe granitique et migmatitique de Dibaya (Région du Kasai, Zaire) par les méthodes Rb/Sr et U/Pb. **Annales Société Géologique Belgique**, v. 98, p. 141–154, 1975.

DIAS, A. N. C. et al. A new approach for electron microprobe zircon fission track thermochronology. **Chemical Geology**, v. 459, n. April, p. 129–136, 2017.

EVANS, B. W. Metamorphism of alpine peridotite and serpentinite. **Annual Review of Earth and Planetary Sciences**, v. 5, n. 1, p. 397–447, 1977.

EVANS, B. W. The Serpentinite Multisystem Revisited: Chrysotile Is Metastable. **International Geology Review**, v. 46, n. 6, p. 479–506, 2004.

FROST, R. B.; BEARD, J. S. On Silica Activity and Serpentinization. **Journal of Petrology**, v. 48, n. 7, p. 1351–1368, 2007.

GALBRAITH, R. F. **Statistics for fission track analysis**. Interdisci ed. Boca Raton, London: Chapman & Hall/CRC, 2005.

GARVER, J. I. et al. Implications for Timing of Andean Uplift from Thermal Resetting of Radiation-Damaged Zircon in the Cordillera Huayhuash, Northern Peru. **The Journal of Geology**, v. 113, n. 2, p. 117–138, 2005.

GARVER, J. I.; KAMP, P. J. J. Integration of zircon color and zircon fission-track zonation patterns in orogenic belts: Application to the Southern Alps, New Zealand. **Tectonophysics**, v. 349, n. 1–4, p. 203–219, 2002.

GIRESSE, P.; HOANG, C.-T.; KOUYOUMONTZAKIS, G. Analysis of vertical movements deduced from a geochronological study of marine Pleistocene deposits, southern coast of Angola. **Journal of African Earth Sciences**, v. 2, n. 2, p. 177–187, 1984.

GIULIANI, A. et al. Southwestern Africa on the burner: Pleistocene carbonatite volcanism linked to deep mantle upwelling in Angola. **Geology**, v. 45, n. 11, p. 971–974, 2017.

GIULIANI, A.; PEARSON, D. G. Kimberlites: From Deep Earth to Diamond Mines. **Elements**, v. 15, n. 6, p. 377–380, 2019.

GLEADOW, A. J. W.; HURFORD, A. J.; QUAIFE, R. D. Fission track dating of zircon: improved etching techniques. **Earth and Planetary Science Letters**, v. 33, p. 273–276, 1976.

GLOBIG, J. et al. New insights into the crust and lithospheric mantle structure of Africa from elevation, geoid, and thermal analysis. **Journal of Geophysical Research: Solid Earth**, v. 121, p. 5389–5424, 2016.

GOMBOSI, D. J.; GARVER, J. I.; BALDWIN, S. L. On the development of electron microprobe zircon fission-track geochronology. **Chemical Geology**, v. 363, p. 312–321, 2014.

GORDON GASTIL, R.; DELISLE, M.; MORGAN, J. Some Effects of Progressive Metamorphism on Zircons. **Geological Society of America Bulletin**, v. 78, n. 7, p. 879–906, 1967.

GREEN, P. F.; MACHADO, V. Pre-rift and synrift exhumation, post-rift subsidence and exhumation of the onshore Namibe Margin of Angola revealed from apatite fission track analysis. **Geological Society, London, Special Publications**, v. 438, p. 99–118, 2015.

GUILLOCHEAU, F. et al. Cenozoic Landscape Evolution in and Around the Congo Basin: Constraints from Sediments and Planation Surfaces. In: DE WIT, M. J.; GUILLOCHEAU, F.; DE WIT, M. C. J. (Eds.). . **Geology and Resource Potential of**

the Congo Basin. Berlin-Heidelberg: Springer, 2015. p. 1–417.

GUIRAUD, M.; BUTA-NETO, A.; QUESNE, D. Segmentation and differential post-rift uplift at the Angola margin as recorded by the transform-rifted Benguela and oblique-to-orthogonal-rifted Kwanza basins. **Marine and Petroleum Geology**, v. 27, n. 5, p. 1040–1068, 2010.

HADDON, I. G. **The Sub-Kalahari Geology and Tectonic Evolution of the Kalahari Basin, Southern Africa**. [s.l.] Witwatersrand, Johannesburg, 2005.

HADDON, I. G.; MCCARTHY, T. S. The Mesozoic-Cenozoic interior sag basins of Central Africa: The Late Cretaceous-Cenozoic Kalahari and Okavango basins. **Journal of African Earth Sciences**, v. 43, p. 316–333, 2005.

HAGGERTY, S. E. Superkimberlites: A geodynamic diamond window to the Earth's core. **Earth and Planetary Science Letters**, v. 122, p. 57–69, 1994.

HAGGERTY, S. E. A diamond trilogy: Superplumes, supercontinents, and supernovae. **Science**, v. 285, n. 5429, p. 851–860, 1999.

HAGGERTY, S. E.; RABER, E.; NAESER, C. W. Fission track dating of kimberlitic zircons. **Earth and Planetary Science Letters**, v. 63, n. 1, p. 41–50, 1983.

HASEBE, N. et al. Geological partial annealing zone of zircon fission-track system: Additional constrains from the deep drilling MITI-Nishikubiki and MITI-Mishima. **Chemical Geology**, v. 199, n. 1–2, p. 45–52, 2003.

HAYMAN, P. C.; CAS, R. A. F.; JOHNSON, M. Characteristics and alteration origins of matrix minerals in volcaniclastic kimberlite of the Muskox pipe (Nunavut, Canada). **Lithos**, v. 112, n. 2009, p. 473–487, 2009.

HEAMAN, L. M.; PHILLIPS, D.; PEARSON, D. G. Dating Kimberlites: Methods and Emplacement Patterns Through Time. **Elements**, v. 15, n. 6, p. 399–404, 2019.

HELMSTAEDT, H.; GURNEY, J. J. **Kimberlites of Southern Africa - Are They Related to Subduction Processes?** [s.l.] Elsevier Science Publishers B.V., 1984. v. 11

JACKSON, M. P. A.; HUDEC, M. R.; HEGARTY, K. A. The great West African Tertiary coastal uplift: Fact or fiction? A perspective from the Angolan divergent margin. **Tectonics**, v. 24, n. 6, p. 1–23, 2005.

JELSMA, H. et al. Tectonic setting of kimberlites. **LITHOS**, v. 112, p. 155–165, 2009.

JELSMA, H. et al. **Kimberlites from Central Angola: A Case Study of Exploration Findings**. (D. G. Pearson et al., Eds.)International Kimberlite Conference 10. **Anais**...Bangalore, India: Springer, 2013

JELSMA, H. A. et al. Preferential distribution along transcontinental corridors of kimberlites and related rocks of Southern Africa. **South African Journal of Geology**, v. 107, n. (1-2), p. 301–324, 2004.

JELSMA, H. A. et al. SHRIMP U-Pb zircon geochronology of basement rocks of the Angolan Shield, western Angola. **23rd Colloquium of African Geology.**, n. January, p. 203, 2011.

KLÖCKING, M. et al. A tale of two domes: Neogene to recent volcanism and dynamic uplift of northeast Brazil and southwest Africa. **Earth and Planetary Science Letters**, v. 547, p. 116464, 2020.

LARSON, E. E.; AMINI, M. H. Fission-track dating of the Green Mountain kimberlite diatreme, near Boulder, Colorado. **Mountain Geologist**, v. 18, n. 1, p. 19–22, 1981.

LAVIER, L. L.; STECKLER, M. S.; BRIGAUD, F. Climatic and tectonic control on the Cenozoic evolution of the West African margin. **Marine Geology**, v. 178, n. 1–4, p. 63–80, 2001.

LINOL, B. et al. Formation and Collapse of the Kalahari Duricrust [’African Surface’] Across the Congo Basin, with Implications for changes in Rates of Cenozoic Off-Shore Sedimentation. **Geology and Resource Potential of the Congo Basin**, n. September, p. 1–417, 2015.

LUNDE, G. et al. Tertiary uplift of the Kwanza Basin in Angola. In: CURNELLE, R. (Ed.). . **Géologie Africaine, Colloques de Geologie de Libreville**. [s.l.] Bull. Cent. de Rech. Explor. Product. Elf Aquitaine Mém, 1992. v. 13p. 99–117.

MCCOURT, S. et al. New U-Pb SHRIMP ages from the Lubango region, SW Angola: insights into the Palaeoproterozoic evolution of the Angolan Shield, southern Congo Craton, Africa. **Journal of the Geological Society**, v. 170, n. 2, p. 353–363, 2013.

MCINNES, B. I. A. et al. Zircon U–Th–Pb–He double dating of the Merlin kimberlite field, Northern Territory, Australia. **Lithos**, v. 112, p. 592–599, 2009.

MITCHELL, R. H. **Kimberlites: Mineralogy, Geochemistry, and Petrology**. 1. ed. New York: Springer Science & Business Media, LLC, 1986.

MITCHELL, R. H.; GIULIANI, A.; O’BRIEN, H. What is a Kimberlite? Petrology and Mineralogy of Hypabyssal Kimberlites. **Elements**, v. 15, n. 6, p. 381–386, 2019.

MONFORTE, A. **O Diamante em Angola nas rochas quimberlíticas e nos jazigos secundários**. Lisboa: Sociedade Portuguesa de empreendimentos, 1988.

MONIÉ, P. et al. The Late Neoproterozoic/Early Palaeozoic evolution of the West Congo Belt of NW Angola: Geochronological (U-Pb and Ar-Ar) and petrostructural constraints. **Terra Nova**, v. 24, n. 3, p. 238–247, 2012.

NAESER, C. W. Geochronology of the Navajo-Hopi Diatremes, Four Corners Area. **Journal of Geophysical Research**, v. 76, n. 20, p. 4978–4985, 1971.

NASDALA, L. et al. Retention of radiation damage in zircon xenocrysts from kimberlites, Northern Yakutia. **Lithos**, v. 206–207, n. 1, p. 252–261, 2014.

NIMIS, P. et al. Phyllosilicate minerals in the hydrothermal mafic-ultramafic-hosted massive-sulfide deposit of Ivanovka (southern Urals): Comparison with modern ocean seafloor analogues. **Contributions to Mineralogy and Petrology**, v. 147, n. 3, p. 363–383, 2004.

PESLIER, A. H.; WOODLAND, A. B.; WOLFF, J. A. Fast kimberlite ascent rates estimated from hydrogen diffusion profiles in xenolithic mantle olivines from southern Africa. **Geochimica et Cosmochimica Acta**, v. 72, n. 11, p. 2711–2722, 2008.

RAHN, M. K. et al. A zero-damage model for fission-track annealing in zircon. **American Mineralogist**, v. 89, n. 4, p. 473–484, 2004.

REINERS, P. W. Zircon (U-TH)/He thermochronometry. **Reviews in Mineralogy and Geochemistry**, v. 58, n. 1936, p. 151–179, 2005.

REINERS, P. W.; BRANDON, M. T. Using thermochronology to understand orogenic erosion. **Annual Review of Earth and Planetary Sciences**, v. 34, n. June 2014, p.

419–466, 2006.

RENNE, P. R. et al. Joint determination of 40K decay constants and 40Ar/40K for the Fish Canyon sanidine standard, and improved accuracy for 40Ar/39Ar geochronology. **Geochimica et Cosmochimica Acta**, v. 74, n. 18, p. 5349–5367, 2010.

ROBERTS, G. G.; WHITE, N. Estimating uplift rate histories from river profiles using African examples. **Journal of Geophysical Research: Solid Earth**, v. 115, n. 2, p. 1–24, 2010.

SCHNEIDER, C. A.; RASBAND, W. S.; ELICEIRI, K. W. NIH Image to ImageJ: 25 years of image analysis. **Nature Methods**, v. 9, n. 7, p. 671–675, 2012.

SCOTT SMITH, B. H. The Fort à la Corne kimberlites, Saskatchewan, Canada: Geology, emplacement and economics. **Journal of the Geological Society of India**, v. 71, n. 1, p. 11–55, 2008.

SCOTT SMITH, B. H. et al. **Kimberlite Terminology and Classification**. (D. G. Pearson et al., Eds.)Proceedings of 10th International Kimberlite Conference. **Anais**...New Delhi: Springer, 2013

SCOTT SMITH, B. H. **Kimberlites – from mantle to mine**. 11th Kimberlite Conference Extended Abstract. **Anais**...Botswana: 2017

SCOTT SMITH, B. H. et al. **A Glossary of Kimberlite and Related Terms**. Vancouver: Scott-Smith Petrology Inc., 2018.

SPARKS, R. S. J. Kimberlite volcanism. **Annual Review of Earth and Planetary Sciences**, v. 41, p. 497–528, 2013.

STANLEY, J. R.; FLOWERS, R. M. Dating kimberlite emplacement with zircon and perovskite (U-Th)/He geochronology. **Geochemistry Geophysics Geosystems**, v. 17, p. 4517–4533, 2016.

STANLEY, J. R.; FLOWERS, R. M.; BELL, D. B. Erosion patterns and mantle sources of topographic change across the southern African Plateau derived from the shallow and deep records of kimberlites. **Geochemistry, Geophysics, Geosystems**, v. 16, p. 1–22, 2015.

STANLEY, J. R.; FLOWERS, R. M.; BELL, D. R. Kimberlite (U-Th)/He dating links surface erosion with lithospheric heating, thinning, and metasomatism in the southern African Plateau. **Geology**, v. 41, n. 12, p. 1243–1246, 2013.

STRIPP, G. R. et al. Post-emplacement serpentinization and related hydrothermal metamorphism in a kimberlite from Venetia, South Africa. **Journal of Metamorphic Geology**, v. 24, n. 6, p. 515–534, 2006.

TACK, L. et al. Early Neoproterozoic magmatism (1000-910 Ma) of the Zadinian and Mayumbian groups (Bas-Congo): Onset of Rodinia rifting at the western edge of the Congo craton. **Precambrian Research**, v. 110, n. 1–4, p. 277–306, 2001.

TAGAMI, T. et al. Revised Annealing Kinetics of Fission Tracks in Zircon and Geological Implications. In: VAN DEN HAUTE, P.; CORTE, F. (Eds.). . **Advances in Fission-Track Geochronology**. [s.l.] Springer Science & Business Media, 1998. p. 99–112.

TAGAMI, T.; SHIMADA, C. Natural long-term annealing of the zircon fission track system around a granitic pluton. **Journal of Geophysical Research**, v. 101, n. B4,

p. 8245–8255, 1996.

TORQUATO, J. R. et al. A evolução geológica do Cinturão Móvel do Quipungo no Ocidente de Angola. **Anais Academia Brasileira de Ciências**, v. 51, p. 133–143, 1979.

TORSVIK, T. H. et al. Diamonds sampled by plumes from the core-mantle boundary. **Nature**, v. 466, n. 7304, p. 352–355, 2010.

USTINOV, V. N. et al. Kimberlites distribution in Angola and prospective areas for new discoveries. **Mineralogy and Petrology**, v. 112, p. 383–396, 2018.

VAN OTTERLOO, J.; CAS, R. A. F. Low-temperature emplacement of phreatomagmatic pyroclastic flow deposits at the monogenetic Mt gambier volcanic complex, south Australia, and their relevance for understanding some deposits in diatremes. **Journal of the Geological Society**, v. 173, n. 4, p. 701–710, 2016.

VERMEESCH, P. RadialPlotter: A Java application for fission track, luminescence and other radial plots. **Radiation Measurements**, v. 44, n. 4, p. 409–410, 2009.

WALKER, R. T. et al. Rapid mantle-driven uplift along the Angolan margin in the late Quaternary. **Nature Geoscience**, v. 9, n. 12, p. 909–914, 14 dez. 2016.

WEBB, K.; HETMAN, C. Magmaclasts in kimberlite. **Lithos**, v. 396–397, p. 106197, 2021.

WHITE, S. H.; BOORDER, H. DE; SMITH, C. B. Structural controls of kimberlite and lamproite emplacement. **Journal of Geoquemical Exploration**, v. 53, p. 245–264, 1995.

YAMADA, R. et al. Annealing kinetics of fission tracks in zircon: an experimental study. **Chemical Geology**, v. 122, n. 1–4, p. 249–258, 1995.

YANG, T. F. et al. Fission-track dating of volcanics in the northern part of the Taiwan-Luzon Arc: eruption ages and evidence for crustal contamination. **Journal of Southeast Asian Earth Sciences**, v. 11, n. 2, p. 81–93, 1995.

ZAUN, P. E.; WAGNER, G. A. Fission-track stability in zircons under geological conditions. **Nuclear Tracks and Radiation Measurements (1982)**, v. 10, n. 3, p. 303–307, 1985.

CAPÍTULO 5 – CONCLUSÕES E CONTRIBUIÇÕES DA TESE

Conforme descrito nos Capítulos 2 e 3, as histórias térmicas das zonas costeiras das porções sudoeste e noroeste do Domo de Angola confirmam resfriamentos no Cenozoico, principalmente a partir do Eoceno, compatíveis com denudação em escala quilométrica (GREEN; MACHADO, 2015; HUDEC; JACKSON, 2002, 2004; JACKSON; HUDEC; HEGARTY, 2005; LUNDE et al., 1992; SILVA et al., 2019). Entretanto, as histórias térmicas do topo da escarpa de Chela (porção sudoeste) e do planalto antigo (porção noroeste) não suportam resfriamentos pronunciados no Cenozoico, indicando que a denudação cenozoica nestas regiões foi substancialmente menor (< 1 km). Uma denudação cenozoica mais limitada (a partir de ~ 40 - 30 Ma) em diversas áreas ao longo do planalto antigo, também é sugerida pela preservação de remanescentes da superfície de aplainamento africana (BURKE; GUNNELL, 2008; DE PUTTER; RUFFET, 2020; GUILLOCHEAU et al., 2018) e da *Upper Surface 2* (GUILLOCHEAU et al., 2015), assim como pela preservação de remanescentes da Formação *Grés Polimorphes* (ARAÚJO; GUIMARÃES, 1992; GUILLOCHEAU et al., 2015; HADDON, 2005; HADDON; MCCARTHY, 2005; LINOL et al., 2015).

Deste modo, os dados coligidos nesta Tese permitem propor que os relevos das porções sudoeste e noroeste do Domo de Angola desenvolveram-se predominantemente no Cenozoico, devido à denudação diferencial entre a zona costeira e o planalto antigo. Esta denudação diferencial é ilustrada pelos índices morfométricos K_{sn} e χ da rede de drenagem da porção sudoeste, os quais indicam que os rios costeiros possuem taxas de incisão fluvial maiores do que os rios interiores e que a bacia de drenagem costeira tende a avançar em direção ao interior. Neste caso, a denudação cenozoica corrobora a hipótese de captura do rio Cunene interior por um rio costeiro no Cenozoico (BUCH, 1997; HOUBEN et al., 2020). Assumindo-se que o Domo de Angola consiste em uma estrutura contínua que tem sido formada por pulsos de soerguimento de longo comprimento de onda (AL-HAJRI; WHITE; FISHWICK, 2009; GUILLOCHEAU et al., 2018; KLÖCKING et al., 2020; ROBERTS; WHITE, 2010; WALKER et al., 2016) e que as variações climáticas têm ocorrido de forma relativamente homogênea ao longo da margem angolana (SÉRANNE; ANKA, 2005), sugere-se que o padrão de denudação observado nestas duas áreas pode ser extrapolado para o restante da margem angolana; no entanto, novas pesquisas são necessárias tanto na zona costeira quanto no planalto antigo para testar tal hipótese.

Estima-se que a superfície de aplainamento reconhecida na região do rio Longa (*Upper surface 2*) possui idade máxima do Paleogeno, baseando-se na sua relação de truncamento com remanescentes da Formação *Grés Polimorphes* (GUILLOCHEAU et al., 2015). Entretanto, como anteriormente mencionado, os resultados de AHe do embasamento Pré-cambriano não detectam resfriamento significativo no cenozoico, indicando que a denudação cenozoica nesta região do planalto foi provavelmente menor do que ~ 1 km. Isto implica que não são necessários vários quilômetros de erosão para formar estas superfícies, ou seja, eventos de resfriamento detectados por meio de métodos termocronológicos de baixa-temperatura, não necessariamente coincidem com a última fase erosiva de determinada superfície, uma vez que estes resfriamentos podem representar fases pretéritas e, portanto, devem ser interpretados com cautela quando utilizados para este propósito.

Conforme descrito no Capítulo 4, a porção noroeste do Escudo Angolano foi afetada por eventos térmicos importantes no Neoproterozoico e no Paleogeno, sendo que este último evento possivelmente corresponde à época de erupção de kimberlitos. Caso esta hipótese se confirme, a ocorrência de kimberlitos diamantíferos na região do rio Longa indica a presença de raiz cratônica espessa e processos de fusão parcial do manto sub-litosférico no Paleogeno. Estas informações combinadas a dados geofísicos prévios (CELLI et al., 2020; KLÖCKING et al., 2020) sugerem que uma fase importante de erosão e afinamento da litosfera vem ocorrendo pelo menos desde o Paleogeno. Tais processos provocam domeamento litosférico e soerguimento de longo comprimento de onda na superfície terrestre (KLÖCKING et al., 2020), possivelmente atrelados à formação do Domo de Angola.

Em resumo, a partir dos resultados obtidos nesta Tese em conjunto com as pesquisas prévias citadas, é proposto um modelo evolutivo para as áreas aqui estudadas dentro do contexto genético Domo de Angola:

i. A fusão do manto sub-litosférico provoca magmatismo kimberlitico e está possivelmente associada ao inicio de uma fase de erosão/afinamento do manto litosférico no Paleogeno;

ii. Tais processos mantélicos iniciam o domeamento e o soerguimento da superfície terrestre;

iii. O soerguimento regional expõe as rochas a processos de denudação e de intemperismo, impulsionados também por condições climáticas favoráveis estabelecidas no Cenozoico;

iv. A denudação ocorre de forma diferenciada, possivelmente devido à reorganização do sistema de drenagem que se adapta as quedas do nível de base, a qual é maior no flanco voltado para o oceano, enquanto que no interior predomina o soerguimento da superfície e a preservação parcial das *etchplains.*

O modelo acima revitaliza em Angola a teoria de (BURKE; GUNNELL, 2008), de que o *Great Escarpment* africano se forma por dissecação das bordas dos Domos regionais a partir da segunda metade do Cenozoico. Se existe evidência da erupção de carbonatitos (GIULIANI et al., 2017) e soerguimentos recentes da superfície do Domo de Angola (WALKER et al., 2016), esta Tese também contribui em sugerir que estes processos estão ativos pelo menos desde o Paleogeno, trazendo mais um capítulo para a elucidação da história tectônica e geomorfológica da região.

De um ponto de vista metodológico, a técnica por EP-FT (DIAS et al., 2017; GOMBOSI; GARVER; BALDWIN, 2014) se mostra promissora para a datação de kimberlitos conforme apresentado no Capítulo 4. A vantagem do método EP-FT em relação às abordagens tradicionais decorre da possibilidade de datação de cristais ricos em urânio, os quais em geral são mais danificados por decaimento radioativo e apresentam temperaturas de fechamento menores, sendo mais sensíveis ao reset total pelas temperaturas associadas à formação de depósitos vulcanoclásticos. Isto é nítido na amostra do kimberlito K-3, no qual a população de idades mais jovem é quase inteiramente representada por cristais com concentrações de urânio acima de 2000 ppm. A vantagem deste método também consiste na possibilidade de se estimar temperaturas, taxas de resfriamento, ou tempo de duração do aquecimento associados à formação de kimberlitos vulcanoclásticos.

Referências

AL-HAJRI, Y.; WHITE, N.; FISHWICK, S. Scales of transient convective support beneath Africa. **Geology**, v. 37, n. 10, p. 883–886, 2009.

ARAÚJO, A. G.; GUIMARÃES, F. Geologia de Angola. **Notícia explicativa da carta geológica à escala 1:1000000**, p. 137p, 1992.

BUCH, M. W. Etosha Pan - The third largest lake in the world? **Madoqua**, v. 20, n. 1, p. 49–64, 1997.

BURKE, K.; GUNNELL, Y. **The african erosion surface: A Continental-Scale Synthesis of Geomorphology, Tectonics, and Environmental Change over the Past 180 Million Years**. Memoir 201 ed. Boulder, Colorado: Geological Society of America, 2008.

CELLI, N. L. et al. African cratonic lithosphere carved by mantle plumes. **Nature Communications**, v. 11, n. 1, 2020.

DE PUTTER, T.; RUFFET, G. Supergene manganese ore records 75 Myr-long Campanian to Pleistocene geodynamic evolution and weathering history of the Central African Great Lakes Region – Tectonics drives, climate assists. **Gondwana Research**, v. 83, p. 96–117, 2020.

DIAS, A. N. C. et al. A new approach for electron microprobe zircon fission track thermochronology. **Chemical Geology**, v. 459, n. April, p. 129–136, 2017.

GIULIANI, A. et al. Southwestern Africa on the burner: Pleistocene carbonatite volcanism linked to deep mantle upwelling in Angola. **Geology**, v. 45, n. 11, p. 971–974, 2017.

GOMBOSI, D. J.; GARVER, J. I.; BALDWIN, S. L. On the development of electron microprobe zircon fission-track geochronology. **Chemical Geology**, v. 363, p. 312–321, 2014.

GREEN, P. F.; MACHADO, V. Pre-rift and synrift exhumation, post-rift subsidence and exhumation of the onshore Namibe Margin of Angola revealed from apatite fission track analysis. **Geological Society, London, Special Publications**, v. 438, p. 99–118, 2015.

GUILLOCHEAU, F. et al. Cenozoic Landscape Evolution in and Around the Congo Basin: Constraints from Sediments and Planation Surfaces. In: DE WIT, M. J.; GUILLOCHEAU, F.; DE WIT, M. C. J. (Eds.). . **Geology and Resource Potential of the Congo Basin**. Berlin-Heidelberg: Springer, 2015. p. 1–417.

GUILLOCHEAU, F. et al. Planation surfaces as a record of mantle dynamics: The case example of Africa. **Gondwana Research**, v. 53, p. 82–98, 2018.

HADDON, I. G. **The Sub-Kalahari Geology and Tectonic Evolution of the Kalahari Basin, Southern Africa**. [s.l.] Witwatersrand, Johannesburg, 2005.

HADDON, I. G.; MCCARTHY, T. S. The Mesozoic-Cenozoic interior sag basins of Central Africa: The Late Cretaceous-Cenozoic Kalahari and Okavango basins. **Journal of African Earth Sciences**, v. 43, p. 316–333, 2005.

HOUBEN, G. J. et al. Stacked megafans of the kalahari basin as archives of paleogeography, river capture, and cenozoic paleoclimate of Southwestern Africa.

Journal of Sedimentary Research, v. 90, n. 9, p. 980–1010, 2020.

HUDEC, M. R.; JACKSON, M. P. A. Structural segmentation, inversion, and salt tectonics on a passive margin: Evolution of the Inner Kwanza Basin, Angola. **Bulletin of the Geological Society of America**, v. 114, n. 10, p. 1222–1244, 2002.

HUDEC, M. R.; JACKSON, M. P. A. Regional restoration across the Kwanza Basin, Angola: Salt tectonics triggered by repeated uplift of a metastable passive margin. **AAPG Bulletin**, v. 88, n. 7, p. 971–990, 2004.

JACKSON, M. P. A.; HUDEC, M. R.; HEGARTY, K. A. The great West African Tertiary coastal uplift: Fact or fiction? A perspective from the Angolan divergent margin. **Tectonics**, v. 24, n. 6, p. 1–23, 2005.

KLÖCKING, M. et al. A tale of two domes: Neogene to recent volcanism and dynamic uplift of northeast Brazil and southwest Africa. **Earth and Planetary Science Letters**, v. 547, p. 116464, 2020.

LINOL, B. et al. Formation and Collapse of the Kalahari Duricrust ['African Surface'] Across the Congo Basin, with Implications for changes in Rates of Cenozoic Off-Shore Sedimentation. **Geology and Resource Potential of the Congo Basin**, n. September, p. 1–417, 2015.

LUNDE, G. et al. Tertiary uplift of the Kwanza Basin in Angola. In: CURNELLE, R. (Ed.). . **Géologie Africaine, Colloques de Geologie de Libreville**. [s.l.] Bull. Cent. de Rech. Explor. Product. Elf Aquitaine Mém, 1992. v. 13p. 99–117.

ROBERTS, G. G.; WHITE, N. Estimating uplift rate histories from river profiles using African examples. **Journal of Geophysical Research: Solid Earth**, v. 115, n. 2, p. 1–24, 2010.

SÉRANNE, M.; ANKA, Z. South Atlantic continental margins of Africa: A comparison of the tectonic vs climate interplay on the evolution of equatorial west Africa and SW Africa margins. **Journal of African Earth Sciences**, v. 43, n. 1–3, p. 283–300, 2005.

SILVA, B. V. et al. Evolution of the Southwestern Angolan Margin: episodic burial and exhumation is more realistic than long-term denudation. **International Journal of Earth Sciences**, v. 108, n. 1, p. 89–113, 2019.

WALKER, R. T. et al. Rapid mantle-driven uplift along the Angolan margin in the late Quaternary. **Nature Geoscience**, v. 9, n. 12, p. 909–914, 14 dez. 2016.